2014

Surface modification of colloidal semiconductor nanocrystal quantum dots

Elham Tavasoli
Iowa State University

Surface modification of colloidal semiconductor nanocrystal quantum dots

by

Elham Tavasoli

A dissertation submitted to the graduate faculty

in partial fulfillment of the requirements for the degree of

DOCTOR OF PHILOSOPHY

Major: Chemistry

Program of Study Committee:
Javier Vela Major Professor
Aaron Sadow
Arthur Winter
Keith Woo
Ning Fang

Iowa State University

Ames, Iowa

2014

DEDICATION

To my mother, who has been a source of encouragement and inspiration to me throughout my life, and my dad who has actively supported me in my determination, to find and realize my potentials, and to make this contribution to our world.

To my husband, who remains willing to engage with the struggle and ensuing discomfort of having a partner who has added the role of wife to the competing demands of business, work, study and personal development.

To my lovely and lonely sister, for her practical and emotional support.

TABLE OF CONTENTS

NOMENCLATURE

QD	Quantum Dot
ADMET	Acyclic Diene Metathesis
PEG	Poly Ethylene Glycol
ROESY	Rotating-frame nuclear Overhauser Effect SpectroscopY
NOESY	Nuclear Overhauser Effect SpectroscopY
DOSY	Diffusion Ordered SpectroscopY
DLS	Dynamic Light Scattering
TEM	Transmission Electron Microscopy
EDX	Energy-Dispersive X-ray spectroscopy

ACKNOWLEDGEMENTS

I would like to thank my Advisor, Dr. Javier Vela for his guidance and support throughout the course of this research. I would also like to thank Professor Malika Jeffries-El for being my mentor for Preparing Future Faculty (PFF) program and giving me invaluable advice. Thank you to Professors Keith Woo, Aaron Sadow, Ning Fang, and Arthur Winter for serving on my Program of Study Committee and being wonderful teachers in and out of the classroom.

In addition, I would also like to thank my friends, colleagues, the department faculties and staff for making my time at Iowa State University a wonderful experience.

Finally, thanks to my family for their encouragement and to my husband for his hours of patience, respect and love.

ABSTRACT

Current quantum dot surface modification strategies rely heavily on ligand exchange that removes the nanocrystal's native ligands originated from its synthesis. This can cause etching and introduce surface defects, affecting the nanocrystal's optical properties. In addition, common ligand exchange method fails to control the degree of functionalization or the number of functional groups introduced per nanocrystal.

We describe our work on surface modification of semiconductor nanocrystal quantum dots investigating a new approach that not only bypasses ligand exchange and introduces native active ligands with original optical properties, but also is able to control the degree of surface loading, called "valence", in semiconductor nanocrystal quantum dots. We show that surface doped quantum dots capped with chemically-active native ligands can be prepared directly from a mixture of ligands with similar chain lengths. Initial ratio between chemically active and inactive ligands is retained on the nanocrystal surface, allowing to control the extent of surface modification.

The extent of surface coverage by a particular functional group will have a large impact on a nanocrystal affinity and permeability to a variety of biological structures. It also affects nanocrystal's ability to localize, penetrate, and transport across specific tissues, cellular and subcellular structures. We show that we are able to control the loading of cholestanone per quantum dot nanocrystal. We observed that samples with higher steroid loading infuse themselves more with the lipid membrane compare to those with no or little steroid.

To further investigate the surface ligand packing, structure and reactivity, we apply advanced solution NMR techniques to determine surface ligand organization and chemistry. Two-dimension ROESY studies show that ligands with the same chain length tend to homogeneously distribute themselves onto the nanocrystal's surface however ligands with the different chain length tend to form islands. Furthermore, we demonstrate that surface ligand organization can affect the reactivity of quantum dots. Formation of rafts as a result of packing ligands of a same length, increase the local concentration of reactive terminal group and facilitate the chemical reactivity at the surface of quantum dots.

We also synthesize multifunctional multidentate polymeric ligand *via* ADMET. Varying the total dienes-to-Ru catalyst ratio allows us to control the extent of ADMET, which enables us to achieve an accurate control over polydentate ligand size. We use the synthetic polymer as a linkage for constructing gold-QD heterostructure.

We hope that this study can provide a new avenue to understand the organic/inorganic boundary of other and more complex nanoparticle/ligand systems.

CHAPTER I

INTRODUCTION

General Introduction

What are Quantum dots? Quantum dots are tiny particles of a semiconducting material that are small enough to exhibit quantum mechanical properties. They usually have diameters in the range of 2-10 nanometers. Quantum dots display unique electronic properties that are intermediate between those of bulk semiconductors and discrete molecules.

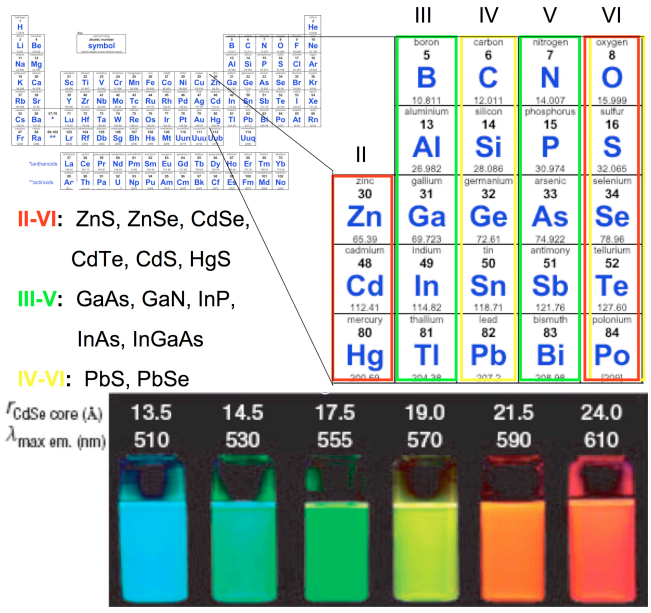

Figure 1. Quantum dost with gradually stepping emission from blue to deep red

Electronic characteristics of a quantum dot are closely related to its size and shape. Generally, as the size of the crystal decreases, the difference in energy between valence band and conduction band increases. More energy is then needed to excite a dot, and concurrently, more energy is released when the crystal returns to its ground state. Since the size of a quantum dot can be controlled when it is made, the excitation and emission of quantum dots can be highly tunable resulting in a color shift from red to blue in the emitted light.

Quantum dot fabrication

Tunable size and unique optical properties make quantum dots appealing materials for variety of applications and new technologies. Quantum dots are particularly important for optical applications due to their bright color, tunable emission with high extinction coefficient, and long lifetime. Solar cells, transistors, ultrafast all-optical switches and logic gates are examples of applications that take advantage of these unique properties. The small size of quantum dots and their ability to go into living organs make them suitable for bio-medical applications such as medical imaging and biosensors.

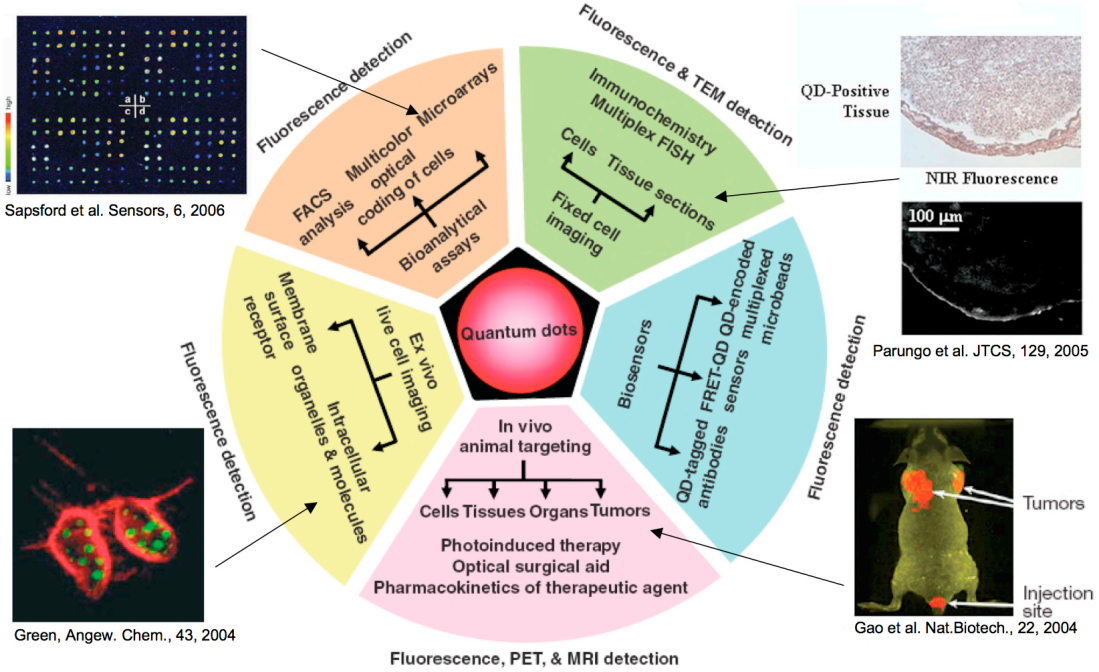

Figure 2. Quantum dots applications

Quantum dot synthesis

In a typical method, quantum dots are synthesized using a three-component system including: metal chalcogenide precursor, organic ligand or surfactant with an active head group to passivate the quantum dot surface upon formation, and a high boiling point inert solvent just to homogenize the reaction mixture. The reaction should be heated to a sufficiently high temperature so that the precursors decompose into monomers that form quantum dots. The nanocrystal growth starts after a nucleation process once the monomers reach supersaturation. The temperature during the growth process must be high enough to allow for rearrangement and annealing of atoms while being low enough to promote crystal growth. Precursor concentration also has to be precisely controlled during nanocrystal growth. Typical dots are made of binary compounds such as cadmium sulfide, cadmium selenide, indium phosphide, and indium arsenide. Dots may also be made from ternary compounds such as cadmium selenide sulfide.

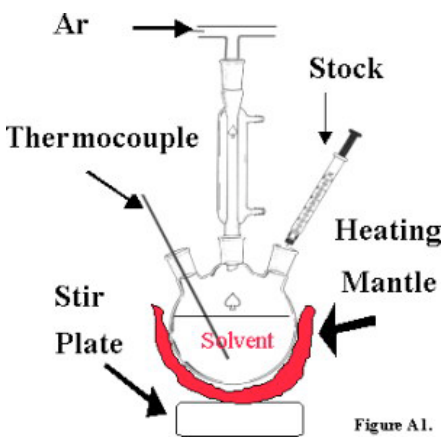

Figure 3. Schematic illustration of traditional synthesis of quantum dots

Surface chemistry of quantum dots

Colloidal nanocrystals synthesized by this approach are inorganic/organic hybrid materials where the inorganic nanocrystal core is passivated by a monolayer of organic ligand (surfactant) layer that was added during their synthesis. Research has long been focused on the inorganic core and its size- and shape-dependent optoelectronic properties.

However, detailed and systematic studies addressing the organic/inorganic interface of colloidal nanocrystals developed only over the last 5−10 years. These native organic ligands typically consist of a functional head group and inert organic tail. The head group binds to the nanocrystal surface and play a crucial role in controlling size and shape of the particles, while the tail group is responsible for colloidal stability and solubility.[1,2]

Ligand Exchange

The state-of-the-art in nanocrystal surface modification includes "thiol ligand exchange". Thiol ligand exchange consists of replacing the nanocrystal's native ligands with chemically active-terminated thiol ligands, usually added in excess. Thiol end of the ligand is attached to the nanocrystal surface and the other end is covalently or non-covalently attached to a molecule or material of interest via a post ligand exchange process.

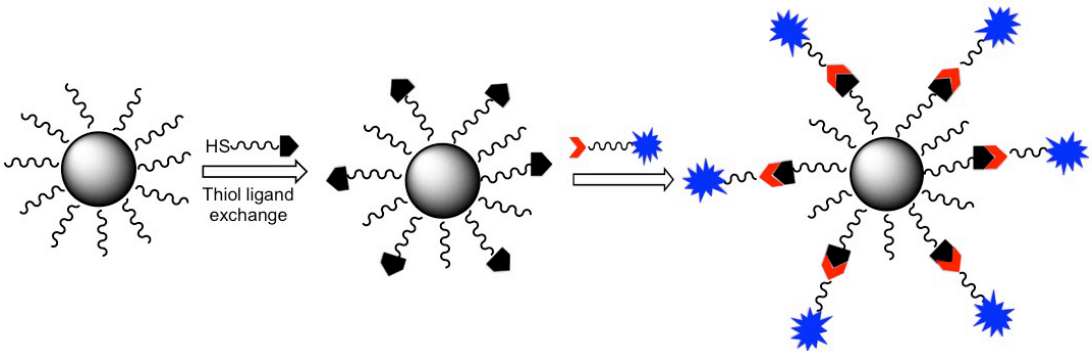

Figure 4. Typical thiol ligand exchange and post ligand exchange surface modification

Several studies have been conducted using thiol-based ligand molecules to modify the surface of QDs. However, removing the nanocrystal's native ligands that originate from its synthesis can cause etching, introduce surface defects, and often leads to a significant loss in quantum yields and poor stability of the colloids in aqueous solutions.

[3,4] Studies have confirmed that thiols generally quench the Photoluminescence (PL) of QDs. [5,6,7]

As a part of our investigation to overcome this problem, we have reported a fundamentally new strategy to directly synthesize CdS nanocrystals with native active surface ligands that can be introduced during the particles growth and bypasses need of routinely implemented ligand exchange.

Another limitation associated with the common "ligand exchange" process is its failure to control the extent of surface modification or number of functional groups per nanocrystal, called "valency". Using the direct synthesis method without ligand exchange, we are able to control the relative population of active ligands on the surface which is proportional to the relative concentration of corresponding ligand used during the nanocrystal synthesis.

Due to increasing demand for appropriate nanocrystals for the study of biological systems and formation of complex, nanocrystal-based superstructures, making nanocrystals in which ligands display a variety of desirable properties *via* capping engineering is a challenging topic in colloidal nanocrystal research. Progress in this respect is tangentially associated to a better understanding of the surface-ligand and ligand-ligand interactions at the nanocrystal-ligand inorganic-organic interface.

Ligand distribution and packing

A key element to exploring the role of surface ligands during synthesis of nanocrystals or the ligand exchange procedures is to understand the nanocrystal-ligand interaction. Among the several methodologies such as infrared spectroscopy, [8] photoluminescence spectroscopy [9,10] and X-ray photoelectron spectroscopy, [11] presented

to investigate these interactions, solution nuclear magnetic resonance spectroscopy (NMR) stands out, where typically ^{1}H, ^{13}C or ^{31}P nuclei are probed. Solution ^{1}H NMR has been used for surface analysis of colloidal NC ligands for more than 20 years. A few initial studies used diffusion ordered spectroscopy (DOSY) to distinguish free from bound ligands and obtain information on the binding of ligands to nanocrystals. [12,13] Nuclear Overhauser effect spectroscopy (NOESY) enabled nanocrystal-ligand interactions to be identified, even with ligands involve in a fast adsorption/ desorption equilibrium.[14] To date, various research groups tried to study the composition of the ligand shell,[15,16,17] analyze the binding between ligands and nanocrystals, [18,19,20,21,22,23]and determine the relative binding strength of different ligands.[24,25] However to the best of our knowledge, there are only a few reports on NOESY characterization of Janus gold nanoparticles, [26,27] NOESY study of mixed Polystyrene/Poly(methyl methacrylate) ligand shell distribution,[28]and morphology determination of gold nanoparticle ligand-shell using 2D NMR.[29]

Quantum dot valency

Nanoparticles labeled with a discrete and controlled number of conjugated ligands are desirable for many purposes. Semiconductor nanoparticles decorated with specific numbers of DNA, streptavidin or antibodies, mimicking valence-dictated molecular self-assembly behaviors, have been successfully used to address a variety of biological applications such as implying the position of single proteins within membranes[30,31,32] and/or visualizing the structure of artificially created nano assemblies. [33,34] Thus, one key issue for some quantum dot applications is the ability to control the number of bio-molecules bound to each nanoparticle. By exactly controlling the number of binding sites

per nanoparticle we can preclude undesirable crosslinking, which can ultimately lead to agglomeration. However, tunable nanocrystal surface functionalization and programmable nano-assembly still remain a challenge. Most of the investigations on controlling the degree of nanocrystal surface functionalization or "valence" had been done on DNA-mediated assemblies of gold nanoparticles.[35,36,37,38,39] Consequently, the resulting assembly's size and composition was defined and demonstrated by gel electrophoresis and TEM techniques.[40,41] To the best of our knowledge we are among the first research groups that synthesize and investigate controlled steroid-mediated quantum dots and study the surface loading effect on affinity of dots toward synthetic lipid bilayers.

Thesis Organization

This thesis is comprised of a new approach to synthesis and surface modifications of semiconductor nanocrystal quantum dots. As the thesis encompasses a diverse range of topics, relevant literature is reviewed in the introduction of each chapter to provide an adequate understanding of the background and significance of the results. Chapter 2 contains material that has already been published and introduces the new approach to one pot synthesis of CdS dots using a single source precursor and mixture of active surfactants. This approach bypasses ligand exchange and introduces controlled number of active native ligands onto the quantum dots surfaces. This chapter also investigates surface ligand orientation and distribution employing advanced two-dimension NMR spectroscopy. Chapter 3 discusses the inorganic-organic-medium interface in colloidal quantum dots and analyses effect of chain length and ligand microstructure on distribution and packing of surface ligands. It also reveals the impact of surface ligand

organization on chemical reactivity of CdS quantum dots. Chapter 4 shows controlled surface decoration of highly fluorescent core-shell CdSe/CdS quantum dots with a series of synthetic steroid conjugated polyethylene glycol ligands, and investigates affinity of such steroid-conjugated quantum dots toward synthetic lipid bilayers. The cholestanone-modified QDs interaction with a lipid bilayer was studied using a homebuilt prism-based total internal reflection fluorescence (TIRF) microscope, performed by Dr. Kyle Marchuk at Iowa State University. Chapter 5 shows synthesis of multifunctional multidentate copolymer via Acyclic Diene Metathesis (ADMET) with controlled chain length and functionality. The synthesized copolymer acts as a linkage to generate nanocrystaline hetero-conjugates. Chapter 6 summarizes the contributions of this work and recommends further investigations for future work.

References

[1] Hyun, B. R.; Chen, H. Y.; Rey, D. A.; Wise, F. W.; Batt, C. A. *J. Phys. Chem. B* **2007**, *111*, 5726–5730.

[2] Hens, Z.; Tallapin, D. V.; Weller, H.; Vanmaekelbergh, D. *Appl. Phys. Lett.* **2002**, *81*, 4245–4247.

[3] Breus, V. V.; Heyes, C. D.; Nienhaus, G. U. *J. Phys. Chem.* C **2007**, *111*, 18589–18594.

[4] Kloepfer, J. A.; Bradforth, S. E.; Nadeau, J. L. *J. Phys. Chem. B* **2005**, *109*, 9996–10003.

[5] Kalyuzhny G., Murray, R. W. *J. Phys. Chem. B*, **2005,** *109*, 7012–7021.

[6] Bullen, C.; Mulvaney, P. *Langmuir* **2006**, *22*, 3007–3013.

[7] Wuister, S. F.; de Mello Donega, C.; Meijerink, A. *J. Phys. Chem. B*, **2004**, *108*, 17393–17397.

[8] Holt, B.; Kudera, S.; Weiss, A.; Schrader, T. E.; Manna, L.; Parak, W. J.; Braun, M. *J. Mater. Chem.* **2008**, *18*, 2728–2732.

[9] Jasieniak, J.; Mulvaney, P. *J. Am. Chem. Soc*. **2007**, *129*, 2841–2848.

[10] Koole, R.; Schapotschnikow, P.; Donega, C. d. M.; Vlugt, T. J. H.; Meijerink, A. *ACS Nano* **2008**, *2*, 1703–1714.

[11] Lobo, A.; Moller, T.; Nagel, M.; Borchert, H.; Hickey, S.; Weller, H. *J. Phys. Chem. B* **2005**, *109*, 17422–17428.

[12] Sachleben, J.; Wooten, E.; Emsley, L.; Pines, A.; Colvin, V.; Alivisatos, A. *Chem. Phys. Lett.* **1992**, *198*, 431–436.

[13] Kohlmann, O.; Steinmetz, W.; Mao, X.; Wuelfing, W.; Templeton, A.; Murray, R.; Johnson, C. *J. Phys. Chem. B* **2001**, *105*, 8801–8809.

[14] Fritzinger, B.; Moreels, I.; Lommens, P.; Koole, R.; Hens, Z.; Martins, J. C. *J. Am. Chem. Soc.* **2009**, *131*, 3024–3032.

[15] Moreels, I.; Fritzinger, B.; Martins, J. C.; Hens, Z. *J. Am. Chem. Soc.* **2008**, *130*, 15081–15086.

[16] Cros-Gagneux, A.; Delpech, F.; Nayral, C.; Cornejo, A.; Coppel, Y.; Chaudret, B. *J. Am. Chem. Soc.* **2010**, *132*, 18147–18157.

[17] Moreels, I.; Justo, Y.; De Geyter, B.; Haustraete, K.; Martins, J. C.; Hens, Z. *ACS Nano* **2011**, *5*, 2004–2012.

[18] Hassinen, A.; Moreels, I.; Donega, C. d. M.; Martins, J. C.; Hens, Z. *J. Phys. Chem. Lett.* **2010**, *1*, 2577–2581.

[19] Fritzinger, B.; Capek, R. K.; Lambert, K.; Martins, J. C.; Hens, Z. *J. Am. Chem. Soc*. **2010**, *132*, 10195–10201.

[20] Donakowski, M. D.; Godbe, J. M.; Sknepnek, R.; Knowles, K. E.; de la Cruz, M. O.; Weiss, E. A. *J. Phys. Chem. C* **2010**, *114*, 22526–22534.

[21] Wallner, A.; Jafri, S. H. M.; Blom, T.; Gogoll, A.; Leifer, K.; Baumgartner, J.; Ottosson, H. *Langmuir* **2011**, *27*, 9057–9067.

[22] Hughes, B. K.; Ruddy, D. A.; Blackburn, J. L.; Smith, D. K.; Bergren, M. R.; Nozik, A. J.; Johnson, J. C.; Beard, M. C. *ACS Nano* **2012**, *6*, 5498–5506.

[23] Coppel, Y.; Spataro, G.; Pages, C.; Chaudret, B.; Maisonnat, A.; Kahn, M. L. *Chem. A Eur. J.* **2012**, *18*, 5384–5393.

[24] Gomes, R.; Hassinen, A.; Szczygiel, A.; Zhao, Q.; Vantomme, A.; Martins, J. C.; Hens, Z. *J. Phys. Chem. Lett.* **2011**, *2*, 145–152.

[25] Hens, Z.; Martins, J. C. *Chem. Mater.* **2013**, *25*, 1211–1221.

[26] Chen, S.; Song, Y. *Chem. Asian J.* **2014**, *9*, 418–430.

[27] Pradhan, S.; Brown, L. E.; Konopelski, J. P.; Chen, S. *J. Nanopart. Res.* **2009,** *11*, 1895–1903.

[28] Guo, Y.; Moffitt, M. G. *Macromolecules* **2007**, *40*, 5868–5878.

[29] Liu, X.; Yu, M.; Kim, H.; Mameli, M.; Stellacci, F. *Nature Commun.* **2012**, 3.

[30] M. Dahan, S. Levi, C. Luccardini, P. Rostaing, B. Riveau, A. Triller, *Science* **2003**, *302*, 442–445.

[31] F. Pinaud, D. King, H.-P. Moore, S. Weiss, *J. Am. Chem. Soc.* **2004**, *126*, 6115–6123.

[32] L. Cognet, C. Tardin, D. Boyer, D. Choquet, P. Tamarat, B. Lounis, *Proc. Natl. Acad. Sci. USA* **2003**, *100*, 11–350.

[33] S. Xiao, F. Liu, A. E. Rosen, J. F. Hainfeld, N. C. Seeman, K. Musier- Forsyth, R. A. Kiel, *J. Nanopart. Res*. **2002**, *4*, 313–317.

[34] S. Beyer, P. Nickels, F. C. Simmel, *Nano Lett*. **2005**, *5*, 719–722.

[35] Suzuki, K.; Hosokawa, K.; Maeda, M. *J. Am. Chem. Soc.* **2009,** *131*, 7518–7519.

[36] Borovok, N.; Gillon, E.; Kotlyar, A. *Bioconj. Chem.* **2012**, *23*, 916–922.

[37] Zhao, W.; Hsing, I. M. *Chem. Commun.* **2010,** *46*, 1314–1316.

[38] Zheng, Y.; Li, Y.; Deng, Z. *Chem. Commun.* **2012,** *48*, 6160–6162.

[39] Pierrat, S.; Zins, I.; Breivogel, A.; Soennichsen, C. *Nano Letters* **2007,** *7*, 259–263.

[40] Sperling, R. A.; Pellegrino, T.; Li, J. K.; Chang, W. H.; Parak, W. J. *Adv. Funct. Mater.* **2006,** *16*, 943–948.

[41] Zanchet, D.; Micheel, C. M.; Parak, W. J.; Gerion, D.; Alivisatos, A. P. *Nano Letters* **2001,** *1*, 32–35.

CHAPTER 2

SURFACE DOPING QUANTUM DOTS WITH CHEMICALLY-ACTIVE NATIVE LIGANDS: CONTROLLING VALANCE WITHOUT LIGAND EXCHANGE

Reprinted with permission form *Chem. Mater.* **2012**, *24*, 4231

Elham Tavasoli, Yijun Guo, Pranaw Kunal, Javier Grajeda, Allison Gerber, Javier Vela

Abstract

Colloidal semiconductor nanocrystals have generated great enthusiasm and found applications in biological imaging, tracking, lighting, photovoltaics, photocatalysis, thermoelectrics, lasing and spintronics. One remaining challenge is learning to control the degree of functionalization or "valency" per nanocrystal. Current quantum dot surface modification strategies rely heavily on ligand exchange, which consists of replacing the nanocrystal's native ligands with carboxylate- or amine-terminated thiols, usually added in excess. Removing the nanocrystal's native ligands can cause etching and introduce surface defects, thus affecting the nanocrystal's optical properties. More importantly, ligand methods fail to control the extent of surface modification or number of functional groups introduced per nanocrystal. Here, we report a fundamentally new surface ligand modification or "doping" approach aimed at controlling the degree of functionalization or valency per nanocrystal while retaining the nanocrystal's original colloidal and photo-stability. We show that surface doped quantum dots capped with chemically-active native ligands can be prepared directly from a mixture of ligands with similar chain lengths. Specifically, vinyl and azide-terminated carboxylic acid ligands survive the high temperatures needed for

nanocrystal synthesis. The ratio between chemically-active and inactive-terminated ligands is maintained on the nanocrystal surface, allowing to control the extent of surface modification by straightforward organic reactions. Using a combination of optical and structural characterization tools, including IR and 2D NMR, we show that carboxylates bind in a bidentate chelate fashion, forming a single monolayer that is perpendicular to the nanocrystal surface. Moreover, we show that mixtures of ligands with similar chain lengths homogeneously distribute themselves on the nanocrystal surface. We expect this new surface doping approach will be widely applicable to other nanocrystal compositions and morphologies, as well as to many specific applications in biology and materials science.

Introduction

Colloidal semiconductor nanocrystal quantum dots, rods, wires[1-4] have found applications in biological imaging,[5-8] tracking,[9-12] lighting,[13-14] photovoltaics,[15] photocatalysis,[16] thermoelectrics,[17] lasing[18] and spintronics.[19] These highly versatile photoactive nanocrystals are well known to benefit from size- and composition-tunable band gaps (300-4000 nm; 4.1-0.3 eV),[1-2,20] broad and intense absorption ($\varepsilon \approx 10^6$ $L \cdot mol^{-1} \cdot cm^{-1}$),[21-22] long-lived excitons (up to 40 ns for CdSe, 500 ns for $CuInS_2$, and 1.8 μs for PbS),[23-24] and good colloidal, chemical and photo stability.[25-27] One remaining challenge in the field of colloidal semiconductor nanocrystals is learning to control the degree of functionalization per nanocrystal, also known as nanocrystal loading or "valency".

The state-of-the-art in quantum dot surface ligand modification includes thiol ligand exchange and the use of biological building blocks. Thiol ligand exchange consists of replacing the nanocrystal's "native" ligands with carboxylate- or amine-terminated thiols, usually added in excess (Scheme 1). The carboxylate or amine groups are then modified

through amidation or layer-by-layer (LBL) ionic pairing. This procedure is well established for soft nanocrystal surfaces with high affinity toward soft "polarizable" thiol ligands.[28] Its use is widespread for II-VI and IV-VI semiconductors such as zinc, cadmium, and mercury-chalcogenides. Biological building blocks have been explored extensively as alternatives for nanocrystal surface modification. The most often used procedure exploits strong binding between streptavidin and biotin.[29-30] One end of the streptavidin–biotin pair is attached to the nanocrystal surface and the other end is covalently or non-covalently attached to a molecule or material of interest. Alternative inorganic modification methods were recently introduced to incorporate functionality onto nanocrystal surfaces. Inorganic ligand exchange with complex anions such as $Sn_2S_6^{4-}$ produces compact nanocrystals with improved carrier mobility or "hopping" across nanocrystal solids.[31] These small ligands improve inter-particle coupling by removing insulating organic ligands.[31-32]

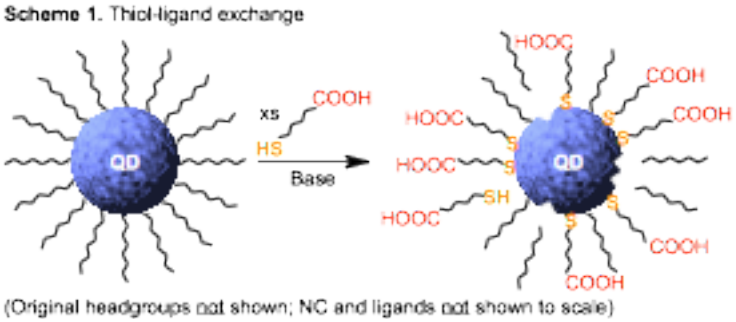

Each one of these known methods has limitations. Thiol ligand exchange does not work well for transition metal oxides, nitrides or other "hard" nanocrystal surfaces.[28] More importantly, ligand exchange removes the nanocrystal's native ligands, i.e., those that originate from its synthesis; this can cause etching and introduce surface defects, affecting

the nanocrystal's optical properties.[33] Biological building blocks require milder reaction conditions but often involve lengthy multistep syntheses on tiny amounts of expensive materials; and their large footprint and thermal instability result in low-surface coverage and chemical incompatibility. Critically, the most important limitation of these methods is their inability to control the extent of surface modification or number of functional groups (valency) introduced per nanocrystal. Here, we report a fundamentally new surface ligand modification or "doping" approach aimed at controlling the degree of functionalization or valency per nanocrystal while retaining the nanocrystal's original colloidal and photo-stability. We also report what changes in ligand organization, surface chemistry and overall nanocrystal properties arise as a result of this approach.

Experimental

Materials. Decanoic acid (≥98%), 9-decenoic acid (≥90%), n-decyl alcohol (99%), potassium ethyl xanthate (96%), and potassium tertiary butoxide (t-BuOK) (95%), N,N,N′,N″,N″-pentamethyldiethylenetriamine (PMDETA) (99%), and Grubbs 2nd generation Ru metathesis catalyst were purchased from Aldrich. 10-Bromodecanoic acid (95%) was purchased from Matrix Scientific, cadmium chloride (anhydrous, 99.995%) from Strem, 9-decen-1-ol (>90%) from AlfaAesar, phenyl ether (Ph_2O) (99%) and 4-(trifluoromethyl) styrene (>98%) from Acros, 10-bromodecan1-ol (95%) from ChemSampCo, carbon disulfide (CS_2) from Fisher, 3-fluorophenylacetylene (98%) from SynQuest, and chloro(1,5-cyclooctadiene)(pentamethyl-cyclopentadienyl)ruthenium(II) ($RuClCp^*(COD)_2$) (98%) from Strem. Methanol, chloroform, tetrahydrofuran (THF), and diethyl ether were purchased from Fisher and used as received. Chloroform-*d* ($CDCl_3$), dichloromethane-d_2 (CD_2Cl_2), and dimethylsulfoxide-d_6 (DMSO-d_6) were purchased from Cambridge Isotopes Labs. 10-

Azidodecanoic acid and 10-azidodecanol were synthesized following reported procedures.[34] ^{1}H NMR chemical shifts (δ) are reported in ppm relative to residual protiated solvent in $CDCl_3$ (7.26 ppm) or DMSO-d_6 (2.50 ppm). Elemental analyses were performed by Galbraith Laboratories.

Synthesis of xanthate precursors. Xanthate precursors were prepared by modified literature procedures.[35-36] *Potassium C10 xanthates.* The linear C10 alcohol (5.32 g for n-decyl alcohol or 5.26 g for 9-decen-1-ol or 6.70 g for 10-azidodecan-1-ol; 33.6 mmol) was added dropwise to a solution of t-BuOK (3.43 g, 30.6 mmol) in anhydrous THF (100 mL) at 0° C under dry N_2. CS_2 (2.0 mL, 33.6 mmol) was added dropwise via syringe. The solution was stirred for 4 h at 0 °C under dry N_2, then diluted with diethyl ether (500 mL) causing formation of a precipitate. The white precipitate was collected by suction filtration, washed twice with diethyl ether and dried under vacuum (88%–94% yield). Potassium decyl-xanthate: ^{1}H NMR (400 MHz, DMSO-d_6): δ 4.15 (t, 2H, α-CH_2, J_{HH} = 6 Hz), 1.56 (m, 2H, β-CH_2), 1.25 (br, 14H, -CH_2-), 0.85 (t, 3H, -CH_3, J_{HH} = 6 Hz). Potassium 9-decenyl-xanthate: ^{1}H NMR (400 MHz, DMSO-d_6): δ 5.80 (m, 1H, -CH=), 4.92 (m, 2H, =CH_2), 4.60 (m, 2H, α-CH_2, J_{HH} = 6 Hz), 2.03 (m, 2H, allylic-CH_2), 1.55 (m, 2H, β-CH_2), 1.32 (br, 10H, -CH_2-). Potassium 10-azidodecyl-xanthate: ^{1}H NMR (400 MHz, $CDCl_3$): δ 3.60 (t, 2H, -CH_2-O), 3.23 (t, 2H, -CH_2-N_3), 1.55 (m, 2H, α-CH_2), 1.27 (m, 14H, -CH_2-). *Cadmium C10 xanthates.* A 0.1 M solution of cadmium chloride (2.70 g, 15.0 mmol in 150 mL H_2O) was added dropwise to a 0.05 M methanolic solution of potassium xanthate (8.03 g for decyl-xanthate or 7.96 g for 9-decenyl-xanthate or 9.23 g for 10-azidodecyl-xanthate; 29.46 mmol; 590 mL) while stirring vigorously, causing the formation of a precipitate. After stirring for 30 min under air, the mixture was centrifuged and the solid washed twice with a water/methanol

mixture (1:3 $^{v}/_{v}$) and once more with methanol. The resulting cadmium xanthate was dried under vacuum (76%–89% yield). Cadmium decyl-xanthate: ^{1}H NMR (400 MHz, $CDCl_3$): δ 4.46 (t, 2H, α-CH_2, J_{HH}= 8 Hz), 1.83 (t, 2H, β-CH_2, J_{HH} = 8 Hz), 1.27 (br, 14H, -CH_2-), 0.88 (t, 3H, -CH_3, J_{HH} = 8 Hz). Anal. Calcd. for $C_{22}H_{42}CdO_2S_4$: C, 45.62; S, 22.14; Cd, 19.41; H, 7.31. Found: C, 43.50; S, 21.90; Cd, 17.50; H, 7.14. Cadmium 9-decenyl-xanthate: ^{1}H NMR (400 MHz, $CDCl_3$): δ 5.80 (m, 1H, -CH=), 4.92 (m, 2H, =CH_2), 4.45 (t, 2H, α-CH_2, J_{HH} = 8 Hz), 2.03 (m, 2H, allylic-CH_2), 1.82 (m, 2H, β-CH_2), 1.30 (m, 10H, -CH_2-). Anal. Calcd. for $C_{22}H_{38}CdO_2S_4$: C, 45.94; S, 22.30; Cd, 19.54; H, 6.66. Found: C, 44.74; S, 22.20; Cd, 20.50; H, 6.64. Cadmium 10-azidodecyl-xanthate: ^{1}H NMR (400 MHz, $CDCl_3$): δ 4.46 (t, 2H, -CH_2-O), 3.26 (t, 2H, -CH_2-N_3), 1.83 (m, 2H, β-CH_2-O), 1.54 (m, 2H, β-CH_2-N_3), 1.30 (m, 12H, -CH_2-).

Synthesis of surface doped cadmium sulfide quantum dots. A mixture of cadmium C10 xanthate (170 mg, 0.290 mmol), Ph_2O (1.80 g), and carboxylic acid ligand (1.02 g, 5.92 mmol for decanoic acid; 1.03 g, 5.91 mmol for 9-decenoic acid; 0.63 g, 2.96 mmol for 10-azidodecanoic acid) were weighed onto a three-neck, 250 mL round bottom flask and sonicated for 30 min. The flask was then fitted with a Teflon-coated stir bar, a condenser, and attached to a Schlenk line. The mixture was degassed for 20 min at room temperature (R.T.), refilled with dry Ar, placed into a pre-equilibrated oil bath at 130 °C and kept at this temperature while stirring for 15 minutes. The oil bath was removed and the mixture allowed to cool down to R.T. After dilution with chloroform (5 mL), nanocrystals were isolated by adding a minimum amount of chilled methanol followed by centrifugation (5000 rpm for 10 min). After re-dissolution in toluene or hexane, precipitation was repeated to remove excess Ph_2O and ligand. Nanocrystals were dried under dynamic vacuum for 2 h. This method was

used to prepare mixed ligand nanocrystals while keeping a 1:10 Cd-to-ligands molar ratio. *Excess ligand recycling.* Concentration of the first supernatant under vacuum allowed us to recover 70-90% of the excess carboxylic acid ligand along with Ph_2O. This ligand/solvent mixture could be re-used up to three times for the synthesis of new nanocrystals.

Surface modification of surface doped CdS quantum dots. *Ru catalyzed click.* 3-Fluorophenyl acetylene was added to a 2 mL THF solution of 10-azido-decanoic acid capped CdS quantum dots in a 1:1 ratio (monitored by ^{1}H NMR). The solution was degassed and taken into the glovebox, where a 0.008 M stock solution of Cp*RuCl(COD) was added to the mixture while stirring. The reaction was further stirred at 50 °C in the absence of light for 24 h. After dilution with chloroform (2 mL), nanocrystals were isolated by adding a minimum amount of chilled methanol followed by centrifugation (5000 rpm for 10 min). *Ru catalyzed metathesis.* 1,4-Trimethylfluoro-styrene (40.0 mg, 230 μmol), Grubb's 2nd generation catalyst (4.0 mg, 4.71 μmol) and CD_2Cl_2 (0.5 mL) were weighed onto a Schlenk tube containing ca. 10-20 mg of dry 9-decenyl capped CdS quantum dots. The mixture was freeze-pump-thawed three times, and allowed to stir at R.T. for 5 h. Nanocrystals were isolated by adding a minimum amount of a chilled methanol and acetone mixture followed by centrifugation (5000 rpm for 10 min).

Structural Characterization. *X-Ray Diffraction*. Powder X-ray diffraction (XRD) was measured using Cu Kα radiation on a Scintag XDS-2000 diffractometer. *Transmission Electron Microscopy*. TEM was conducted on carbon-coated copper grids using an FEI Tecnai G2 F20 field emission scanning transmission electron microscope (STEM) at 200 kV (point-to-point resolution <0.25 nm, line-to-line resolution <0.10 nm). Elemental composition was characterized by energy-dispersive spectroscopy (EDS). *Particle Analysis*.

Dimensions were measured manually or with ImageJ for >50-100 particles. Averages are reported ± standard deviations.

Optical Characterization. *Absorption spectra* were measured with a photodiode-array Agilent 8453 UV-Vis spectrophotometer. Solvent absorption was recorded and subtracted from all spectra. *Steady-state photoluminescence* (PL) spectra were measured with a Horiba-Jobin Yvon Nanolog scanning spectrofluorometer equipped with a photomultiplier detector. Nanocrystal quantum dots were diluted in chloroform to give an optical density of 0.05-0.2 at 390 nm. Excitation wavelength was 350 nm, and emission was recorded between 365 and 685 nm. *Vibrational infrared spectra* were recorded with a Bruker IFS66V FT-IR spectrometer equipped with a DTGS detector with 64 scans at a resolution of 4 cm^{-1}. The samples were prepared either as dropcast thin films on KBr plates or diluted with KBr and pressed onto a pellet. Background spectra were collected under identical conditions. Samples were continuously purged with dry N_2 to minimize water vapor absorbance.

NMR Characterization. *^{1}H NMR*. ^{1}H NMR spectra were carried out in a Varian 400MR spectrometer operating at a ^{1}H frequency of 399.80 MHz. Spectra were recorded using standard pulse sequences from VNMRJ 3.1 pulse program library. ^{1}H NMR spectra (64 scans) were recorded with a relaxation delay (d_1) between scans of 2 s for free ligands and 10 s for surface-bound ligands to allow full relaxation of all ^{1}H nuclei. Single-pulse ^{1}H spin-lattice relaxation measurements (10 scans) were recorded with a pulse width of 156 μs and a recycle delay of 10 s. *DOSY*. Diffusion Ordered Spectroscopy (DOSY) experiments were collected using a Bruker DRX 400 spectrometer operating at a ^{1}H frequency of 400.39 MHz equipped with normal geometry probe. Spectra were recorded using standard pulse sequences from TopSpin 1.3 pulse program library. The duration of the magnetic field pulse gradients

(δ) was optimized for each diffusion time (Δ) to obtain a signal decay of roughly 90% at the maximum gradient strength. A series of 16 spectra with 32,768 data points in each spectrum were collected. In each pulsed-field gradient NMR experiment, the value of δ was set to 3.6 ms, and the value of Δ (diffusion time) was set to 600 ms. The gradient strength was varied from 2 to 95% (space) of the maximum strength using a sine gradient shape. *ROESY.* Rotating-frame Overhauser Effect Spectroscopy (ROESY) experiments were recorded using an Avance III 600 spectrometer operating a ^{1}H frequency of 600.39 MHz equipped with 5 mm BBFO Smart Probe. Spectra were recorded using standard pulse sequences from TopSpin 3.0 pulse program library. ROESY spectra were collected using a spin lock time of 200 ms and 256 t_1 increments, with each t_1 slice consisting of 36 scans of 2048 sampled data points, each recorded with a 2 s relaxation delay.

Results and Discussion

In view of the problems and limitations commonly associated with quantum dot surface modification by thiol ligand exchange and similar methods, we investigated the synthesis of nanocrystals capped with *chemically-active native ligands*. Our first question was whether such "surface doped" nanocrystals could actually be made, NOT by ligand exchange as it has been done routinely and repeatedly in the past, but by direct nanocrystal synthesis in the presence of two (or more) different capping ligands. For example, one ligand may contain a chemically-active, terminally unsaturated group such as a vinyl (-CH=CH_2) or azide (-N_3); another ligand may be completely saturated (aliphatic), and end with a methyl (-CH_3) (Scheme 2). If such mixed-ligand nanocrystals could be made directly, this would solve two important problems: (1) Simply varying the active-to-inactive ligand ratio used during nanocrystal synthesis (x-to-y in Scheme 2a) would allow us to control the number of

chemically-active groups, and thus control the amount or degree of functionality (valency) that could be introduced per nanocrystal; and (2) surface modification could then be easily accomplished by direct reaction of the chemically-active, unsaturated groups *without resorting to ligand exchange*[37] (A-to-C transformation in Scheme 2b).

Scheme 2. Synthesis and direct modification of quantum dots capped with **chemically-active native ligands** (A)

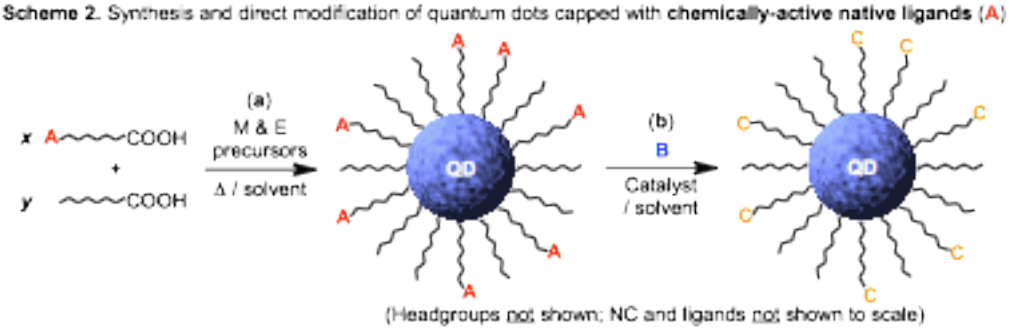

(Headgroups not shown; NC and ligands not shown to scale)

Synthesis of surface doped quantum dots. To test the feasibility of this concept, we prepared as models ca. 2 nm diameter, zinc-blende (cubic) CdS quantum dots using cadmium xanthate single source precursors.[35,38-40] In the presence of 10-20 equivalents of commercially available, ten-carbon-long (C10) carboxylic acids, the cadmium xanthate precursors decompose cleanly at 120-140°C to give C10 carboxylate-capped CdS nanocrystals (Figure 1). IR and NMR analyses reveal that the organic group in the xanthate precursor does not compete with the 10-20 equivalents of extra added carboxylate ligand for binding to the nanocrystal surface (Figures 2 and 3). The asymmetric carboxylate stretching frequency, $\nu_{as}(COO^-)$ shifts from 1700 cm^{-1} in the free ligands to 1540 cm^{-1} in the surface-bound ligands; while the symmetric carboxylate stretching frequency, $\nu_s(COO^-)$ remains unchanged at ca. 1410 cm^{-1} in both free and surface-bound ligands (Figure 2). In other words, the difference between asymmetric and symmetric carboxylate stretching frequencies,

$\nu_{as}(COO^-) - \nu_s(COO^-)$, decreases from 290 cm^{-1} in the free ligands to only 130 cm^{-1} in the surface-bound ligands. This is consistent with bidentate (chelate) coordination of carboxylate groups to surface cadmium ions on all nanocrystals.[41] This is true even for azide-capped nanocrystals, where the IR spectrum clearly indicates that there is no azide ($-N_3$) binding to the nanocrystal surface. In both free and surface-bound ligands, the asymmetric and symmetric azide stretching frequencies, $\nu_{as}(N_3)$ and $\nu_s(N_3)$, remain unchanged at 2090 cm^{-1} and 1250 cm^{-1}, respectively (Figure 2c).[42]

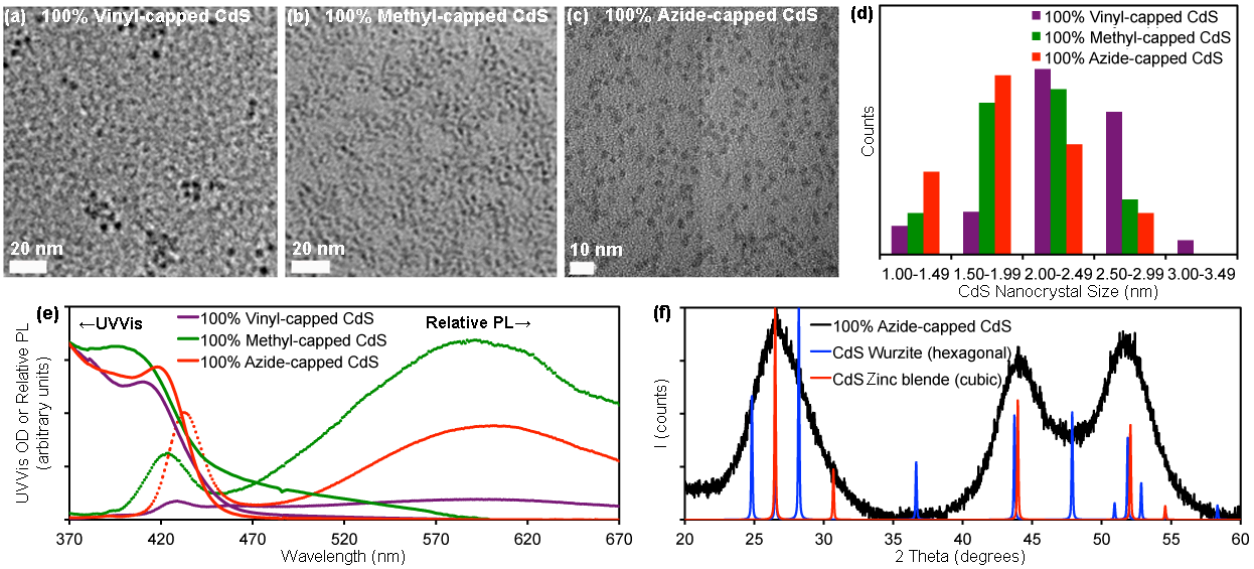

Figure 1. Representative TEM images, particle size histograms, optical spectra (UV-Vis/PL) and XRD pattern of CdS quantum dots capped with vinyl, methyl, and azide-terminated C10 carboxylate ligands.

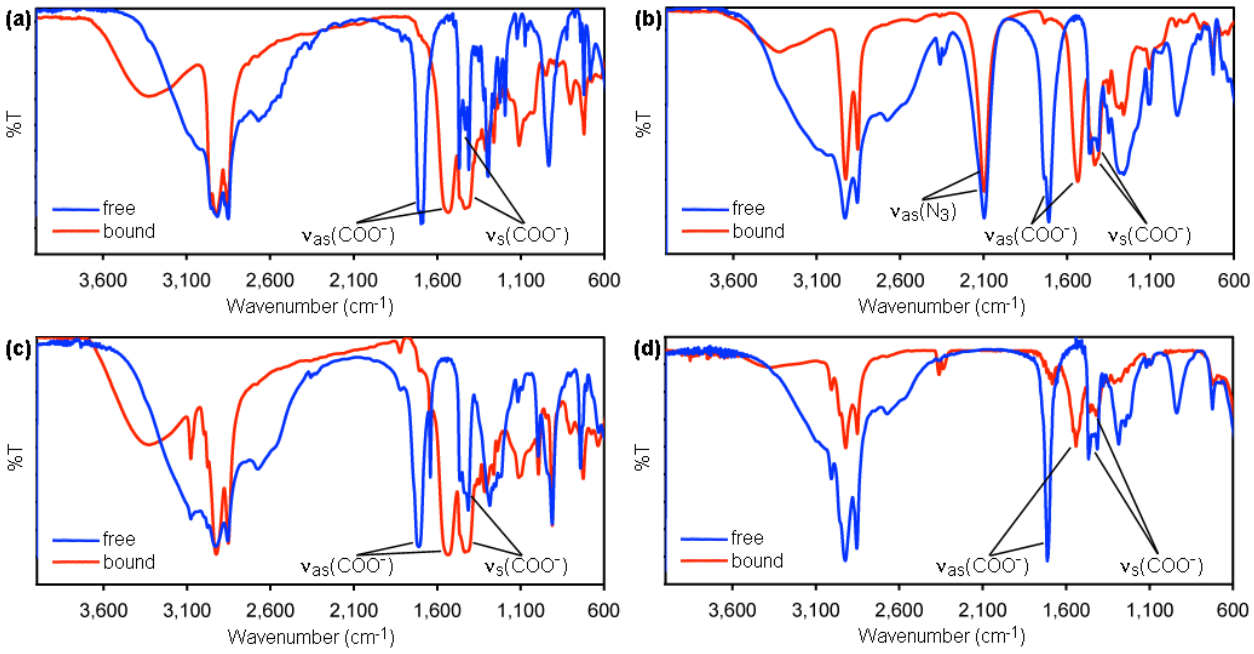

Figure 2. Infrared spectra of free (blue) and CdS surface-bound (red) decanoic acid (a), 9-decenoic acid (b), and 10-azide-decanoic acid (c). Oleic acid (blue) and bis(oleate)cadmium (red) are shown for comparison (d). Labels show key asymmetric (ν_{as}) and symmetric (ν_s) stretching frequencies. The broad peak at 3360 cm^{-1} arises from trace leftover moisture in some of the samples.

The formation of surface doped CdS nanocrystals proceeds equally well in either 1-octadecene (ODE) or phenyl ether (Ph_2O) as solvent. However, the olefinic resonances in ODE make it difficult to distinguish whether double bond resonances observed by NMR arise either from capping ligands or from residual ODE solvent. In contrast, unlike ODE, Ph_2O lacks isolated double bonds, facilitating unambiguous assignment of olefinic (double bond) NMR resonances.[43] To illustrate why this is important, we questioned whether ligands containing chemically-active groups such as vinyl or azide could survive the high temperatures needed for nanocrystal synthesis. We were particularly concerned that terminal double bonds in vinyl-terminated ligands could isomerize to thermodynamically more stable internal double bonds at high temperature during nanocrystal synthesis.[43] It was difficult to

answer this question when we used 1-octadecene (ODE) as solvent because, even after two washes by crashing and centrifugation, CdS nanocrystals showed internal double bonds from trace amounts of ODE as judged by their characteristic ^{1}H NMR multiplet (m) resonance at δ 5.5 ppm. In contrast, when we used Ph_2O as solvent, CdS nanocrystals did not contain internal double bonds regardless of the number of washes, allowing us to conclude that vinyl group isomerization does not occur during nanocrystal synthesis. Only terminal double bonds from vinyl-terminated ligands were observed on CdS nanocrystals made in Ph_2O by ^{1}H NMR at δ 5.9 ppm (m) and 5.0 ppm (m) (Figure 3).

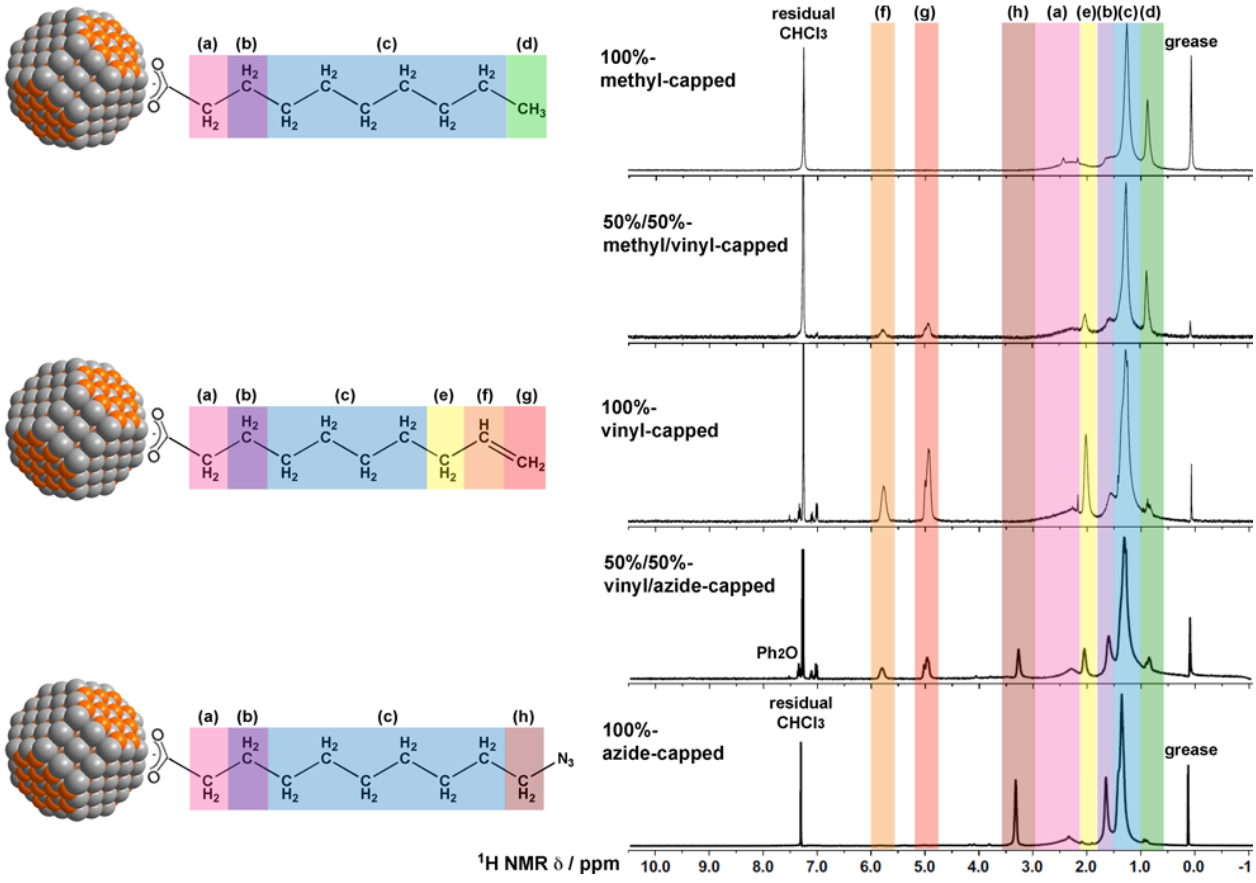

Figure 3. ^{1}H NMR spectra of CdS nanocrystal quantum dots capped with mixtures of methyl (-CH_3), vinyl (-$CH{=}CH_2$) and azide (-N_3) terminated C10 carboxylate ligands. Relative

surface ligand populations are proportional to the relative ligand concentrations used during nanocrystal synthesis.

Using this direct synthesis method and without resorting to ligand exchange, we prepared as test models surface doped CdS quantum dots capped with methyl- (saturated), vinyl- (unsaturated) and azide-terminated C10 ligands, as well as with mixtures of these (Figures 1, 2 and 3). The resulting colloidal CdS nanocrystals are highly soluble in chloroform, toluene and hexane. After careful purification by cold acetone- or methanol-induced precipitation ("crashing") and centrifugation to remove excess ligands, we observe NMR resonances predominantly from surface-bound ligands and not from free ligands,[44] along with a few weak NMR resonances from trace amount of synthesis solvent (Ph_2O, Figure 3). As predicted, the relative population of the different surface ligands is proportional to the relative ligand concentrations used during nanocrystal synthesis (Figure 3). Several unique and key features allow us to distinguish surface-bound ligands from free ligands by NMR: (1) First, resonances from surface-bound ligands are characteristically broadened (Figure 3); (2) second, resonances from surface-bound ligands show faster ^1H NMR T_1 relaxation times compared to those from free ligands (Figure 4); and (3) third, Diffusion Ordered Spectroscopy (DOSY) (below) shows resonances from surface-bound ligands have very slow diffusion rates that are about one order of magnitude slower (one-tenth) compared to resonances from free ligands and trace solvent, unambiguously demonstrating that after two washes and centrifugation we completely or nearly completely (>99%) removed free or excess ligands. We believe effects (1) and (2) are a manifestation of the same phenomenon, namely the close proximity of surface-bound ligand protons to unpaired electrons localized on surface trap states. The NMR peak width ($\nu_{1/2}$) is inversely proportional to the spin-lattice

or "longitudinal" T_1 relaxation time according to Heisenberg's uncertainty principle: $\nu_{1/2} = 1 / (\pi \cdot T_1)$. Semiconductor nanocrystals are strong light absorbers ($\varepsilon \approx 10^6$ $L \cdot mol^{-1} \cdot cm^{-1}$),[21-22] become red-ox-active upon illumination even under ambient light, and remain red-ox-active after dark-storage for several hours.[45] Photo-generated charge carriers are known to localize on surface defects or "dangling bonds" (unpassivated ions) on the nanocrystal surface. Thus, ^{1}H NMR peak broadening does not arise from fast equilibration between surface-bound and free ligands.[46-50] Instead, surface-trapped electrons behave as paramagnetic impurities on the CdS nanocrystal inorganic-organic ligand interface, leading to the observed fast ^{1}H NMR T_1 relaxation times and consequent broadening of surface-bound ligand resonances (Figure 5). Interestingly, the extent of peak broadening ($\nu_{1/2}$) and T_1 relaxation time shortening correlates with the nanocrystal's optical properties. Specifically, the ratio between band-edge photoluminescence (PL) and "surface" trap PL intensity increases as the density of paramagnetic impurities decreases (Figures 1e and 4). This suggests that detailed ^{1}H NMR measurements may be a useful way to measure the amount of paramagnetic impurities, and thus the density of surface defects in colloidal semiconductor nanocrystals (quantum dots, rods, wires).[49,51-53]

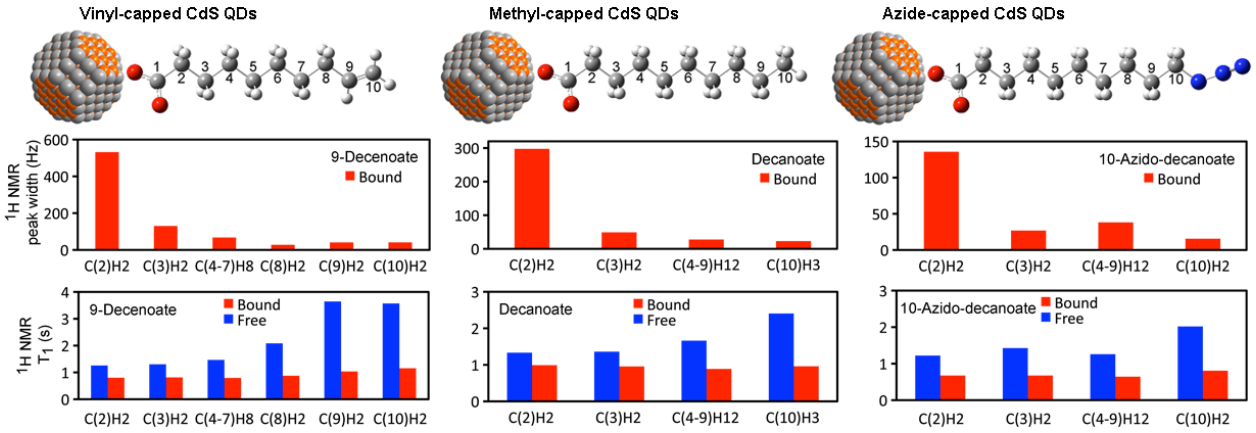

Figure 4. ^{1}H NMR peak widths ($\nu_{1/2}$) and T_1 relaxation times of CdS nanocrystal quantum dots capped with methyl (-CH_3), vinyl (-$CH{=}CH_2$) and azide (-N_3) terminated C10 carboxylate ligands.

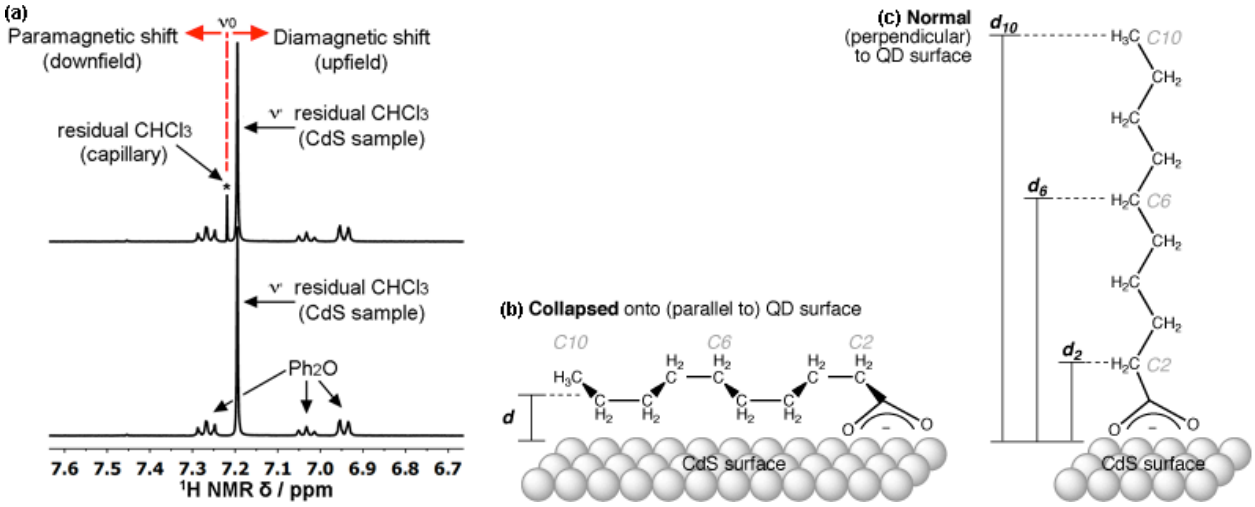

Figure 5. Assessing paramagnetic impurities by ^{1}H NMR (a) and surface ligand orientation (collapsed, b *vs.* normal to the surface, c) in surface doped CdS nanocrystal quantum dots.

Attempt to quantify paramagnetic impurities on the nanocrystal surface. We sought to collect further evidence for the presence of paramagnetic impurities on the nanocrystal surface by measuring the paramagnetic-susceptibility of our samples using the Evans method.[54-56] A solution phase NMR technique, the Evans method consists of measuring the change in chemical shift ($\Delta\nu = \nu' - \nu_0$) in the residual protiated solvent peak (ν_0) when exposed to a paramagnetic sample (ν_0). When compared to the pure solvent, usually contained in a sealed capillary within the same NMR tube, paramagnetism causes the solvent peak to move downfield (higher δ, $\nu_0 > 0$), whereas diamagnetism causes it to move upfield (lower δ, $\nu_0 < 0$) (Figure 5a). For small paramagnetic molecules, the solvent's and the sample's (χ^{dia}) diamagnetic susceptibilities are small or negligible, the paramagnetic susceptibility (χ^{p}) dominates, and the paramagnetic susceptibility can be easily calculated.

However, for large paramagnetic species such as supramolecular assemblies, biomolecules or nanoparticles, paramagnetism is often only a small contributor to the observed change in chemical shift (v_0). Indeed, we find that the diamagnetic susceptibility is the dominant contribution to the overall downfield shift (lower δ) observed for CdS quantum dots (Figure 5a). Reliable determination of the magnetic susceptibility of such large species requires independent determination of the much larger diamagnetic contribution, typically by using an appropriate diamagnetic model of comparable mass and density where the paramagnetic center has been removed, for example in metal-free supramolecular assemblies or apoproteins.[55] Unfortunately, we do not presently have such a model for CdS quantum dots. We are currently exploring EPR to characterize and quantify trapped unpaired electrons and other paramagnetic impurities on the nanocrystal surface.

Assessing ligand orientation and surface organization. We observed that the extent of ^1H NMR peak broadening varies significantly along the length of the capping ligands. Specifically, peak broadening ($\nu_{1/2}$) decreases and relaxation times (T_1) increase when going from the surface-bound carboxylate (COOH) head groups toward the tail end groups (Figure 3).[57] In all cases we measured, peak broadening is highest for the methylene protons ($C(2)H_2$) on the second carbon that is adjacent to the surface-binding carboxylic head group. Peak broadening then progressively decreases down the chain and is the lowest for the tenth carbon protons, namely the vinyl ($C(10)H_2$), methyl ($C(10)H_3$), and azide-adjacent-methylene protons ($C(10)H_2$) of unsaturated-, saturated-, and azide-terminated ligands, respectively. This is inconsistent with a scenario where ligands collapse onto the nanocrystal surface, because such arrangement would lead to more regular and less variable peak broadening among distinct protons along each ligand chain (Figure 5a).[58] In contrast, because

peak broadening actually decreases as the separation from the surface-bound head group increases, we conclude ligands orient themselves normal (perpendicular) to the nanocrystal surface to form a self-assembled monolayer (SAM) (Figure 5b).

Within this single ligand layer, two (or more) different ligands can assemble together to form islands or rafts of identical composition (Figure 6a), or they can mix together and distribute homogeneously (at random) on the nanocrystal surface (Figure 6b). This question has been the subject of intense research in plasmonic gold nanocrystals,[59-63] but it has not been addressed in semiconductor nanocrystals. Distinguishing between these two possible scenarios (rafts vs. mixing) is important in controlling quantum dot valency and assembly through surface ligand doping. To answer this question, we used Rotating-frame Overhauser Effect Spectroscopy (ROESY). A variant of Nuclear Overhauser Effect Spectroscopy (NOESY), ROESY is useful for intermediate-to-high molecular weight species (>1-3 kDa), for which the NOE can be hard to observe.[64-67] ROESY cross peaks have a sign opposite to that of the the diagonal (red in Figure 7), allowing easier distinction of through-space vs. through-bond correlations (black vs. red, respectively, Figure 7). ROESY spectra of carefully washed samples bearing only surface-bound ligands consistently show strong through-space hetero-correlations between dissimilar ligands for all mixed ligand samples we studied. For example, the ROESY spectrum of a 50%/50% methyl/vinyl-capped CdS quantum dot sample clearly shows through-space hetero-ligand coupling between the protons on the methyl end group ($C(10)H_3$) of the saturated ligand and the protons on the vinyl end group ($C(10)H_2$, C(9)H) as well as on the allylic position ($C(8)H_2$) of the unsaturated ligand (blue arrows in Figure 7). Similarly, the ROESY spectrum of a 50%/50% vinyl/azide-capped CdS quantum dot sample also shows through-space hetero-ligand coupling between the protons on the last

methylene ($C(10)H_2$) of the azide ligand and the protons on the vinyl end group ($C(10)H_2$, C(9)H) as well as on the allylic position ($C(8)H_2$) of the unsaturated ligand (blue arrows in Figure 7). Selective gradient-enhanced unidimensional (1D) ROESY experiments, where one particular proton resonance is pulsed while the others are allowed to relax, fully confirm these results (see Supporting Information). In all cases we studied, the experimentally observed through-space (NOE) hetero-ligand correlations are either stronger or at least as strong as the homo-ligand correlations, which can arise from within individual ligands (Figure 7). Therefore, we conclude that CdS nanocrystal quantum dots capped by a mixture of two different C10 carboxylates have a significant amount of random, homogeneous ligand distribution on their surface.

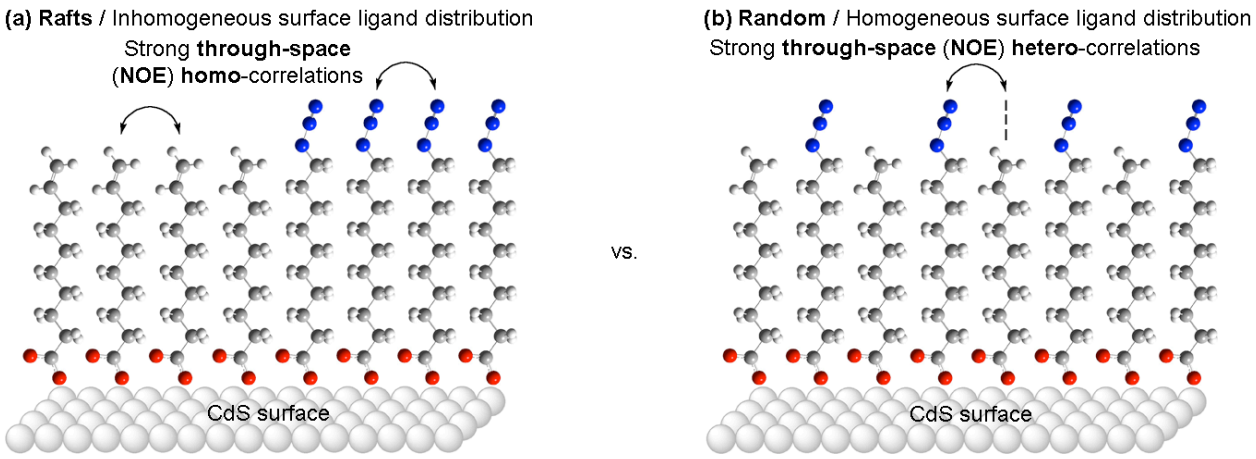

Figure 6. Possible inhomogeneous (raft assembly, a) *vs.* homogeneous (random, b) surface ligand distributions in mixed ligand CdS nanocrystal quantum dots.

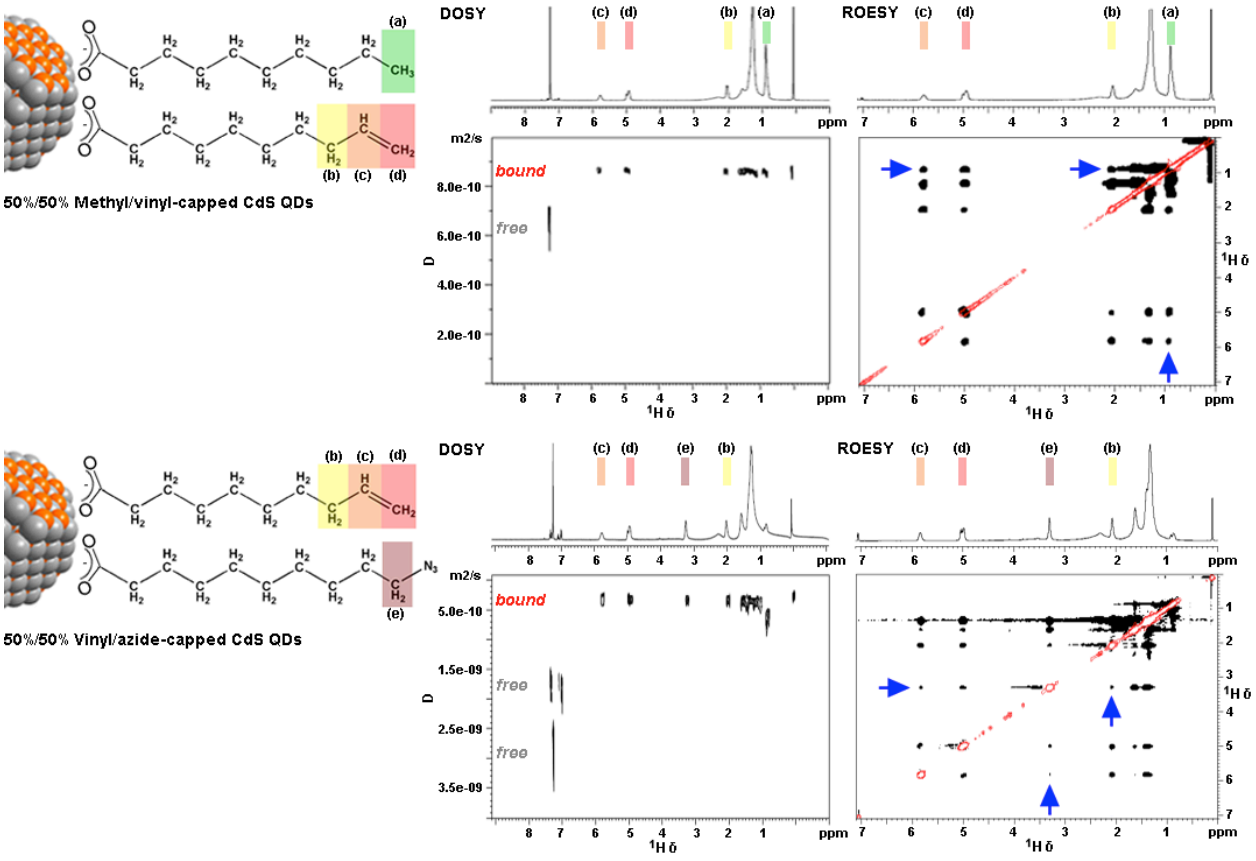

Figure 7. Representative DOSY and ROESY spectra of mixed ligand CdS nanocrystal quantum dots.

Proof of principle: Does this type of surface doping strategy work? To test the feasibility of this surface doping approach in controlling the degree of functionalization (valency) per nanocrystal, we subjected vinyl- and azide-capped quantum dots to cross-metathesis[68-69] and "click" (Huisgen's [3+2]-cycloaddition)[70-72] conditions. To facilitate our initial screening, we used small fluorinated molecules as model substrates, and followed the surface modification reactions by UV-Vis, PL, NMR, XRD, TEM and energy-dispersive X-ray spectroscopy (EDX). The presence of fluorine in the model substrates enables the use of ^{19}F NMR, and enhances the value of EDX elemental mapping in assessing the outcome of these reactions. In the presence of Grubb's 2nd generation catalyst, vinyl-capped CdS

quantum dots react with para-trimethylfluoro-styrene to produce p-CF_3-styrene-capped quantum dots (Scheme 3). A 20-fold excess of styrene, relative to the number of vinyl equivalents in solution (ca. 50-150 per dot), helps prevent undesirable side reactions, such as previously reported dendronization and cross-linking.[73-74] UV-Vis, PL, XRD and TEM showed that metathesis proceeds without affecting the particle size or optical properties. After removal of free soluble unreacted styrene and the self-metathesis byproduct by crashing and centrifugation, both 100% vinyl-capped and 50%/50% vinyl/methyl-capped CdS dots show ca. 50-60% conversion, as evidenced by the internal-to-terminal olefin ratio observed by ^{1}H NMR (Scheme 3). Critically, EDX confirms that the final loading of fluorinated groups per quantum dot is proportional to the original population of surface-active native vinyl ligands in the original nanocrystals (Scheme 3). To the best of our knowledge, this is one of only a couple of examples of valency control on semiconductor nanocrystal quantum dots,[75-77] and the only one that does not use ligand exchange.

Scheme 3. Surface doping and valency control of CdS quantum dots via cross metathesis.

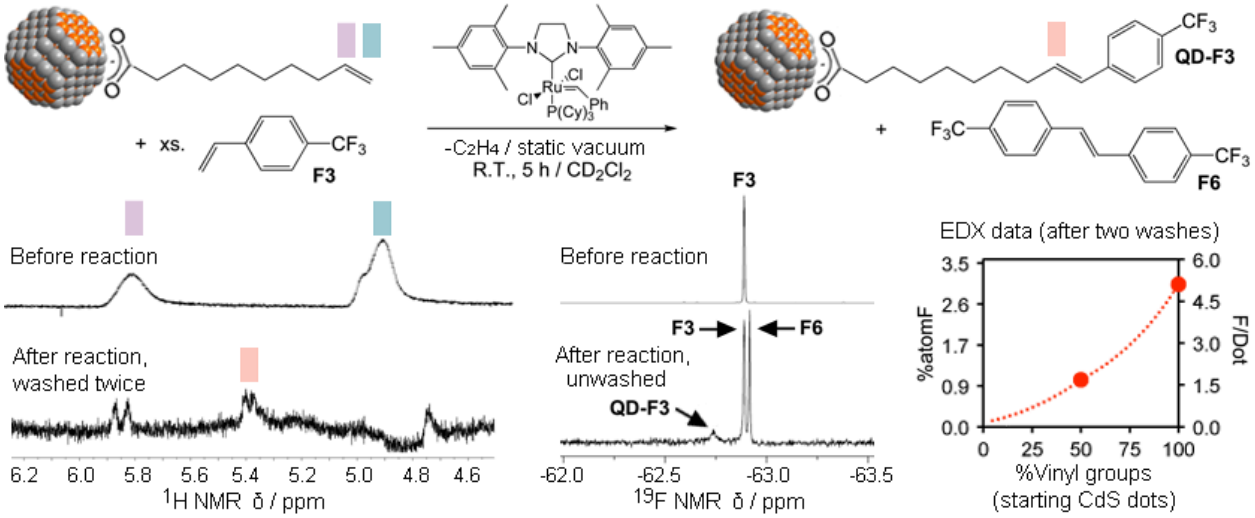

Similarly, in the presence of different copper catalysts, azide-capped CdS quantum dots react with meta-fluoro-phenyl-acetylene to produce m-F-phenyl-azole-capped quantum dots (Scheme 4). ^{1}H NMR and ^{19}F NMR show complete conversion of chemically-active surface azide groups to azole groups. As in the metathesis case above, the degree of quantum dot surface fluorination is proportional to the population of azide surface ligands in the original nanocrystals. However, in contrast to the metathesis reaction, we found that copper click catalysts behave in a "non-innocent" way, adsorbing onto the CdS surface and red-shifting the dots' UV-Vis absorption and PL spectra (Scheme 4). This is not surprising based on several fully documented examples of metal ion diffusion into colloidal nanocrystals.[78-79] Our initial attempts to suppress this problem by using copper wire[80] as a slowly releasing heterogeneous click catalyst temporarily slowed the observed red shift, but did not completely stop it (Scheme 4). Nevertheless, we found that we can completely avoid this problem by using a much more robust, ligated ruthenium click catalyst, Cp*Ru(COD)Cl, which was recently reported in the literature (Scheme 4).[81]

Scheme 4. Surface doping of CdS quantum dots with different click catalysts.

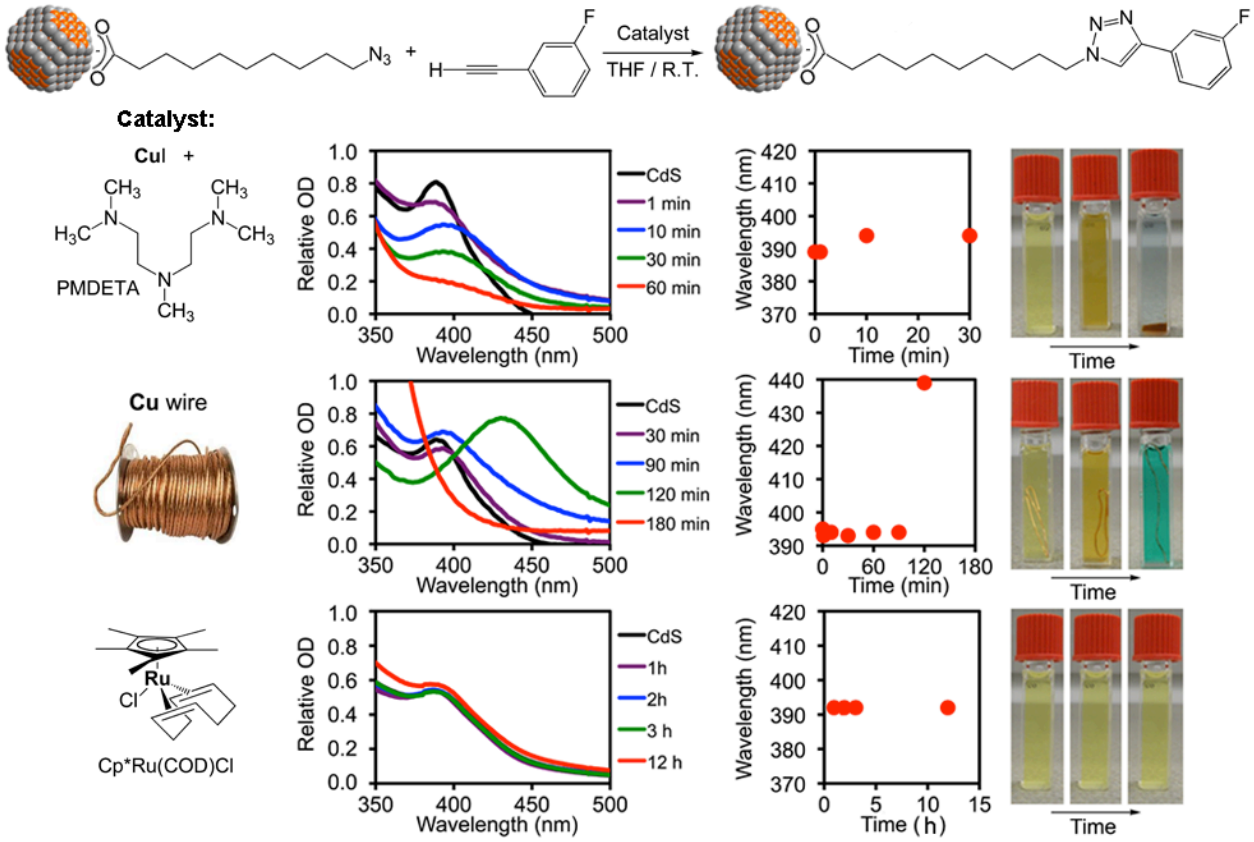

Conclusions

In summary, we have explored a fundamentally new surface ligand modification or "doping" strategy aimed at controlling the degree of loading or "valency" in semiconductor nanocrystal quantum dots. Unlike currently used surface modification methods, which rely heavily on thiol ligand exchange, our approach preserves the nanocrystal's native ligands, avoiding etching and retaining optical properties. We have shown that surface doped quantum dots capped with chemically-active native ligands can be prepared directly from a mixture of ligands with similar chain lengths. Vinyl and azide-terminated carboxylic acid ligands survive the high temperatures needed for nanocrystal synthesis. The ratio between chemically active and inactive-terminated ligands is maintained in the nanocrystals, and allows to control the extent of surface modification by straightforward organic reactions.

Using a combination of optical and structural characterization tools, including IR and 2D NMR, we have shown that carboxylates bind to the nanocrystals in a bidentate chelate fashion, forming a single monolayer that is perpendicular to the nanocrystal surface. Moreover, we have shown that mixtures of ligands with similar chain lengths homogeneously distribute themselves on the nanocrystal surface. We are currently working toward gaining a deeper understanding of surface paramagnetic impurities by EPR, the dispersion in the degree of surface doping across individual quantum dots by AFM-PL, and the effect of inorganic surface composition and ligand structure on raft formation by NMR and STEM. We believe that the surface doping approach presented here will be widely applicable to many nanocrystal compositions (Cu_2S, CZTS, CIGS, InP, Cu, Au), shapes (dots, rods, wires, tetrapods), and specific applications. In energy and materials science, the ability to fine-tune the number and relative configuration of energy and charge transfer donors and acceptors will provide unprecedented control over quantum dot exciton decay and chemical reaction pathways across the inorganic(crystal)-organic(ligand)-solvent(medium) interface. In biology, the extent of surface coverage by a particular functional group will have a large impact on a nanocrystal's affinity and permeability to a variety of biological structures, and thus on its ability to localize, penetrate, and be transported across specific tissues, and cellular and subcellular structures.

Acknowledgments

J.V. gratefully acknowledges the National Science Foundation for funding of this work through the Division of Chemistry (NSF- 1253058).

References

[1] Smith, A. M.; Nie, S. M. Semiconductor Nanocrystals: Structure, Properties, and Band Gap Engineering. *Acc. Chem. Res.* **2010,** *43*, 190–200.

[2] Talapin, D. V.; Lee, J. S.; Kovalenko, M. V.; Shevchenko, E. V. Prospects of Colloidal Nanocrystals for Electronic and Optoelectronic Applications. *Chem. Rev.* **2010,** *110*, 389–458.

[3] Kuno, M. An Overview of Solution-Based Semiconductor Nanowires: Synthesis and Optical Studies. *Phys. Chem. Chem. Phys.* **2008,** *10*, 620–639.

[4] Buhro, W. E.; Wang, F. D.; Dong, A. G.; Sun, J. W.; Tang, R.; Yu, H. Solution-Liquid-Solid Growth of Semiconductor Nanowires. *Inorg. Chem.* **2006,** *45*, 7511–7521.

[5] Michalet, X.; Pinaud, F. F.; Bentolila, L. A.; Tsay, J. M.; Doose, S.; Li, J. J.; Sundaresan, G.; Wu, A. M.; Gambhir, S. S.; Weiss, S. Quantum Dots for Live Cells, In Vivo Imaging, and Diagnostics. *Science* **2005,** *307*, 538–544.

[6] Li, A. D. Q.; Tian, Z. Y.; Wu, W. W. Photoswitchable Fluorescent Nanoparticles: Preparation, Properties and Applications. *Chemphyschem* **2009,** *10*, 2577–2591.

[7] Mattoussi, H.; Palui, G.; Na, H. B. Luminescent Quantum Dots as Platforms for Probing In Vitro and In Vivo Biological Processes. *Adv. Drug Deliv. Rev.* **2012,** *64*, 138–166.

[8] Marchuk, K.; Guo, Y. J.; Sun, W.; Vela, J.; Fang, N. High-Precision Tracking with Non-blinking Quantum Dots Resolves Nanoscale Vertical Displacement. *J. Am. Chem. Soc.* **2012,** *134*, 6108–6111.

[9] Alivisatos, A. P.; Fu, A. H.; Gu, W. W.; Boussert, B.; Koski, K.; Gerion, D.; Manna, L.; Le Gros, M.; Larabell, C. A. Semiconductor Quantum Rods as Single Molecule Fluorescent Biological Labels. *Nano Lett.* **2007,** *7*, 179–182.

[10] Medintz, I. L.; Mattoussi, H. Quantum Dot-Based Resonance Energy Transfer and Its Growing Application in Biology. *Phys. Chem. Chem. Phys.* **2009,** *11*, 17–45.

[11] Vela, J.; Htoon, H.; Chen, Y.; Park, Y.-S.; Ghosh, Y.; Goodwin, P. M.; Werner, J. H.; Wells, N. P.; Casson, J. L.; Hollingsworth, J. A. Effect of Shell Thickness and Composition on Blinking Suppression and the Blinking Mechanism in 'Giant' CdSe/CdS Nanocrystal Quantum Dots. *J. Biophotonics* **2010,** *3*, 706–717.

[12] Algar, W. R.; Susumu, K.; Delehanty, J. B.; Medintz, I. L. Semiconductor Quantum Dots in Bioanalysis: Crossing the Valley of Death. *Anal. Chem.* **2011,** *83*, 8826–8837.

[13] Shields, A. J. Semiconductor Quantum Light Sources. *Nat. Photonics* **2007,** *1*, 215–223.

[14] Bulovic, V.; Anikeeva, P. O.; Halpert, J. E.; Bawendi, M. G. Quantum Dot Light-Emitting Devices with Electroluminescence Tunable over the Entire Visible Spectrum. *Nano Lett.* **2009,** *9*, 2532–2536.

[15] Kamat, P. V. Meeting the Clean Energy Demand: Nanostructure Architectures for Solar Energy Conversion. *J. Phys. Chem. C* **2007,** *111*, 2834–2860.

[16] Kamat, P. V. Quantum Dot Solar Cells. Semiconductor Nanocrystals as Light Harvesters. *J. Phys. Chem. C* **2008,** *112*, 18737–18753.

[17] Dresselhaus, M. S.; Chen, G.; Tang, M. Y.; Yang, R. G.; Lee, H.; Wang, D. Z.; Ren, Z. F.; Fleurial, J. P.; Gogna, P. New Directions for Low-Dimensional Thermoelectric Materials. *Adv. Mater.* **2007,** *19*, 1043–1053.

[18] Klimov, V. I.; Ivanov, S. A.; Nanda, J.; Achermann, M.; Bezel, I.; McGuire, J. A.; Piryatinski, A. Single-Exciton Optical Gain in Semiconductor Nanocrystals. *Nature* **2007,** *447*, 441–446.

[19] Felser, C.; Fecher, G. H.; Balke, B. Spintronics: A Challenge for Materials Science and Solid-State Chemistry. *Angew. Chem. Int. Ed.* **2007,** *46*, 668–699.

[20] Rogach, A. L.; Eychmuller, A.; Hickey, S. G.; Kershaw, S. V. Infrared-Emitting Colloidal Nanocrystals: Synthesis, Assembly, Spectroscopy, and Applications. *Small* **2007,** *3*, 536–557.

[21] Yu, W. W.; Qu, L. H.; Guo, W. Z.; Peng, X. G. Experimental Determination of the Extinction Coefficient of CdTe, CdSe, and CdS Nanocrystals. *Chem. Mater.* **2003,** *15*, 2854–2860.

[22] Mulvaney, P.; Jasieniak, J.; Smith, L.; van Embden, J.; Califano, M. Re-Examination of the Size-Dependent Absorption Properties of CdSe Quantum Dots. *J. Phys. Chem. C* **2009,** *113*, 19468–19474.

[23] García-Santamaría, F.; Chen, Y.; Vela, J.; Schaller, R. D.; Hollingsworth, J. A.; Klimov, V. I. Suppressed Auger Recombination in "Giant" Nanocrystals Boosts Optical Gain Performance. *Nano Lett.* **2009,** *9*, 3482–3488.

[24] Li, L. A.; Pandey, A.; Werder, D. J.; Khanal, B. P.; Pietryga, J. M.; Klimov, V. I. Efficient Synthesis of Highly Luminescent Copper Indium Sulfide-Based Core/Shell Nanocrystals with Surprisingly Long-Lived Emission. *J. Am. Chem. Soc.* **2011,** *133*, 1176–1179.

[25] Hermier, J. P.; Mahler, B.; Spinicelli, P.; Buil, S.; Quelin, X.; Dubertret, B. Towards Non-Blinking Colloidal Quantum Dots. *Nature Mater.* **2008,** *7*, 659–664.

[26] Chen, Y.; Vela, J.; Htoon, H.; Casson, J. L.; Werder, D. J.; Bussian, D. A.; Klimov, V. I.; Hollingsworth, J. A. "Giant" Multishell CdSe Nanocrystal Quantum Dots with Suppressed Blinking. *J. Am. Chem. Soc.* **2008,** *130*, 5026–5027.

[27] Krauss, T. D.; Wang, X. Y.; Ren, X. F.; Kahen, K.; Hahn, M. A.; Rajeswaran, M.; Maccagnano-Zacher, S.; Silcox, J.; Cragg, G. E.; Efros, A. L. Non-Blinking Semiconductor Nanocrystals. *Nature* **2009,** *459*, 686–689.

[28] Pearson, R. G. Hard and Soft Acids and Bases - the Evolution of a Chemical Concept. *Coord. Chem. Rev.* **1990,** *100*, 403–425.

[29] Medintz, I. L.; Uyeda, H. T.; Goldman, E. R.; Mattoussi, H. Quantum Dot Bioconjugates for Imaging, Labelling and Sensing. *Nature Mater.* **2005,** *4*, 435–446.

[30] Erathodiyil, N.; Ying, J. Y. Functionalization of Inorganic Nanoparticles for Bioimaging Applications. *Acc. Chem. Res.* **2011,** *44*, 925–935.

[31] Talapin, D. V.; Kovalenko, M. V.; Scheele, M. Colloidal Nanocrystals with Molecular Metal Chalcogenide Surface Ligands. *Science* **2009,** *324*, 1417–1420.

[32] Talapin, D. V.; Lee, J. S.; Kovalenko, M. V.; Huang, J.; Chung, D. S. Band-Like Transport, High Electron Mobility and High Photoconductivity in All-Inorganic Nanocrystal Arrays. *Nature Nanotech.* **2011,** *6*, 348–352.

[33] Jeong, S.; Achermann, M.; Nanda, J.; Lvanov, S.; Klimov, V. I.; Hollingsworth, J. A. Effect of the Thiol-Thiolate Equilibrium on the Photophysical Properties of Aqueous CdSe/ZnS Nanocrystal Quantum Dots. *J. Am. Chem. Soc.* **2005,** *127*, 10126–10127.

[34] Amara, N.; Mashiach, R.; Amar, D.; Krief, P.; Spieser, S. A. H.; Bottomley, M. J.; Aharoni, A.; Meijler, M. M. Covalent Inhibition of Bacterial Quorum Sensing. *J. Am. Chem. Soc.* **2009,** *131*, 10610–10619.

[35] Pradhan, N.; Katz, B.; Efrima, S. Synthesis of High-Quality Metal Sulfide Nanoparticles from Alkyl Xanthate Single Precursors in Alkylamine Solvents. *J. Phys. Chem. B* **2003,** *107*, 13843–13854.

[36] Gonzalez-Roura, A.; Casas, J.; Llebaria, A. Synthesis and Phospholipase C Inhibitory Activity of D609 Diastereomers. *Lipids* **2002,** *37*, 401–406.

[37] Jennings, T. L.; Becker-Catania, S. G.; Triulzi, R. C.; Tao, G. L.; Scott, B.; Sapsford, K. E.; Spindel, S.; Oh, E.; Jain, V.; Delehanty, J. B.; Prasuhn, D. E.; Boeneman, K.; Algar, W. R.; Medintz, I. L. Reactive Semiconductor Nanocrystals for Chemoselective Biolabeling and Multiplexed Analysis. *ACS Nano* **2011,** *5*, 5579–5593.

[38] Li, Y. C.; Ye, M. F.; Yang, C. H.; Li, X. H.; Li, Y. F. Composition- and Shape-Controlled Synthesis and Optical Properties of $Zn_xCd_{1-x}S$ Alloyed Nanocrystals. *Adv. Funct. Mater.* **2005,** *15*, 433–441.

[39] Nair, P. S.; Radhakrishnan, T.; Revaprasadu, N.; Kolawole, G.; O'Brien, P. Cadmium Ethylxanthate: A Novel Single-Source Precursor for the Preparation of CdS Nanoparticles. *J. Mater. Chem.* **2002,** *12*, 2722–2725.

[40] Barreca, D.; Gasparotto, A.; Maragno, C.; Seraglia, R.; Tondello, E.; Venzo, A.; Krishnan, V.; Bertagnolli, H. Synthesis and Characterization of Zinc Bis(O-isopropylxanthate) as a Single-Source Chemical Vapor Deposition Precursor for ZnS. *Appl. Organomet. Chem.* **2005,** *19*, 1002–1009.

[41] Zelenak, V.; Vargova, Z.; Gyoryova, K. Correlation of Infrared Spectra of Zinc(II) Carboxylates with their Structures. *Spectrochim. Acta A* **2007,** *66*, 262–272.

[42] Lieber, E.; Rao, C. N. R.; Chao, T. S.; Hoffman, C. W. W. Infrared Spectra of Organic Azides. *Anal. Chem.* **1957,** *29*, 916–918.

[43] Vela, J.; Lief, G. R.; Shen, Z. L.; Jordan, R. F. Ethylene Polymerization by Palladium Alkyl Complexes Containing Bis(aryl)phosphino-Toluenesulfonate Ligands. *Organometallics* **2007,** *26*, 6624–6635.

[44] Cros-Gagneux, A.; Delpech, F.; Nayral, C.; Cornejo, A.; Coppel, Y.; Chaudret, B. Surface Chemistry of InP Quantum Dots: A Comprehensive Study. *J. Am. Chem. Soc.* **2010,** *132*, 18147–18157.

[45] Banin, U.; Costi, R.; Saunders, A. E.; Elmalem, E.; Salant, A. Visible Light-Induced Charge Retention and Photocatalysis with Hybrid CdSe-Au Nanodumbbells. *Nano Lett.* **2008,** *8*, 637–641.

[46] Kalyuzhny, G.; Murray, R. W. Ligand Effects on Optical Properties of CdSe Nanocrystals. *J. Phys. Chem. B* **2005,** *109*, 7012–7021.

[47] Querner, C.; Reiss, P.; Bleuse, J.; Pron, A. Chelating Ligands for Nanocrystals' Surface Functionalization. *J. Am. Chem. Soc.* **2004,** *126*, 11574–11582.

[48] Sachleben, J. R.; Colvin, V.; Emsley, L.; Wooten, E. W.; Alivisatos, A. P. Solution-State NMR Studies of the Surface Structure and Dynamics of Semiconductor Nanocrystals. *J. Phys. Chem. B* **1998,** *102*, 10117–10128.

[49] Kuno, M.; Lee, J. K.; Dabbousi, B. O.; Mikulec, F. V.; Bawendi, M. G. The Band Edge Luminescence of Surface Modified CdSe Nanocrystallites: Probing the Luminescing State. *J. Chem. Phys.* **1997,** *106*, 9869–9882.

[50] Ji, X. H.; Copenhaver, D.; Sichmeller, C.; Peng, X. G. Ligand Bonding and Dynamics on Colloidal Nanocrystals at Room Temperature: The Case of Alkylamines on CdSe Nanocrystals. *J. Am. Chem. Soc.* **2008,** *130*, 5726–5735.

[51] Cossairt, B. M.; Juhas, P.; Billinge, S. J. L.; Owen, J. S. Tuning the Surface Structure and Optical Properties of CdSe Clusters Using Coordination Chemistry. *J. Phys. Chem. Lett.* **2011,** *2*, 3075–3080.

[52] Mercado, C. C.; Knorr, F. J.; McHale, J. L.; Usmani, S. M.; Ichimura, A. S.; Saraf, L. V. Location of Hole and Electron Traps on Nanocrystalline Anatase TiO_2. *J. Phys. Chem. C* **2012,** *116*, 10796–10804.

[53] Knorr, F. J.; Zhang, D.; McHale, J. L. Influence of $TiCl_4$ Treatment on Surface Defect Photoluminescence in Pure and Mixed-Phase Nanocrystalline TiO_2. *Langmuir* **2007,** *23*, 8686–8690.

[54] Schubert, E. M. Utilizing the Evans Method with a Superconducting NMR Spectrometer in the Undergraduate Laboratory. *J. Chem. Ed.* **1992,** *69*, 62–62.

[55] Piguet, C. Paramagnetic Susceptibility by NMR: The "Solvent Correction" Removed for Large Paramagnetic Molecules. *J. Chem. Ed.* **1997,** *74*, 815–816.

[56] Grant, D. H. Paramagnetic-Susceptibility by NMR - the Solvent Correction Reexamined. *J. Chem. Ed.* **1995,** *72*, 39–40.

[57] Li, Y. J.; Lei, X. G.; Lawler, R. G.; Murata, Y.; Komatsu, K.; Turro, N. J. Distance-Dependent Paramagnet-Enhanced Nuclear Spin Relaxation of H-2@C-60 Derivatives Covalently Linked to a Nitroxide Radical. *J. Phys. Chem. Lett.* **2010,** *1*, 2135–2138.

[58] Berrettini, M. G.; Braun, G.; Hu, J. G.; Strouse, G. F. NMR Analysis of Surfaces and Interfaces in 2-nm CdSe. *J. Am. Chem. Soc.* **2004,** *126*, 7063–7070.

[59] Carney, R. P.; DeVries, G. A.; Dubois, C.; Kim, H.; Kim, J. Y.; Singh, C.; Ghorai, P. K.; Tracy, J. B.; Stiles, R. L.; Murray, R. W.; Glotzer, S. C.; Stellacci, F. Size Limitations for the Formation of Ordered Striped Nanoparticles. *J. Am. Chem. Soc.* **2008,** *130*, 798–799.

[60] DeVries, G. A.; Brunnbauer, M.; Hu, Y.; Jackson, A. M.; Long, B.; Neltner, B. T.; Uzun, O.; Wunsch, B. H.; Stellacci, F. Divalent Metal Nanoparticles. *Science* **2007,** *315*, 358–361.

[61] Centrone, A.; Hu, Y.; Jackson, A. M.; Zerbi, G.; Stellacci, F. Phase Separation on Mixed-Monolayer-Protected Metal Nanoparticles: A Study by Infrared Spectroscopy and Scanning Tunneling Microscopy. *Small* **2007,** *3*, 814–817.

[62] Hung, A.; Mwenifumbo, S.; Mager, M.; Kuna, J. J.; Stellacci, F.; Yarovsky, I.; Stevens, M. M. Ordering Surfaces on the Nanoscale: Implications for Protein Adsorption. *J. Am. Chem. Soc.* **2011,** *133*, 1438–1450.

[63] Kuna, J. J.; Voitchovsky, K.; Singh, C.; Jiang, H.; Mwenifumbo, S.; Ghorai, P. K.; Stevens, M. M.; Glotzer, S. C.; Stellacci, F. The Effect of Nanometre-Scale Structure on Interfacial Energy. *Nature Mater.* **2009,** *8*, 837–842.

[64] Moreels, I.; Martins, J. C.; Hens, Z. Solution NMR Techniques for Investigating Colloidal Nanocrystal Ligands: A Case Study on Trioctylphosphine Oxide at InP Quantum Dots. *Sensor Actuat B-Chem* **2007,** *126*, 283–288.

[65] Fritzinger, B.; Moreels, I.; Lommens, P.; Koole, R.; Hens, Z.; Martins, J. C. In Situ Observation of Rapid Ligand Exchange in Colloidal Nanocrystal Suspensions Using Transfer NOE Nuclear Magnetic Resonance Spectroscopy. *J. Am. Chem. Soc.* **2009,** *131*, 3024–3032.

[66] Hassinen, A.; Moreels, I.; Donega, C. D.; Martins, J. C.; Hens, Z. Nuclear Magnetic Resonance Spectroscopy Demonstrating Dynamic Stabilization of CdSe Quantum Dots by Alkylamines. *J. Phys. Chem. Lett.* **2010,** *1*, 2577–2581.

[67] Gomes, R.; Hassinen, A.; Szczygiel, A.; Zhao, Q. A.; Vantomme, A.; Martins, J. C.; Hens, Z. Binding of Phosphonic Acids to CdSe Quantum Dots: A Solution NMR Study. *J. Phys. Chem. Lett.* **2011,** *2*, 145–152.

[68] Connon, S. J.; Blechert, S. Recent Developments in Olefin Cross-Metathesis. *Angew. Chem. Int. Ed.* **2003,** *42*, 1900–1923.

[69] Connon, S. J.; Rivard, M.; Zaja, M.; Blechert, S. Practical Olefin Metathesis in Protic Media under an Air Atmosphere. *Adv. Synth. Cat.* **2003,** *345*, 572–575.

[70] Kolb, H. C.; Finn, M. G.; Sharpless, K. B. Click Chemistry: Diverse Chemical Function from a Few Good Reactions. *Angew. Chem. Int. Ed.* **2001,** *40*, 2004–2005.

[71] Hawker, C. J.; van Berkel, K. Y.; Piekarski, A. M.; Kierstead, P. H.; Pressly, E. D.; Ray, P. C. A Simple Route to Multimodal Composite Nanoparticles. *Macromolecules* **2009,** *42*, 1425–1427.

[72] Gole, A.; Murphy, C. J. Azide-Derivatized Gold Nanorods: Functional Materials for "Click" Chemistry. *Langmuir* **2008,** *24*, 266–272.

[73] Elmer, S. L.; Lemcoff, N. G.; Zimmerman, S. C. Exploring the Reversibility of the Ring-Closing Metathesis Mediated Cross-Linking of Dendrimers. *Macromolecules* **2007,** *40*, 8114–8118.

[74] Guo, W. H.; Li, J. J.; Wang, Y. A.; Peng, X. G. Luminescent CdSe/CdS Core/Shell Nanocrystals in Dendron Boxes: Superior Chemical, Photochemical and Thermal Stability. *J. Am. Chem. Soc.* **2003,** *125*, 3901–3909.

[75] Blanco-Canosa, J. B.; Medintz, I. L.; Farrell, D.; Mattoussi, H.; Dawson, P. E. Rapid Covalent Ligation of Fluorescent Peptides to Water Solubilized Quantum Dots. *J. Am. Chem. Soc.* **2010,** *132*, 10027–10033.

[76] Liu, W.; Howarth, M.; Greytak, A. B.; Zheng, Y.; Nocera, D. G.; Ting, A. Y.; Bawendi, M. G. Compact Biocompatible Quantum Dots Functionalized for Cellular Imaging. *J. Am. Chem. Soc.* **2008,** *130*, 1274–1284.

[77] Han, H. S.; Devaraj, N. K.; Lee, J.; Hilderbrand, S. A.; Weissleder, R.; Bawendi, M. G. Development of a Bioorthogonal and Highly Efficient Conjugation Method for Quantum Dots Using Tetrazine-Norbornene Cycloaddition. *J. Am. Chem. Soc.* **2010,** *132*, 7838–7839.

[78] Pietryga, J. M.; Schaller, R. D.; Werder, D.; Stewart, M. H.; Klimov, V. I.; Hollingsworth, J. A. Pushing the Band Gap Envelope: Mid-Infrared Emitting Colloidal PbSe Quantum Dots. *J. Am. Chem. Soc.* **2004,** *126*, 11752–11753.

[79] Son, D. H.; Hughes, S. M.; Yin, Y. D.; Alivisatos, A. P. Cation Exchange Reactions in Ionic Nanocrystals. *Science* **2004,** *306*, 1009–1012.

[80] Monteiro, M. J.; Urbani, C. N.; Bell, C. A.; Whittaker, M. R. Convergent Synthesis of Second Generation AB-Type Miktoarm Dendrimers Using "Click" Chemistry Catalyzed by Copper Wire. *Macromolecules* **2008,** *41*, 1057–1060.

[81] Boren, B. C.; Narayan, S.; Rasmussen, L. K.; Zhang, L.; Zhao, H. T.; Lin, Z. Y.; Jia, G. C.; Fokin, V. V. Ruthenium-Catalyzed Azide-Alkyne Cycloaddition: Scope and Mechanism. *J. Am. Chem. Soc.* **2008,** *130*, 8923–8930.

CHAPTER 3

SURFACE LIGAND MICROSTRUCTURE, ORGANIZATION AND REACTIVITY: INVESTIGATING THE INORGANIC-ORGANIC-MEDIUM INTERFACE IN COLLOIDAL QUANTUM DOTS

Abstract

Over the past decades, there have been several studies on shape and morphology of quantum dots (QDs) but not many groups focused on the surface ligand packing and organization. Therefore, a thorough understanding of the composition and morphology of the ligand shell is essential for controlling the properties and behavior of nanocrystals. Herein, using DOSY spectroscopy we demonstrate that a dynamic equilibrium exists between bound and free ligands. The ligands are tightly bound to the particle surface when they are dispersed in a ligand-free solvent, while they rapidly exchange when an excess of free ligands are present in solution. We show that carboxylic acid head group is responsible for this type of exchange at the inorganic-organic interface. Removing the head group simply removes the rapid cap exchange and results in distinguished diffusion coefficient for the free and bound ligands. We also demonstrate that bound and free ligands have strongly different NOE spectra wherein only bound ligands develop strong and negative NOEs. We used one-dimensional and two-dimensional NMR as a powerful tool to determine the ligand shell structure of a series of particles capped with mixture of C10-N_3, C10-Me, C16-N3 and C16-Me ligand. ROESY analysis shows that particles have a homogeneous coating, when capped with ligand composition of same length, while they show a raft structure composed of phase-separated domains when ligand shell is constituted of ligands of different length. Furthermore, we demonstrate that surface ligand organization can affect the reactivity of

quantum dots. Formation of rafts as a result of packing ligands of a same length, increases the local concentration of reactive terminal group and facilitate the chemical reactivity at the surface of quantum dots. We conclude that solution-state NMR is a very powerful tool to characterize colloidal nanocrystal dispersions stabilized by organic ligands. This study can provide a new avenue to understand the organic/inorganic boundary of other and more complex nanoparticle/ligand systems.

Introduction

Semiconductor nanoparticles[1] signify a unique class of nanomaterials that display great potential in diverse applications such as nanoelectronic devices,[2] multifunctional catalysts,[3] (bio)- chemical sensors,[4] biological labeling,[5] and data storage.[6] However, to use these exceptional properties for the fabrication of various devices, not only design and synthesis of nanoscale building blocks, but also controlled assemblies of these structural units has to be addressed.[7] Since the chemical and physical properties of semiconducting nanocrystals are the combination of inorganic cores and organic protecting shells, the properties of materials can be readily manipulated by surface.[8] To date, a great deal of research has been focused on monolayer-protected nanoparticles.

Song and Co-workers[9] summarized several leading methods for the preparation of nanometersized Janus particles and highlighted the important properties and applications of these Janus nanoparticles in electrochemistry, sensing, and catalysis.

Recently Stellacci and co-workers investigated scanning tunneling microscopy (STM)[10, 11] and infrared spectroscopy,[12] of gold nanoparticles coated with a mixture of ligands that were known to phase separate into randomly sized and shaped domains when co-assembled on flat gold surfaces.[13,14] In a very recent Nature Communication[15] they show that a combination of

one-dimensional and two-dimensional NMR can be used to determine the ligand shell structure of a series of particles covered with aliphatic and aromatic ligands of varying composition.

Hens and coworkers introduced solution NMR as a powerful toolbox for surface ligand analysis, highlighting 1D ^{1}H, diffusion ordered (DOSY) and nuclear Overhauser effect (NOESY) spectroscopy as NMR techniques that enable bound ligands to be distinguished from free ligands.[16] They also used a combination of 1D and 2D NMR measurements to investigate the surface chemistry of CdTe QDs synthesized in the presence of phosphonic acids and amines. They find that upon addition of oleic acid, neither amine or phosphonate anhydride ligands are released from the QDs. On the other hand, the addition of phosphonic acids to CdTe QDs partially capped by oleic acid moieties through a high temperature ligand exchange process leads to the ready, one to one release of oleic acid.[17]

Weiss and co-workers, categorized the analytical work such as NMR, FT-IR, XPS, and ultrafast spectroscopy on the ligand shells of QDs in a review published in Chem Mater. 2012. [18]

While the cost of instrumentation for a few of these techniques described here may be prohibitive for researchers who are considering working with semiconductor QDs, standard and well-established analytical methods, such as NMR can be very effective in establishing the composition and structure of QD ligand shell. They are therefore a practical starting point for in-depth chemical characterization of these exciting nanomaterials. In our previous studies we show that C10 ligands tend to randomly distribute themselves onto the nanocrystal surface however effect of chain length on the ligand organization and assembly has yet to be investigated. This chapter discusses the inorganic-organic-medium interface in

colloidal quantum dots and analyses effect of chain length and ligand microstructure on distribution and packing of surface ligands employing advanced 2D ROESY NMR spectroscopy. It also reveals impact of surface ligand organization on chemical reactivity of CdS quantum dots.

Experimental

Materials. Decanoic acid (≥98%), 9-decenoic acid (≥90%), oleic acid (>90%), sodium azide, hexadecanoic acid, were purchased from Aldrich. 16-Hydroxyhexadecanoic acid (95%) was purchased from ChemSampCo, phenyl ether (Ph_2O) (99%), 3-fluorophenylacetylene (98%) from SynQuest, and chloro(1,5-cyclooctadiene)(pentamethyl-cyclopentadienyl) ruthenium(II) RuClCp*(COD) (98%) from Strem. Glacial acetic acid, hydrogen bromide (48%), methanol, ethanol, chloroform, and tetrahydrofuran (THF), were purchased from Fisher and used as received. Chloroform-*d* ($CDCl_3$), and tetrahydrofuran-d_8 (THF-d_8) were purchased from Cambridge Isotopes Labs. 10-Azidodecanoic acid and 16-azidohexadecanoic acid, Cadmium decyl-xanthate, 10-azidodecanoate capped-CdS, and 9-decenoate capped CdS were synthesized following reported procedures.[19] ^{1}H NMR chemical shifts (δ) are reported in ppm relative to residual protiated solvent in $CDCl_3$ (7.26 ppm) or THF-d_8 (1.72, 3.58 ppm).

General procedure for synthesis of surface doped cadmium sulfide quantum dots with mixed ligands on the surafec. A mixture of cadmium C10 xanthate (50 mg, 0.087 mmol), Ph_2O (500 mg), and carboxylic acid ligand (150 mg for decanoic acid, 148 mg for 9-decenoic acid, 185 mg for 10-azidodecanoic acid, 259 mg for 16-azidohexadecanoic acid, 223 mg for hexadecanoic acid, 245 mg for oleic acid; 0.870 mmol) were weighed onto a three-neck, 250 mL round bottom flask and sonicated for 45 min. The flask was then fitted with a Teflon-

coated stir bar, a condenser, and attached to a Schlenk line. The mixture was degassed for 20 min at room temperature (R.T.), refilled with dry Ar, placed into a pre-equilibrated oil bath at 150 °C and kept at this temperature while stirring for 15 minutes. The oil bath was removed and the mixture allowed to cool down to R.T. After dilution with chloroform (5 mL), nanocrystals were isolated by adding a minimum amount of chilled methanol followed by centrifugation (5000 rpm for 10 min). After re-dissolution in toluene or chloroform, precipitation was repeated to remove excess Ph_2O and ligand. Nanocrystals were dried under argon flow for 20 min. This method was used to prepare mixed ligand nanocrystals while keeping a 1:10 Cd-to-ligand molar ratio. *Excess ligand recycling.* Concentration of the first supernatant under vacuum allowed us to recover 70-90% of the excess carboxylic acid ligand along with Ph_2O. This ligand/solvent mixture could be re-used up to three times for the synthesis of new nanocrystals.

Ru catalyzed click reaction on azide-terminated CdS quantum dots. A mixture of 3-Fluorophenyl acetylene and Cp*RuCl(COD) catalyst (5% mol) was added to a 0.4 mL THF-d_8 solution of 10-azidodecanoic acid or 16-azidohexadecanoic acid capped CdS quantum dots inside the glovebox and was monitored by ^{1}H NMR to obtain a 1:3 azide: acetylene ratio. The reaction was further stirred at R.T. in the absence of light and was monitored by ^{1}H NMR for the disappearance of azide peak over the time.

NMR Characterization. *^{1}H NMR.* ^{1}H NMR spectra were carried out in a Varian 400MR spectrometer operating at a ^{1}H frequency of 399.80 MHz. Spectra were recorded using standard pulse sequences from VNMRJ 3.1 pulse program library. ^{1}H NMR spectra (64 scans) were recorded with a relaxation delay (d_1) between scans of 2 s for free ligands and 10 s for surface-bound ligands to allow full relaxation of all ^{1}H nuclei. Single-pulse ^{1}H spin-

lattice relaxation measurements (10 scans) were recorded with a pulse width of 156 μs and a recycle delay of 10 s. *DOSY*. Diffusion Ordered Spectroscopy (DOSY) experiments were collected using a Bruker DRX 400 spectrometer operating at a ^{1}H frequency of 400.39 MHz equipped with normal geometry probe. Spectra were recorded using standard pulse sequences from TopSpin 1.3 pulse program library. The duration of the magnetic field pulse gradients (δ) was optimized for each diffusion time (Δ) to obtain a signal decay of roughly 90% at the maximum gradient strength. A series of 16 spectra with 32,768 data points in each spectrum were collected. In each pulsed-field gradient NMR experiment, the value of δ was set to 2 ms, and the value of Δ (diffusion time) was set to 150 ms. The gradient strength was varied from 2 to 90% (space) of the maximum strength using a sine gradient shape. *ROESY*. Rotating-frame Overhauser Effect Spectroscopy (ROESY) experiments were recorded using an Avance III 600 spectrometer operating a ^{1}H frequency of 600.39 MHz equipped with 5 mm BBFO Smart Probe. Spectra were recorded using standard pulse sequences from TopSpin 3.0 pulse program library. ROESY spectra were collected using a spin lock time of 200-500 ms and 256 t_1 increments, with each t_1 slice consisting of 256 scans of 1024 sampled data points, each recorded with a 2 s relaxation delay.

Optical Characterization. *Absorption spectra* were measured with a photodiode-array Agilent 8453 UV-Vis spectrophotometer. Solvent absorption was recorded and subtracted from all spectra. *Steady-state photoluminescence* (PL) spectra were measured with a Horiba-Jobin Yvon Nanolog scanning spectrofluorometer equipped with a photomultiplier detector. Nanocrystal quantum dots were diluted in chloroform or toluene to give an optical density of 0.05-0.2 at 390 nm. Excitation wavelength was 350 nm, and emission was recorded between 365 and 685 nm.

Results and Discussion

Figure 1 shows DOSY spectra of vinyl-capped CdS in presence of 10-azidedecanoic acid free ligand at room temperature as well as reduced temperature. 10-azidedecanoic acid was chosen as a free ligand instead of 9-decenoic acid to avoid resonance overlap of free ligands and bound ligands. The DOSY spectrum of this mixture at room temperature didn't show any difference between diffusion rates of free ligands vs. bound ligands. Hence, the temperature was lowered to slow down the exchange process that is happening on the surface of nanocrystal QDs and facilitate the diffusion rate detection. Figure 1-b and 1-c, show DOSY spectra of the same mixture at 0 °C and -23 °C, respectively. As it is obvious from the corresponding spectra, reducing the temperature caused peak streaking and did not help on the diffusion rate detection of free and bound ligands. Figure 1d illustrates the DOSY spectrum of vinyl capped CdS at -23 °C and shows that peak streaking is not characteristics of this system at low temperature.

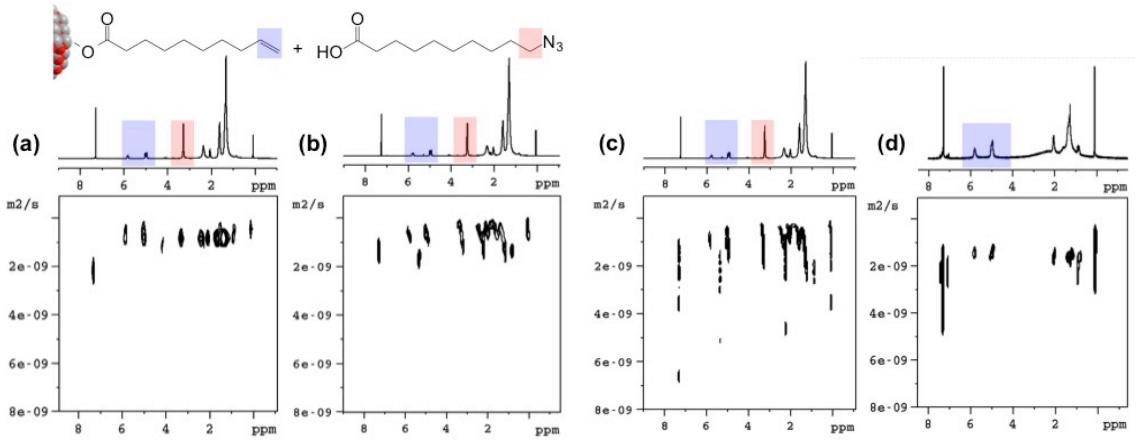

Figure 1. DOSY spectra of 9-decenoate-capped CdS after addition of free 10-azidodecanoic acid (a) R.T., (b) 273K, and (c) 250K in CDCl3, (d) DOSY spectrum of 9-decenoate-capped CdS at 250K is given for comparison

Figure 2 shows the DOSY spectra of a series of different examples at room temperature. Figure 2a, shows DOSY of azide-capped CdS in presence of excess of 10-azidodecanoic acid. Similar to the previous system in Fig. 1, we did not observe any separation for this mixture either. However, when we block the carboxylic acid head group in free ligand we were able to clearly observe that free ligand is diffusing faster than the bound ligand (Figure 2b). In Figure 2c and 2d, we completely removed the carboxylic acid functional groups on free ligands and looked at the diffusion rates of bound ligands vs. 9-decene and 10-azidodecane, respectively. DOSY spectra unambiguously indicated slower diffusion rates for bound system compare to free ligands.

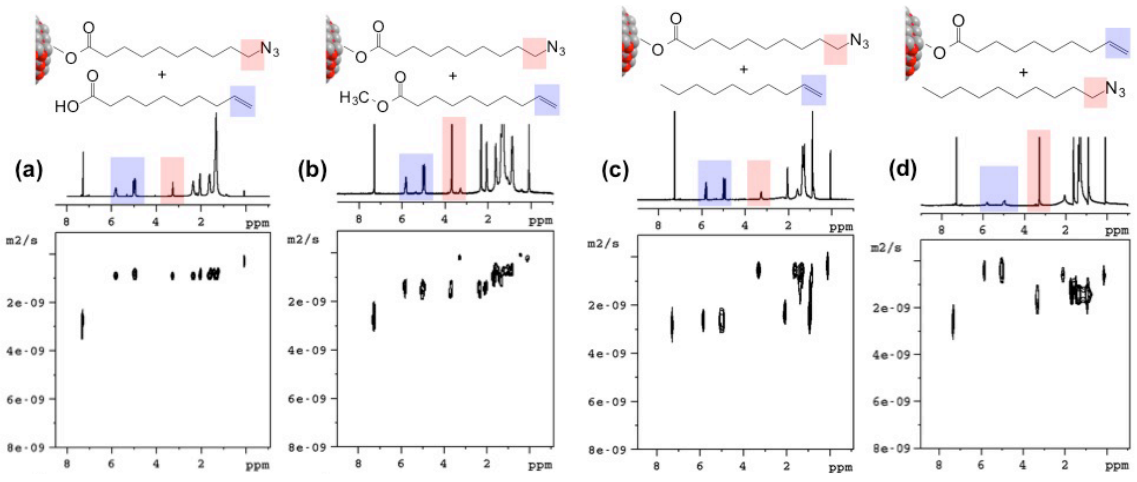

Figure 2. DOSY spectra of 10-azidodecenoate-capped CdS and free (a) 9-decenoic acid, (b) 9-methyldecenoate, (c) 9-decene, and (d) 9-decenoate-capped CdS and free 10-azido decene in $CDCl_3$ at R.T.

Following the reported procedure in our previous study, we were able to optimize a condition for synthesis of CdS using a single cadmium xanthate precursor and a mixture of long and short chain ligands.[19] Figure 3a shows ^{1}H NMR of CdS capped with 50%-50% mixture of C10-methyl and C16-azide terminated ligands. Figure 3b demonstrates the T1 relaxation values of corresponding mixed C10-C16 bound ligands compared with mixed

C10-C16 free ligands. In general, protons of the bound ligands relax much faster than protons of free ligands. We also synthesized CdS with different combinations of short and long chain ligands employing direct synthesis procedure form our previous paper.[19]

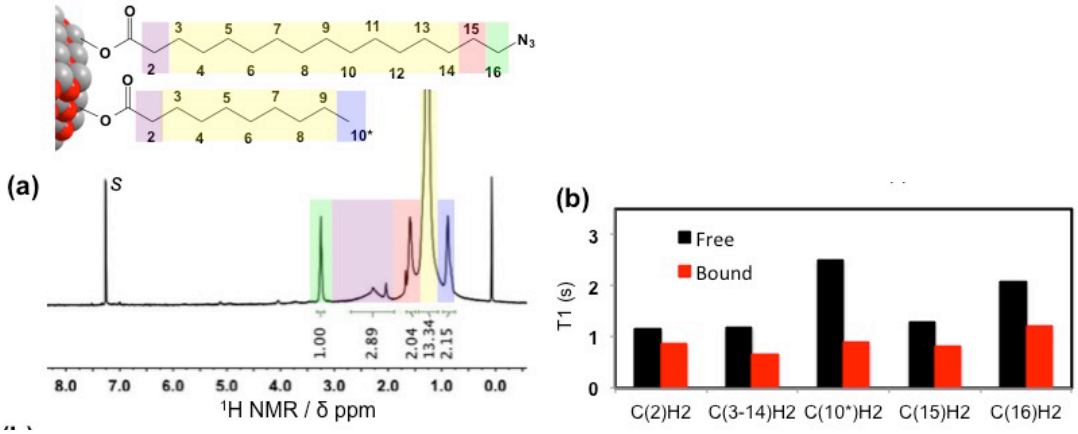

Figure 3. (a) ^{1}H NMR spectrum, and (b) *T1* relaxation times of CdS capped with mixture of C16-azide and C10-methyl terminated ligands

In Figure 4 we investigated effect of chain length on surface ligand distribution by employing 2D ROESY NMR technique. Figure 4a, 4b demonstrate ROESY spectra of CdS capped with mixture of short and long chain ligands. Unidimension ROESY (Figure S3) as well as 2D ROESY studies showed very weak hetero-correlation between two ligands of different chain length.

To further investigate if the weak hetero-correlation is as a result of far distance between the end groups of each ligand or if it is caused by homogeneous distribution of surface ligands, we designed a control experiment to look at the space correlation of C10-azide terminated and C18-oleate ligand bound to the surface of QDs to take the advantage of close proximity of CH_2-N_3 and CH_2=CH_2 protons. From Figure 4c, ROESY study of the corresponding system still shows a vey weak hetero correlation (CH_2-N_3 and CH_2=CH_2) but a strong homo correlation (CH_2=CH_2 and CH_2=CH_2). Therefore, ROESY observations

confirmed the hypothesis that ligands with different chain length form island or raft, however, our previous study on surface ligand distribution of ligands with the same chain length showed a heterogeneous distribution of ligands onto the nanocrystal surface.

As an additional example to support this hypothesis, we choose another model in which CdS capped with the same chain length surface ligands. Figure 4d shows ROESY spectrum of CdS capped with mixture of C10-azide and C10-methyl terminated ligands with relatively strong hetero-correlation between CH_2-N_3 and -CH_3. This is in consistent with our previous studies in which ROESY of CdS capped with different combination of C10 ligands were showed to have a strong hetero-correlation.

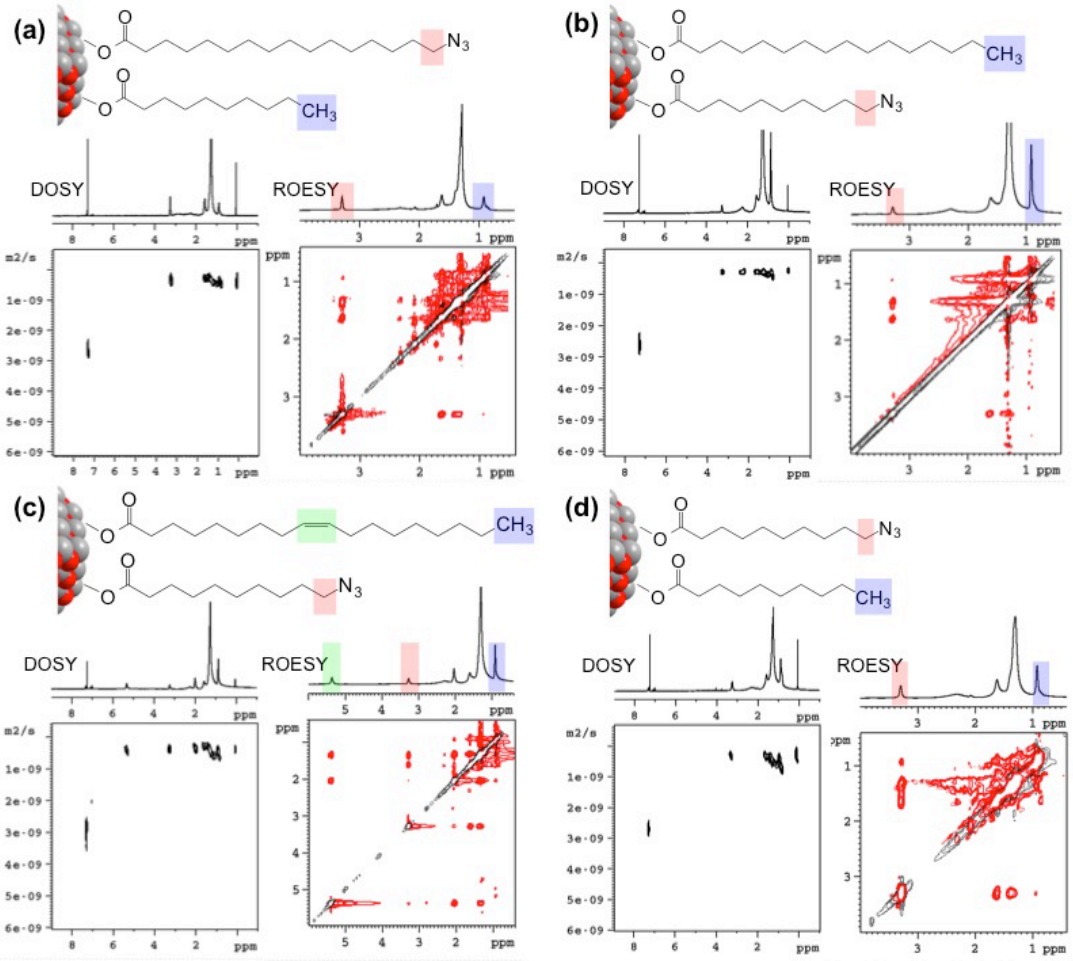

Figure 4. DOSY and ROESY spectra of CdS capped with 50%-50% mixture of (a) C16-azide and C10-methyl, (b) C10-azide and C16-methyl, (c) C10-azide and C18-Oleate, and (d) C10-azide and C10-methyl terminated ligands in CDCl3 at R.T.

We studied the relationship between chemical reactivity of our synthesized CdS capped with mixture of C10-C16 ligands *vs.* CdS capped with mixture of C10-C10 ligands. Since our azide capped CdS is capable of participating in click, we first optimized the Ru-catalyzed click condition for free 10-azidodecanoic acid with different acetylene substrates in different solvents (Table 1).

Table 1. Optimize condition for Ruthenium catalyzed click reaction on 10-azido decanoic acid and different acetylene substrates.

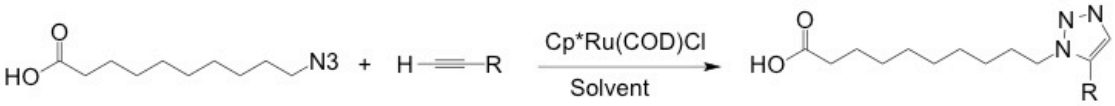

R	Solvent	Catalyst (% mol)	T (°C)	t (h)	Conversion(%)
CH_2NH_2	THF	5%	R.T.	4	0
CH_2NH_2	THF	10%	40	24	0
CH_2NH_2	Toluene	5%	R.T.	Several days	0
CH_2NH_2	Benzene	5%	R.T.	Several days	0
CH_2OH	THF	5%	R.T.	4	0
CH_2OH	THF	10%	40	24	0
CH_2OH	Toluene	5%	R.T.	Several days	0
CH_2OH	Benzene	5%	R.T.	Several days	0
C_6H_5	THF	5%	R.T.	4	16
C_6H_5	THF	10%	40	24	100
3-Fluorophenyl	THF	5%	R.T.	12	100

Then we performed a click reaction on our azide-terminated capped CdS with F-phenylacetylene substrate at R.T. in THF-d_8 using Cp*Ru(COD)Cl as a catalyst. We

monitored progress of click reaction on three different models by ^{1}H NMR over 3 days as it is shown in Figure 5.

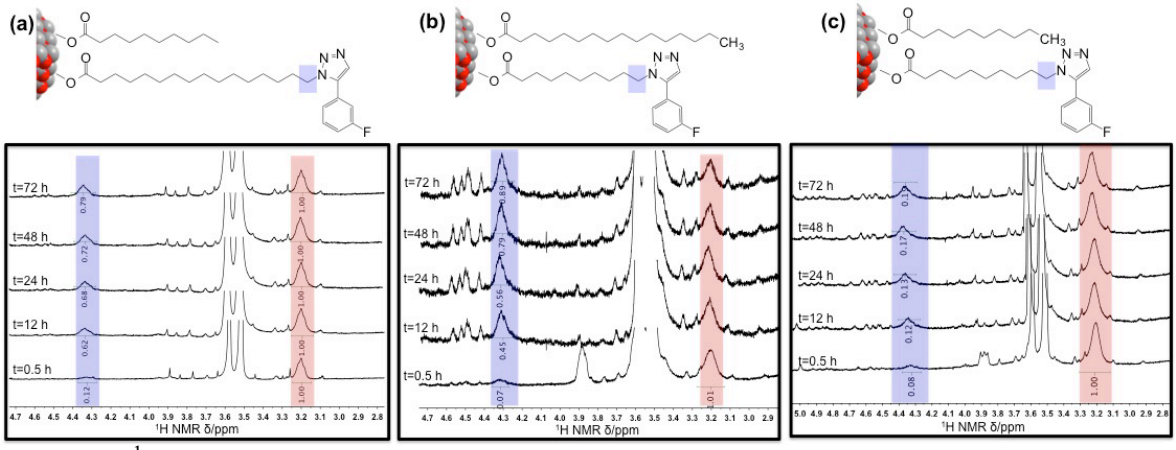

Figure 5. ^{1}H NMR spectra of CdS capped with 50%-50% mixture of (a) C16-azide and C10-methyl, (b) C10-azide and C16-methyl, and (c) C10-azide and C10-methyl terminated ligands participated in Ru catalyzed click with F-acetylene substrate in THF-d_8 at R.T.

CdS capped with C16-azide and C10-methyl terminated ligands shows very similar kinetic to CdS capped with C10-azide and C16-methyl terminated ligands (Figures 5a,b). However, the click reaction progress was very slow and only about 10% conversion in the same condition and same catalyst loading when we performed click on CdS capped with C10-azide and C10-methyl terminated ligands (Figure 5c).

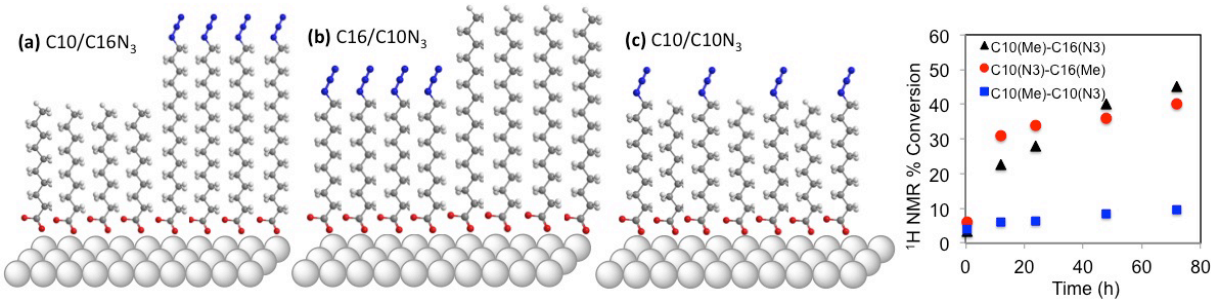

Figure 6. Ligand distribution effect on surface reactivity toward click reaction

Figure 6 shows the click reaction percent conversion driven from ^{1}H NMR over time using the same solvent, catalyst loading and temperature for three different cases we studied. It

seems that local concentration of azide on the surface of nanocrystals comforts accessibility of azide functional group and favors kinetic of click reaction onto the surface.

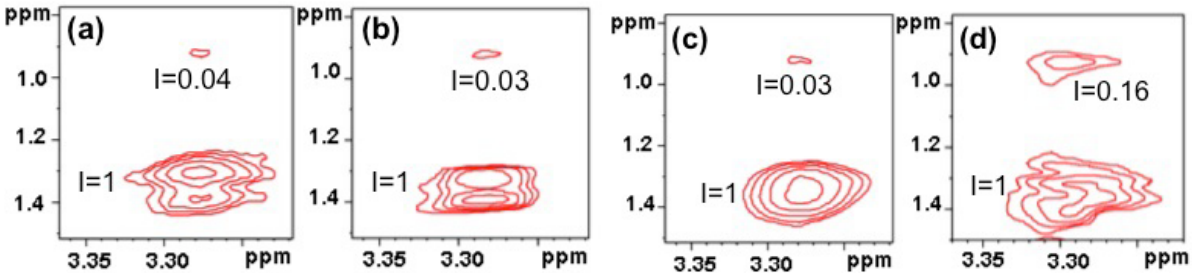

Figure 7. Relative Backbone to hetero correlation ROESY resonance intensity of (a) $C10/C16N_3$, (b) $C16/C10N_3$, (c) $C10N_3$/oleate, and (d) $C10/C10N_3$

Our data clearly shows that ligand distribution has a great impact on the reactivity of the QD's surface. It also further confirms that raft formation increases the local concentration of azide-terminated ligands and facilitates click reaction onto the surface on NC QDs. Figure 7 shows the relative ROESY peak intensity of backbone to hetero correlation for three different systems we studied in this paper.

Conclusions

DOSY spectroscopy shows a rapid ligand exchange on the surface on CdS quantum dots in the presence of free ligands. Attempts to freeze the ligand exchange at low temperature and distinguish free vs. bound ligands diffusion coefficient only resulted in peak smearing. However removing the carboxylate head group which is responsible for the surface binding lead to two separate peaks in the DOSY spectrum related to the differences in the free and bound ligand diffusion coefficients. We performed ROESY to study the effect of length differences on the ligand organization and formation of patterns. This data predicts that when one type of ligand is significantly longer than all others, the longer ligands preferentially align themselves to form the islands. Ligand organization proved to have a

significant affect on the quantum dot surface reactivity. Particles with raft ligand packing participated in click reaction much faster than particles with homogeneous distribution.

Acknowledgements

J.V. gratefully acknowledges the National Science Foundation for funding of this work through the Division of Chemistry (NSF- 1253058).

References

[1] a) M. Brust, M. Walker, D. Bethell, D. J. Schiffrin, R. Whyman, *J. Chem. Soc. Chem. Commun*. **1994**, 801–802; b) P. D. Jadzinsky, G. Calero, C. J. Ackerson, D. A. Bushnell, R. D. Kornberg, *Science* **2007**, *318*, 430–433; c) H. H kkinen, *Nat. Chem*. **2012**, *4*, 443–455.

[2] a) A. Coskun, J. M. Spruell, G. Barin, W. R. Dichtel, A. H. Flood, Y. Y. Botros, J. F. Stoddart, *Chem. Soc. Rev.* **2012**, *41*, 4827–4859; b) R. P. Andres, J. D. Bielefeld, J. I. Henderson, D. B. Janes, V. R. Kolagunta, C. P. Kubiak, W. J. Mahoney, R. G. Osifchin, *Science* **1996**, *273*, 1690–1693; c) C. A. Berven, L. Clarke, J. L. Mooster, M. N. Wybourne, J. E. Hutchison, *Adv. Mater*. **2001**, *13*, 109 – 113.

[3] a) G. A. Somorjai, J. Y. Park, Top. Catal. 2008, 49, 126 –135; b) V. Polshettiwar, R. S. Varma, *Green Chem*. **2010**, *12*, 743–754; c) N. Yan, C. X. Xiao, Y. Kou, *Coord. Chem. Rev*. **2010**, *254*, 1179 –1218; d) H. Lee, C. Kim, S. Yang, J. W. Han, J. Kim, *Catal. Surv. Asia* **2012**, *16*, 14–27; e) C. Mohr, H. Hofmeister, J. Radnik, P. Claus, *J. Am. Chem. Soc*. **2003**, *125*, 1905 –1911; f) L. N. Lewis, *Chem. Rev.* **1993**, *93*, 2693–2730.

[4] a) E. Katz, I. Willner, J. Wang, *Electroanalysis* **2004**, *16*, 19– 44; b) S. W. Zeng, K. T. Yong, I. Roy, X. Q. Dinh, X. Yu, F. Luan, *Plasmonics* **2011**, *6*, 491–506; c) V. K. K. Upadhyayula, *Anal. Chim. Acta* **2012**, *715*, 1–18; d) S. Tokonami, Y. Yamamoto, H. Shiigi, T. Nagaoka, *Anal. Chim. Acta* **2012**, *716*, 76– 91; e) S. R. Emory, W. E. Haskins, S. M. Nie, *J. Am. Chem. Soc*. **1998**, *120*, 8009–8010; f) M. Zayats, A. B. Kharitonov, S. P. Pogorelova, O. Lioubashevski, E. Katz, I. Willner, *J. Am. Chem. Soc*. **2003**, *125*, 16006 –16014.

[5] J. F. Hainfeld, *Science* **1987**, *236*, 450 –453.

[6] a) J. Kane, J. Ong, R. F. Saraf, *J. Mater. Chem*. **2011**, *21*, 16846–16858; b) S. H. Sun, C. B. Murray, D. Weller, L. Folks, A. Moser, *Science* **2000**, *287*, 1989–1992; c) T. Sun, K. Seff, *Chem. Rev*. **1994**, *94*, 857–870.

[7] J. Z. Zhang, Z. L. Wang, J. Liu, S. W. Chen, G.-y. Liu, Self-Assembled Nanostructures, Kluwer, New York, **2003**.

[8] a) A. C. Templeton, M. P. Wuelfing, R. W. Murray, *Acc. Chem. Res*. **2000**, *33*, 27–36; b) M. G. Warner, S. M. Reed, J. E. Hutchison, *Chem. Mater*. **2000**, *12*, 3316–3320; c) R.

Shenhar, V. M. Rotello, *Acc. Chem. Res*. **2003**, *36*, 549–561; d) H. Wellsted, E. Sitsen, A. Caragheorgheopol, V. Chechik, *Anal. Chem*. **2004**, *76*, 2010–2016; e) A. R. Rothrock, R. L. Donkers, M. H. Schoenfisch, *J. Am. Chem. Soc*. **2005**, *127*, 9362–9363.

[9] Song, Y.; Chen, Y. *Chem. Asian J.* **2014**, *9*, 418 – 430.

[10] Ying, H.; Uzun, H.; Dubois, C.; Stellacci, F. *J. Phys. Chem. C* **2008**, *112*, 6279–6284.

[11] Jackson, A. M.; Hu, Y.; Jacob Silva, P.; Stellacci, F. *J. Am. Chem. Soc.* **2006**, *128*, 11135.

[12] Centrone, A.; Hu, Y.; Jackson, A. M.; Zerbi, G.; Stellacci, F. *Small* **2007**, *3*, 814.

[13] Smith, R. K.; Reed, S. M.; Lewis, P. A.; Monnell, J. D.; Clegg, R. S.; Kelly, K. F.; Bumm, L. A.; Hutchison, J. E.; Weiss, P. S. *J. Phys. Chem. B* **2001**, *105*, 1119.

[14] Stranick, S. J.; Atre, S. V.; Parikh, A. N.; Wood, M. C.; Allara, D. L.; Winograd, N.; Weiss, P. S. *Nanotechnology* **1996**, *7*, 438.

[15] Liu, X.; Yu, M.; Kim, H.; Mameli, M.; Stellacci, F. *Nat. Commun*. **2013**, *3*,1182.

[16] Hens, Z.; Martins, J. *Chem. Mater.* **2013**, *25*, 1211−1221.

[17] Hassinen, A.; Gomes, R.; De Nolf, K.; Zhao, Q.; Vantomme, A.; C. Martins, J.; Hens, Z. *J. Phys. Chem. C* **2013**, *117*, 13936−13943.

[18] Morris-Cohen, A. J.; Malicki, M.; Peterson, M. D.; Slavin, J. W. J.; Weiss, E. A. *Chem. Mater.* **2013**, *25*, 1155–1165.

[19] Tavasoli, E.; Guo, Y. J.; Kunal, P.; Grajeda, J.; Gerber, A.; Vela, J. *Chem. Mater.* **2012**, *24*, 4231–4241.

CHAPTER 4

NANOCRYSTAL VALANCY: EFFECT OF SURFACE LOADING ON THE AFFINITY OF STEROID CAPPED GIANT QUANTUM DOTS TOWARD LIPID BILAYERS

Abstract

We incorporated three different steroids onto the surface of fluorophore giant quantum dots through DHLA-PEG ligand exchange method. In particular, we show that we are able to control the loading of cholestanone per quantum dot nanocrystals. Three samples with different percentage loading of cholestanone showed dissimilar affinities towards the synthetic lipid bilayer surface. Since there was almost no interaction between the lipid bilayer and the QDs without cholestanone, we inferred the interaction is due to the cholestanone integrating itself with the lipid bilayer. Particle landing on the lipid membrane is directly proportional to steroid loading. We observed that samples with higher steroid loading infuse themselves more with the lipid membrane compare to those with no or little steroid. Furthermore, we have shown through experiment that we can estimate the number of ligands interacting with the surface and how they affect lateral motion. We also investigated ligand distribution on the nanocrystals surface using 1D gradient ROESY technique for a simulated model system.

Introduction

Nanoparticle interactions with cell membranes play a crucial role in biomedical applications. Controlling the specific interactions and movements of the nanoparticles within biologically relevant systems is of great interest within the fields of biomedicine and

nanomedicine. Therefore, much effort has been put into the functionalization of nanoparticle surfaces for applications such as biosensing, imaging, and molecular delivery.[1]

While there are many routes to change the functionalization of nanoparticles, controlling the surface loading of particles has only been done with a select few molecules at low surface coverage. Interest in controlling specific ligand count on each particle has risen mostly for creating assembly structures with oligonucleotides[2 3 4] and DNA[5 6], but has also been performed with bifunctional polyethylene glycol.[7 8] These particles have been limited with specific loading from single to tens of ligands, and typically need to be separated into their respective ligand count through electrophoresis.

Herein we show that single particle surface loading has biologically relevant consequences by tracking many individual QDs interacting with synthetic lipid membranes.

Experimental

Materials. Polyethylene glycol (PEG) (average MW:600), diethylene glycol (DEG) (99%), (±)-α-lipoic acid (TA) (≥99%), N,N′-dicyclohexylcarbodiimide (DCC) (99%), diisopropyl azodicarboxylate (DIAD), N-Hydroxyphthalimide (97%), hydrazine hydrate (64% hydrazine), 5α-Cholestan-3-one, 4-dimethylamino-pyridine (99%), pyridine anhydrous, methanesulfonyl chloride (99.7%), 4-methylcyclohexanone (99%), triethylamine (Et_3N), and Celite® 503, ε-Caprolactone (97%), trimethylaluminum (97%) were purchased from Aldrich. Tiphenylphosphine was purchased from Alfa Aesar. Sodium chloride (NaCl) and magnesium sulfate ($MgSO_4$, anhydrous) were purchased from Fisher. Diethyl ether, dichloromethane (CH_2Cl_2), and tetrahydrofuran (THF) were purified by passage through activated alumina and "deoxygenating" columns from Vacuum Atmospheres Co. (Hawthorne, CA). Hexane, ethanol, methanol, and ethyl acetate were purchased from Fisher

and used as received. Chloroform-*d* ($CDCl_3$) was purchased from Cambridge Isotopes Laboratories, Inc. TA-PEG600-OH,[9] TA-PEG600 capped giant dots,[9] and CdSe/CdS giant quantum dots.[10] were synthesized following literature procedures. ^{1}H NMR chemical shifts (δ) are reported in ppm relative to residual protiated solvent in $CDCl_3$ (7.26 ppm). ^{13}C NMR spectra are referenced to residual $CDCl_3$ (77.16 ppm).

Synthesis of TA-PEG600/DEG-ONH$_2$ ligands (6)/(14). A solution of diisopropyl azodicarboxylate (1.04 g, 4.95 mmol) in THF (5 mL) was added dropwise to a stirred solution of N-hydroxyphthalimide (900 mg, 5.52 mmol) mixed with triphenylphosphine (1.45 g, 5.52 mmol), and one of the TA-PEG600-OH (2.87 g, 3.68 mmol) or TA-DEG-OH (1.21 g, 4.12 mmol) in THF (50 mL) at 0 °C. The solution was allowed to warm up to room temperature (R.T.) and stirred for 12 h under dry N_2. The solvent was evaporated and the mixture was concentrated under vacuum. The crude was subjected to a reduction step without further purifications.

A solution of hydrazine hydrate (553 mg, 11.0 mmol) for TA-PEG600-ONH$_2$ or (617 mg, 12.3 mmol) for TA-DEG-ONH$_2$ in CH_2Cl_2 (5 mL) was added dropwise to the stirred solution of N-alkoxyphthalimide-terminated PEG/DEG crude product in CH_2Cl_2 (50 mL) at R.T. The solution was allowed to stir for 12 h under dry N_2. The solvent was evaporated and the mixture was concentrated under vacuum. The product was purified by automated column chromatography on silica gel with CH_2Cl_2: MeOH (97:3 (vol/vol)) for TA-PEG600-ONH$_2$ or CH_2Cl_2: EtOAc (50:50 (vol/vol)) for TA-DEG-ONH$_2$ as the eluent. Solvent evaporation yield 2.60 g (3.27 mmol, 91%) of TA-PEG600-ONH$_2$ or 660 mg (2.13 mmol, 51%) of TA-DEG-ONH$_2$. The compound was stored refrigerated in an inert environment. TA-DEG-ONH$_2$: ^{1}H NMR (400 MHz, $CDCl_3$, 22 ºC) δ 4.24 (t, 2H, J = 4.8 Hz); 3.65-3.74 (m, 4H); 3.60 (t, 2H, J

= 4.8 Hz); 3.53-3.58 (m, 1H); 3.07-3.20 (m, 2H); 2.41-2.50 (m, 1H); 2.35 (t, 2H, *J* = 7.6 Hz); 1.85-1.93 (m, 1H); 1.60-1.74 (m, 4H); 1.40-1.52 (m, 2H). ^{13}C NMR (100 MHz, $CDCl_3$, 22ºC) δ 173.57, 74.81, 72.42, 69.59, 63.46, 61.82, 56.41, 40.33, 38.59, 34.70, 34.07, 28.82, 24.74. TA-PEG600-ONH_2: ^{1}H NMR (400 MHz, $CDCl_3$, 22 ºC) δ 5.52 (br s, 2H); 4.21 (t, 2H, *J* = 4.8 Hz); 3.83 (t, 2H, *J* = 4.8 Hz); 3.58-3.71 (m, 48H); 3.51-3.58 (m, 1H); 3.07-3.20 (m, 2H); 2.41-2.50 (m, 1H); 2.33 (t, 2H, *J* = 7.6 Hz); 1.85-1.93 (m, 1H); 1.60-1.74 (m, 4H); 1.36-1.52 (m, 2H). ^{13}C NMR (100 MHz, $CDCl_3$, 22 ºC) δ 173.57, 74.84, 70.72, 69.70, 69.25, 63.55, 56.41, 40.30, 38.56, 34.68, 34.02, 28.82, 24.74.

Synthesis of TA-PEG600-Cholestanone or TA-PEG600-Castatsterone-terminated ligands (7, 8, 10). A solution of 5α-Cholestan-3-one (4 mg, 0.0107 mmol) or Castatsterone (5 mg, 0.0107 mmol) or 3-methylcyclohexanone (2 mg, 0.0178 mmol) in anhydrous pyridine (1mL) was added to the stirred solution of TA-PEG600-ONH_2 (9 mg, 0.0113 mmol) at R.T. and the reaction mixture was stirred under dry N_2. After 7 days, for steroid or 12h for cyclohexanone, solvent was pumped down and the crude product was concentrated under vacuum to give 12 mg of cholestanone- or 13 mg of Castatsterone- or 10 mg of methylcyclohexane-terminated PEG as yellow oil. TA-PEG600-Cholestanone: ^{1}H NMR (400 MHz, $CDCl_3$, 22 ºC) δ 4.19 (t, 2H, *J* = 4.8 Hz); 4.10 (t, 2H, *J* = 5.0 Hz); 3.64-3.69 (m, 4H); 3.60-3.61 (m, 42H); 3.50-3.56 (m, 1H); 3.04-3.17 (m, 2H); 2.33-2.46 (m, 1H); 2.31 (t, 2H, *J* = 7.4 Hz); 1.85-1.93 (m, 1H); 1.60-1.74 (m, 4H); 1.36-1.52 (m, 2H). ^{13}C NMR (100 MHz, $CDCl_3$, 22ºC) δ 173.57, 74.84, 70.72, 69.70, 69.25, 63.55, 56.41, 40.30, 38.56, 34.68, 34.02, 28.82, 24.74. TA-PEG600-castasterone: ^{1}H NMR (400 MHz, $CDCl_3$, 22ºC) δ 4.21 (t, 2H, *J* = 4.8 Hz); 4.13 (t, 2H, *J* = 5.0 Hz); 3.52-3.71 (m, 42H); 3.50-3.56 (m, 1H); 3.06-3.22 (m, 2H); 2.40-2.48 (m, 1H); 2.33 (t, 2H, *J* = 7.4 Hz); 2.14-2.18 (m, 2H); 1.96-2.05 (m, 1H); 1.85-1.95

(m, 6H); 1.50-1.74 (m, 4H); 1.36-1.52 (m, 4H); 1.22 (s, 3H); 0.80-0.95 (m, 4H); 2.40-2.48 (m, 1H); 0.73 (s, 3H); 0.66 (s, 3H). ^{13}C NMR (100 MHz, $CDCl_3$, 22 ºC) δ 173.57, 160.53, 74.64, 70.72, 69.70, 69.25, 63.45, 61.66, 56.31, 42.45, 40.20, 38.46, 37.71, 36.80, 34.58, 33.91, 32.01, 30.72, 29.66, 28.72, 25.78, 25.37, 24.58, 20.73, 13.56, 11.90, 10.11. TA-PEG600-methylcyclohexanone: ^{1}H NMR (400 MHz, $CDCl_3$, 22ºC) δ 4.20 (t, 2H, J = 4.6 Hz); 4.13 (t, 2H, J = 4.8 Hz); 3.70-3.65 (m, 2H); 3.45-3.63 (m, 40H); 3.51-3.58 (m, 1H); 3.07-3.19 (m, 2H); 2.40-2.48 (m, 2H); 2.33 (t, 2H, J = 7.4 Hz); 1.95-2.00 (m, 2H); 1.86-1.91 (m, 1H), 1.74-1.83 (m, 2H); 1.58-1.70 (m, 4H); 1.41-1.54 (m, 4H); 1.16-1.36 (m, 4H); 1.00-1.14 (m, 4H), 0.92-1.01 (m 2H); 0.63 (s, 3H). ^{13}C NMR (100 MHz, $CDCl_3$, 22 ºC) δ 173.39, 160.28, 72.49, 70.55, 69.68, 69.13, 63.44, 61.69, 56.21, 53.90, 46.60, 45.32, 42.51, 40.19, 39.92, 39.47, 38.45, 37.33, 36.05, 35.75, 34.57, 33.91, 31.78, 28.70, 27.97, 24.58, 24.17, 23.79, 22.80, 22.54, 21.18, 18.64, 12.04, 11.3133.96, 28.64, 28.46, 28.25, 24.60, 22.29.

Synthesis of TA-PEG600-hydroxyamide (11). (25 uL, 0.0188 mmol) trimethylaluminum was added to the stirred solution of capralactone (8 mg, 0.0700 mmol) and TA-PEG600-ONH_2 (50 mg, 0.0629 mmol) in 2 mL CH_2Cl_2 at 0 °C. Reaction mixture was warmed up to R.T. and stirred for 1 h. The crude product was washed with 2×10 mL brine and extracted by DCM. The organic layer was dried over $MgSO_4$ and concentrated by vacuum to give 35 mg (60% yield) of product as yellow oil. TA-PEG600-hydroxyamide: ^{1}H NMR (400 MHz, $CDCl_3$, 22 ºC) δ 4.34 (t, 2H, J = 4.6 Hz); 4.13 (t, 2H, J = 4.8 Hz); 3.90-3.91 (m, 1H); 3.70-3.73 (m, 2H); 3.45-3.63 (m, 42H); 3.50-3.56 (m, 1H); 2.97-3.10 (m, 2H); 2.66-2.69 (m, 2H); 2.32-2.39 (m, 2H); 2.30 (t, 2H, J = 7.4 Hz); 1.76-1.82 (m, 2H); 1.66-1.75 (m, 4H); 1.52-1.61 (m, 4H); 1.31-1.42 (m, 2H). ^{13}C NMR (100 MHz, $CDCl_3$, 22 ºC) δ 183.95, 174.54, 160.53,

74.49, 72.55, 68.90, 64.15, 59.11, 56.34, 53.22, 40.21, 38.50, 34.52, 34.37, 33.96, 28.64, 28.46, 28.25, 24.60, 22.29.

Synthesis. Synthesis of TA-DEG-OH ligand (12). A solution of lipoic acid (3.00g, 0.0145 mol) in CH_2Cl_2 (5 mL) was added dropwise within 20 min to the stirred solution of diethylene glycol (DEG) (15.4 g, 0.145 mol) mixed with DMAP (0.53 g, 4.35 mmol) and DCC (3.30 g, 0.0159 mol) in CH_2Cl_2 (50 mL) at 0 °C. The solution was kept at this temperature for 2 h, warmed up to R.T., and stirred for 24 h under dry N_2. The mixture was filtered through Celite® 503, washed with saturated aqueous $NaHCO_3$, and extracted by ether (3 × 50 mL). The solution was dried over anhydrous $MgSO_4$, filtered and concentrated under vacuum and subjected to column chromatography on silica gel with CH_2Cl_2: EtOAc (100:30 (vol/vol)) as the eluent to yield 2.80 g (9.52 mmol, 51 %) of ligand as a yellow oil. ^{1}H NMR (400 MHz, $CDCl_3$, 22 ºC) δ 4.24 (t, 2H, *J* = 4.8 Hz); 3.74 (t, 2H, *J* = 4.6 Hz); 3.70 (t, 2H, *J* = 4.6 Hz); 3.60 (t, 2H, *J* = 4.8 Hz); 3.53-3.58 (m, 1H); 3.08-3.20 (m, 2H); 2.42-2.50 (m, 1H); 2.35 (t, 2H, *J* = 7.6 Hz); 1.86-1.94 (m, 1H); 1.62-1.74 (m, 4H); 1.40-1.55 (m, 2H). ^{13}C NMR (100 MHz, $CDCl_3$, 22 ºC) δ 173.59, 72.43, 69.26, 63.46, 61.85, 56.46, 40.35, 38.61, 34.70, 34.07, 28.84, 24.74.

Synthesis of mesyl-terminated DEG ligands (13). A solution of methanesulfonyl chloride (875 mg, 7.64 mmol) in CH_2Cl_2 (5 mL) was added dropwise to the stirred solution of TA-DEG-OH (1.50 g, 5.09 mmol) mixed with triethylamine (1.54 g, 15.27 mmol) in CH_2Cl_2 (50 mL). The solution was stirred for 24 h under dry N_2 at R.T. The mixture was then diluted with water (100 mL) and organic layer was washed with 1M HCl (2 × 50 mL) and neutralized with brine (2 × 50 mL). Combined organic layers was then dried over anhydrous $MgSO_4$, filtered and concentrated under vacuum to yield 1.50 g (4.03 mmol, 79 %) of ligand

as a yellow oil. ^{1}H NMR (400 MHz, $CDCl_3$, 22 ºC) δ 4.37 (t, 2H, *J* = 4.4 Hz); 4.23 (t, 2H, *J* = 4.8 Hz); 3.76 (t, 2H, *J* = 4.4 Hz); 3.71 (t, 2H, *J* = 4.8 Hz); 3.60 (t, 2H, *J* = 4.8 Hz); 3.53-3.60 (m, 1H); 3.09-3.20 (m, 2H); 3.05 (s, 3H); 2.42-2.50 (m, 1H); 2.35 (t, 2H, *J* = 7.6 Hz); 1.86-1.94 (m, 1H); 1.62-1.74 (m, 4H); 1.40-1.55 (m, 2H). ^{13}C NMR (100 MHz, $CDCl_3$, 22 ºC) δ 173.44, 69.43, 69.06, 63.25, 61.85, 56.46, 40.35, 38.61, 37.80, 34.70, 34.03, 28.84, 24.72.

Synthesis of 4-methylcyclohexanone-terminated DEG ligands (15). 4-methylcyclohexanone (275 mg, 2.45 mmol) was added to the stirred solution of TA-DEG-ONH_2 (800 mg, 2.58 mmol) in anhydrous pyridine (1.5 mL) under inert condition. The solution was stirred for 24 h under dry N_2 at 60 °C. The mixture was then concentrated under vacuum to yield 500 mg (4.03 mmol, 48 %) of ligand as a yellow oil. ^{1}H NMR (400 MHz, $CDCl_3$, 22 ºC) δ 4.22 (t, 2H, *J* = 4.8 Hz); 4.15 (t, 2H, *J* = 4.8 Hz); 3.72 (t, 2H, *J* = 4.8 Hz); 3.70 (t, 2H, *J* = 4.8 Hz); 3.60 (t, 2H, *J* = 4.8 Hz); 3.54-3.58 (m, 1H); 3.08-3.20 (m, 2H); 2.42-2.48 (m, 1H); 2.35 (t, 2H, *J* = 7.6 Hz); 2.04-2.10 (m, 1H); 1.86-1.94 (m, 1H); 1.83-1.87 (m, 2H); 1.74-1.80 (m, 2H); 1.62-1.74 (m, 4H); 1.59-1.63 (m, 2H); 1.40-1.55 (m, 2H), 1.04-1.18 (m, 2H); 0.93 (d, 3H, *J* = 6.6 Hz);. ^{13}C NMR (100 MHz, $CDCl_3$, 22 ºC) δ 173.59, 160.60, 72.60, 69.79, 69.26, 63.67, 61.85, 56.46, 40.35, 38.61, 35.13, 34.74, 34.09, 33.91, 32.07, 31.62, 28.87, 24.75, 21.70.

Cap exchange of dioctylamine-capped CdsSe/Cds QDs with TA-PEG600 or TA-DEG-based ligands. 0.5 mL of crude CdS/CdSe was diluted with chloroform and precipitated with a minimum amount of methanol. The precipitate was dried under vacuum for 1 hour. 0.65 mmol of pure ligand or mixed ligands (1%, 10%, and 25% steroid) was dissolved in 0.5 mL of ethanol for PEG or chloroform for DEG and then added to the precipitate. The vial was then sealed and purged with nitrogen for 5 min. The mixture was allowed to stir for 4 h

under UV lamp (350 nm). Once homogenized, adding a mixture of hexane and chloroform for PEG-derivetized or methanol for DEG-derivetized QDs. The turbid mixture was centrifuged for 10 min to precipitate the sample. Washing cycle was repeated another time to remove the excess of free ligands.

Optical Characterization. *Absorption spectra* were measured with a photodiode-array Agilent 8453 UV-Vis spectrophotometer. Solvent absorption was recorded and subtracted from all spectra. *Steady-state photoluminescence* (PL) spectra were measured with a Horiba-Jobin Yvon Nanolog scanning spectrofluorometer equipped with a photomultiplier detector. Nanocrystal quantum dots were diluted in chloroform to give an optical density of 0.05-0.2 at 390 nm. Excitation wavelength was 350 nm, and emission was recorded between 365 and 685 nm. *Vibrational infrared spectra* were recorded with a Bruker IFS66V FT-IR spectrometer equipped with a DTGS detector with 64 scans at a resolution of 4 cm^{-1}. Samples were prepared as either drop cast thin films on KBr plates or solid KBr pellets. Background spectra were collected and subtracted under identical conditions. During spectral collection, samples were continuously purged with dry N_2 to minimize water vapor absorbance.

Structural Characterization. *Transmission Electron Microscopy*. TEM was conducted on carbon-coated copper grids using an FEI Tecnai G2 F20 field emission scanning transmission electron microscope (STEM) at 200 kV (point-to-point resolution <0.25 nm, line-to-line resolution <0.10 nm). Elemental composition was characterized by energy-dispersive spectroscopy (EDS). *Particle Analysis*. Dimensions were measured manually or with ImageJ for >50-100 particles. Averages are reported ± standard deviations.

NMR characterization. All NMR spectra were carried out on a Varian 400MR spectrometer operating at a ^{1}H frequency of 399.80 MHz and ^{13}C frequency of 100.51 MHz

equipped with a oneNMR pulse-field-gradient probe. All spectra were recorded using standard pulse sequences from the VNMRJ 3.1 pulse program library. The 1D ^{1}H NMR spectra were recorded with a spectral width of 12.00 ppm, 16 scans, and a 2 s relaxation delay (d_1) between scans. The ^{13}C NMR spectra were recorded with a spectral width of 12.00 ppm, 16 scans, and a 2 s relaxation delay (d_1) between scans. Single-pulse ^{1}H spin−lattice relaxation measurements (10 scans) were recorded with a pulse width of 200 μs and a recycle delay of 12 s. DOSY. Diffusion ordered spectroscopy (DOSY) experiments were collected using a Bruker DRX 400 spectrometer operating at a ^{1}H frequency of 400.39 MHz equipped with normal geometry probe. Spectra were recorded using standard pulse sequences from TopSpin 1.3 pulse program library. The duration of the magnetic field pulse gradients (δ) was optimized for each diffusion time (Δ) to obtain a signal decay of roughly 90% at the maximum gradient strength. A series of 16 spectra with 32,768 data points in each spectrum were collected. In each pulsed-field gradient NMR experiment, the value of δ was set to 1.2 ms (gradient duration), and the value of Δ (diffusion time) was set to 200 ms. The gradient strength was ramped from 2 to 95% of the maximum strength using a sine gradient shape. ROESY. Rotating-frame Overhauser Effect Spectroscopy (ROESY) experiments were recorded using an Avance III 600 spectrometer operating a ^{1}H frequency of 600.39 MHz equipped with 5 mm BBFO Smart Probe. Spectra were recorded using standard pulse sequences from TopSpin 3.0 pulse program library. ROESY spectra were collected using a spin lock time of 200 ms and 256 t_1 increments, with each t_1 slice consisting of 36 scans and 1024 sampled data points, each recorded at a 2 s relaxation delay.

Single Quantum Dot Affinity Studies. The instrument used was a homebuilt prism-based total internal reflection fluorescent microscope (TIRFM) previously described.[11]

Samples were illuminated using a 532-nm CW laser (Gem model, LaserQuantum, San Jose, CA) with power set at 50 mW. A 532-nm RazorEdge long pass filter (Semrock, Rochester, NY) was placed between the sample and the Andor iXon^{EM}+ 897 EMCCD camera (Belfast, Northern Ireland; 512 × 512 imaging array, 16 μm × 16 μm pixel size). All videos were recorded at 50 ms exposure in frame transfer mode with gain set to 100.

Samples were imaged in a quartz micro-chamber. Two strips of double-sided tape 50 μm thick (3M) were placed on a clean 25 mm × 51 mm quartz microscope slide (SPI, West Chester, PA) to use as spacers. A clean Corning (Lowell, MA) 22 mm × 22 mm glass slide was then place on top of the tape to complete the chamber. To create the bilayer, lipid solution was flowed into the chamber and allowed to incubate at room temperature for 20 min. The chamber was first rinsed with two chamber volumes of PBS buffer (pH 7.4) followed by two chamber volumes of 1 mg/ml BSA solution.

Raw QD samples were diluted to an appropriate concentration using high purity 18-MΩ MilliQ water before one chamber volume of diluted solution was injected. The ends of the chamber were then sealed with a thin strip of one-sided tape to reduce solution evaporation and placed under the microscope. The sample was then allowed to sit for 30 minutes to reach surface-binding equilibrium. Before data collection the autofluorescence of the lipid bilayer was bleached for 5 minutes under 532-nm illumination.

Synthetic Lipid Bilayer Preparation. Lipid films composed of 1-palmitoyl-2-oleoyl-sn-glycero-3-phosphocholine (POPC, Avanti Polar Lipids) were prepared following the published procedure[12] with the exceptions that no Texas-Red DHPE was used due to the fluorescence overlap.

Diffusion Calculation. A particle tracking plugin for ImageJ developed by the MOSAIC Group was used in the image analysis software ImageJ to produce time traces of multiple QDs. The resulting traces were filtered to only traces longer than 100 frames recorded at 50 ms exposure time in frame transfer mode. The sub-pixel localization was then used to calculate the mean squared displacement (MSD) for each particle. The diffusion coefficient was calculated using the linear portion of the MSD and averaged for more than 100 particles for both the 10% and 25% cholestanone samples.

Determining Particle Drag. The particles were assumed to have an even distribution of cholestanone attached to the QD surface. Since there was almost no interaction between the lipid bilayer and the QDs without cholestanone, we inferred the interaction is due to the cholestanone integrating itself with the lipid bilayer. The diffusion coefficient of a QD in a water environment with a hydrodynamic radius r = 13.45 nm was calculated from equation 1.

$$D_t = \frac{k_b T}{6\pi\eta_w r}$$

The resulting lateral diffusion of the QDs in water (η_w = 1 cP) D_t = 16.04 μm^2/s. Since our measured values for both samples are two orders of magnitude lower we expect there to be much surface interaction.

To estimate the diffusion coefficient of QDs interacting with the surface membrane, we calculated the drag force using the Einstein relation (equation 2).

$$D_t = \frac{k_B T}{f}$$

where f is the sum of the drag forces induced on the particle from both water f_w and the force of the ligands f_{lig}. The drag force of water upon the QDs can be calculated from equation 3.

$$f_w = \frac{2k_B T}{D_t}$$

The estimation of the drag force of cholestanone molecules incorporating into the surface was calculated by the Saffman-Delbruck model.[13] We assumed the molecule to be a cylinder with a radius r_{lip} = 0.25 nm and height h = 1.9 nm. The drag force can then be calculated from equation 4 below.

$$f_{lip} = 4\pi\eta_m h \left(\ln \frac{\eta_m h}{\eta_w r_{lip}} - \gamma_E \right)^{-1}$$

where η_m is the viscosity of the membrane (200 cP) and γ_E is the Euler constant.

We next need to calculate the amount of cholestanone ligands we can expect to find interacting with the membrane surface. The total amount of ligands per nanocrystal is estimated to be ~2500. Assuming the cholestanone will integrate into the membrane to its full height h = 1.9 nm, an inverted "dome" with diameter d = 9.6 nm will come into contact with the membrane surface resulting in a contact area that is 13.2% of the QDs total surface area as seen in equation 5.

$$\frac{A_{con}}{A_{tot}}(100) = \frac{h^2 + \left(\frac{d}{2}\right)^2}{4r_{QD}^2}$$

where A_{con} is the particle contact area, A_{tot} is the total are of the QD, and r_{QD} is the radius of the QD. For the QD-10 sample we find that there are ~33 cholestanone ligands available to interact with the membrane surface, while there are ~83 for the QD-25 sample.

If N is the number of cholestanone molecules interacting with the surface we can calculate the diffusion coefficient for the cholestanone QDs using equation 6.

$$D_t = \frac{k_B T}{f_w + N \cdot f_{lip}}$$

We find that if N = 33 cholestanone molecules, D_t = 0.170 μm^2/s, which agrees well with the measured D_t = 0.179 ± 0.453 μm^2/s for sample QD-10. If N = 83 cholestanone molecules D_t = 0.068 μm^2/s, which is also in good agreement with the measured D_t = 0.041 ± 0.226 μm^2/s for QD-25.

Results and Discussion

Figure 1 show the chemical structures of three steroid aimed to study in this paper.

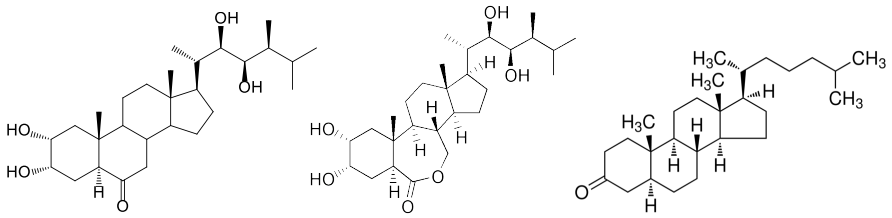

Figure 1. Chemical structure of steroids

Scheme 1 shows the synthesis of TA-PEG600-steroid terminated ligands for surface modification of CdSe/CdS giant dots. Compound **4** was prepared previously by DCC coupling of lipoic acid and polyethylene glycol (Mw=600).[14] This approach provides the bidentate chelate interactions with the QD surfaces afforded by the dithiolane ring, in addition to with hydrophilic nature of the PEG chain to maintain water solubility. Compound **4** was subjected to the Mitsunobu reaction condition using PhthNOH as a nucleophile and DEAD and PPh_3 as activators. Subsequent hydrazinolysis of **5** produced desired compound **6** in 91% yield from **4.** Treatment of alkoxyamine **6** with castasterone **1**, or 5-a-cholestane-3-one **3** in dry pyridine for several days at R.T., gave rise to the desired TA-PEG600-steroid-terminated ligands **7** and **8**. Corresponding ^{1}H NMR, ^{13}C NMR, and MS for all the intermediates as well as final ligands are reported in the supporting information.

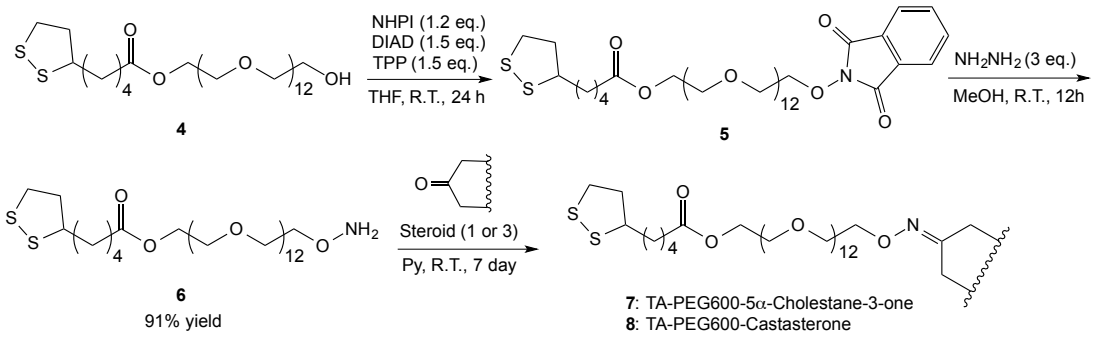

Scheme1. Synthesis of steroid terminated ligands

The fourier transform infrared spectra in Figure 2 show the transformation of hydroxyl functional group in **4** to alkoxyamine **6** and then to oxime **7**or **8**.

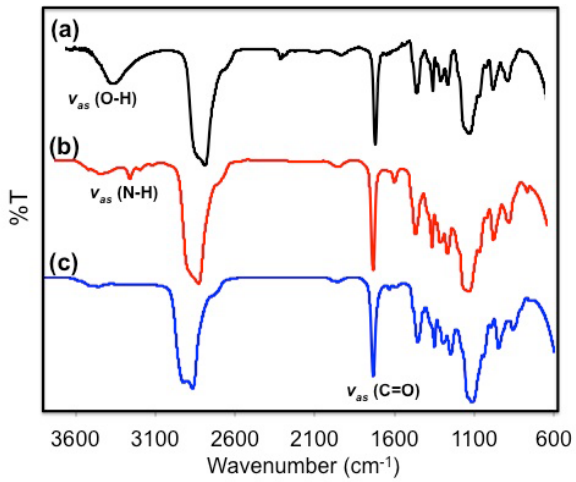

Figure 2. Infrared spectra of transformation from (a) hydroxy (**4**) to (b) alkoxyamine (**6**) to (c) oxime (**10**) terminated ligand

In Scheme 2 we demonstrate photo-mediated phase transfer of luminescent CdSe/CdS giant quantum dots from hydrophobic to polar and hydrophilic media as a result of the cap exchange. In particular, we used UV-irradiation (λ =350nm) to promote the in situ ligand exchange on hydrophobic CdSe QDs with mixture of TA-PEG600-hydroxyl terminated **4** and TA-PEG600-cholestanone terminated **7** ligands and facilitate QD transfer to polar

solvents such as ethanol. By varying the ratio of **4** to **7** during the thiol cap exchange process we were able to label the corresponding QDs with as low as 1% and as high as 35% cholestanone. Scheme 2b shows that PL quenched after the cap exchange however the QDs are still fluorescent.

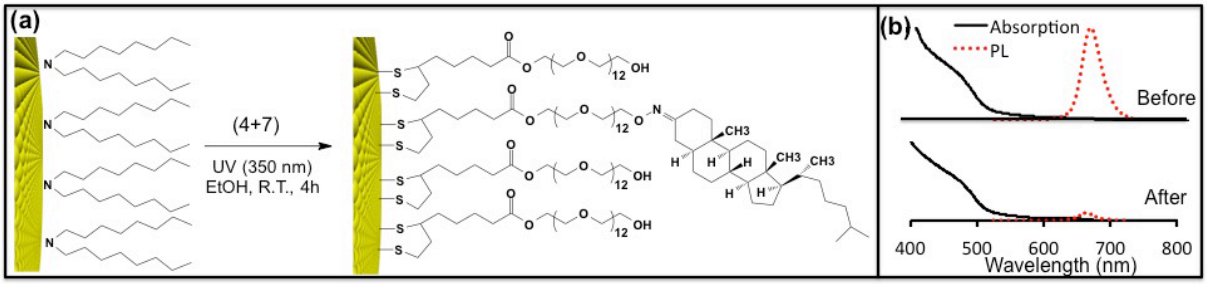

Scheme 2. (a) Thiol ligand exchange to introduce 1-35% of 5α-Cholestan-3-one onto the surface. Mixture of ligands was used to keep the water solubility. (b) Absorption and emission (at 510 nm) of CdSe/CdS quantum dots before and after ligand exchange

The cholestanone modified QDs lipid bilayer interactions were studied using a homebuilt prism-based total internal reflection fluorescence (TIRF) microscope. Cholesterol is a known component of cell membranes[15] and its derivative cholestanone is known to incorporate itself into synthetic lipid bilayers.[16] We found that QDs modified with cholestanone bind to the surface with much higher affinity than QDs modified only with PEG.

We studied three samples of QDs on a synthetic 1-palmitoyl-2-oleoyl-*sn*-glycero-3-phosphocholine (POPC) lipid bilayer; QDs functionalized with 100% PEG (QD-PEG), QDs functionalized with 10% cholestanone and 90% PEG, (QD-10), and QDs functionalized with 25% cholestanone and 75% PEG (QD-25). Synthetic POPC membranes were prepared in quartz chambers that allowed the injection of dilute QD solutions. Once the samples were

prepared and placed under the microscope, they were incubated for 45 minutes to allow the QD adsorption and desorption rates to reach equilibrium (Figure 3).

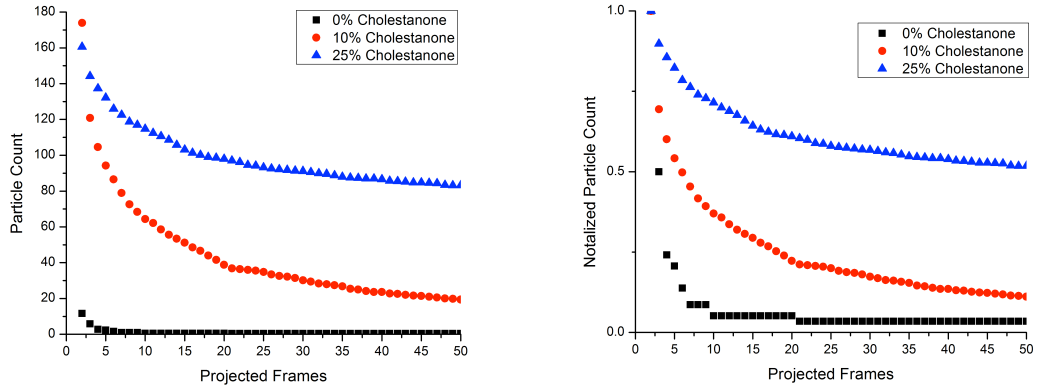

Figure 3. Adsorption and desorption rates to reach equilibrium for three samples with 0% steroid in black, 10% steroid in red, and 25% steroid in blue.

With incubation complete the sample was illuminated for an additional 5 minutes with 532-nm laser illumination under TIRF to reduce the lipid auto-fluorescence before data was collected. A 532-nm long pass filter was placed between the sample and the EMCCD which recorded QD emission at 50 ms exposure under frame transfer mode.

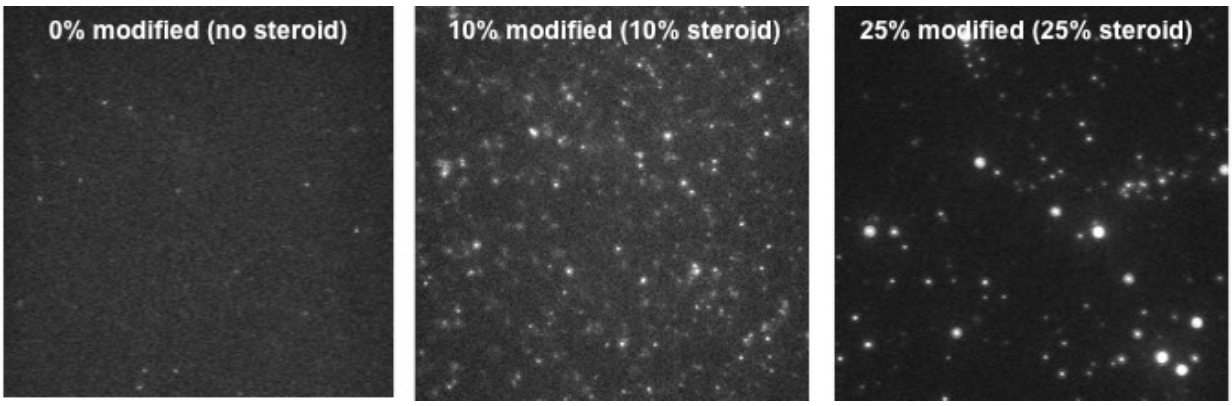

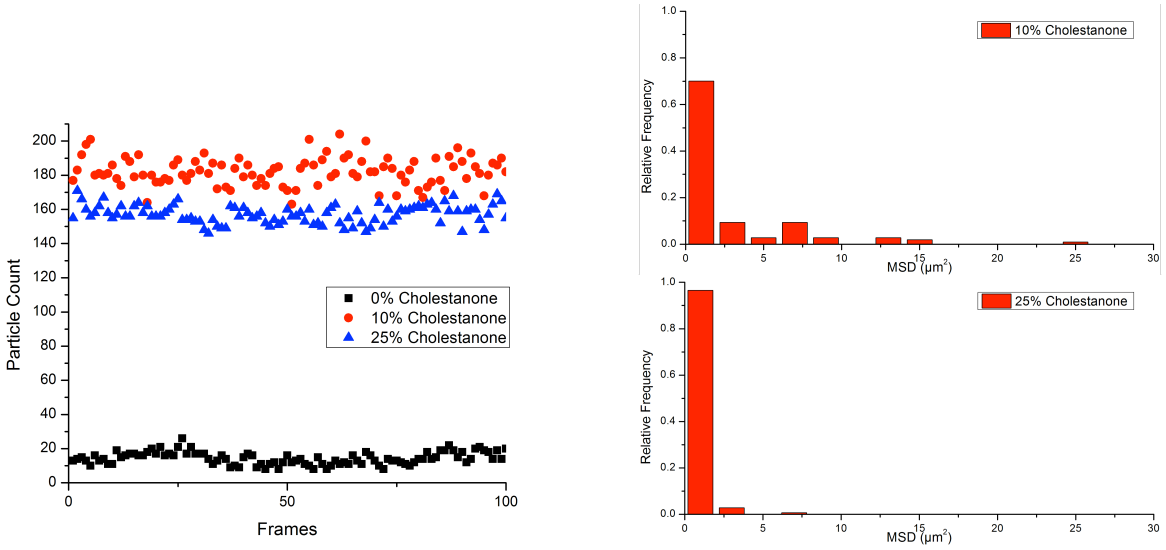

Figure 4. Landing and lateral diffusion of 5-α-cholestane-3-one-modified thick-shelled CdSe/14CdS QDs on a lipid bilayer (TIRF)

As shown in Figure 4, the three samples show differing affinities towards the surface. Samples QD-10 and QD-25 show a much higher particle density on the lipid surface compared to QD-PEG, which shows very little coverage. Since both the PEG and cholestanone terminated groups are neutral in charge, the affinity for the particles to incorporate themselves on the surface lies in the ability of the cholestanone to infuse itself with the lipid membrane.

The coverage of the QDs with the cholestanone also affects the adsorption and desorption of the particles. Sample QD-10, while in equilibrium, desorbs at a faster rate (8.4 particles/s·100 μm^2) compared to the QD-25 sample (2.8 particles/s·100 μm^2). This corresponds to the lateral diffusion coefficients calculated for the cholestanone samples. Using an ImageJ plugin over 100 single particle trajectories were used to calculate the mean square displacements (MSD). Following $MSD(t) = 4D_t t$ we find the lateral diffusion coefficient $D_t = 0.179 \pm 0.453$ $\mu m^2/s$ for QD-10 and $D_t = 0.041 \pm 0.226$ $\mu m^2/s$ for QD-25. We

suspect the cholestanone acts as anchoring points in the lipids for each of the nanoparticles, and the increased ratio allows for more anchors. To investigate the effects the cholestanone has on the lateral diffusion of the molecule on the lipid membrane we performed the following calculations.

In water the lateral diffusion coefficient of the QDs treated as a sphere with a hydrodynamic diameter of 26.9 nm is calculated to be 16.04 $\mu m^2/s$. While interacting with the lipid membranes, the QDs experience a greatly reduced lateral diffusion coefficient. As the cholestanone incorporates itself into the lipid membrane each molecule will produce a drag on the motion of the particle. To calculate the increased drag due to the cholestanone we used a method similar to Pierrat *et al.*[12]

The particle has a loading capacity of ~2500 ligands creating a sphere 26.9 nm in diameter. Each cholestanone was treated as a cylinder that incorporated itself into the membrane with a radius of 0.5 nm and a height of 1.9 nm. Under these conditions the QD can "sink" into the membrane surface 1.9 nm increasing the surface contact area to 15.3% of the total particle. Sample QD-10 will therefore have ~38 ligands interacting with the membrane surface creating enough drag to slow the lateral diffusion to $D_t = 0.170\ \mu m^2/s$, while sample QD-25 have ~96 ligands that will slow it to $D_t = 0.068\ \mu m^2/s$. These numbers are in good agreement with the measured values.

Figure 5 shows T1 relaxation time measured from the ^1H NMR spectra of QDs capped with 100% hydroxyl terminated TA-PEG600, 100% cholestanone terminated TA-PEG600, and 50%-50% mixture of two ligands. In general bound ligands relax much faster than the free ligands base on the collected T1 relaxation data. We also looked at NMR analysis of

mixtures utilizing Pulsed Gradient Spin Echo (PGSE) NMR, called Diffusion Ordered SpectroscopY (DOSY).

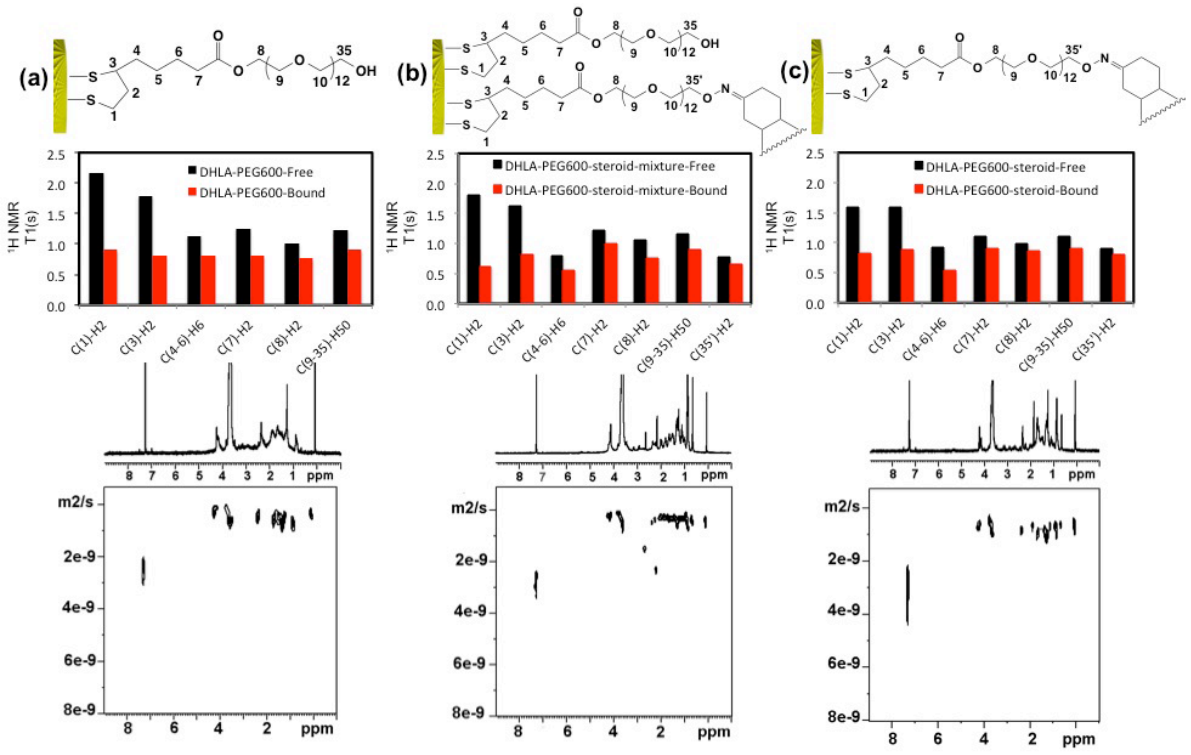

Figure 5. ^{1}H NMR T1 relaxation times and representative DOSY spectra of CdSe/CdS nanocrystal quantum dots capped with (a) 0% steroid, (b) 50% steroid, and (c) 100% cholestanone-terminated ligand

This method relies on the different rates of diffusion of molecules through a solution, due to the inherent difference in the physical properties, to separate the components making up the mixture. The diffusion rate of these capped systems in the chloroform-*d* solution at R.T. assured absence of any free ligands.

As another example of steroid capped QDs that can be used for cell imaging, we synthesized castasterone terminated QDs applying the UV-induced thiol ligand exchange method to transfer the QDs from hydrophobic to hydrophilic media using a mixture of **4** and

8. Emission spectrum of the corresponding dots slightly quenched after ligand exchange (Scheme 3).

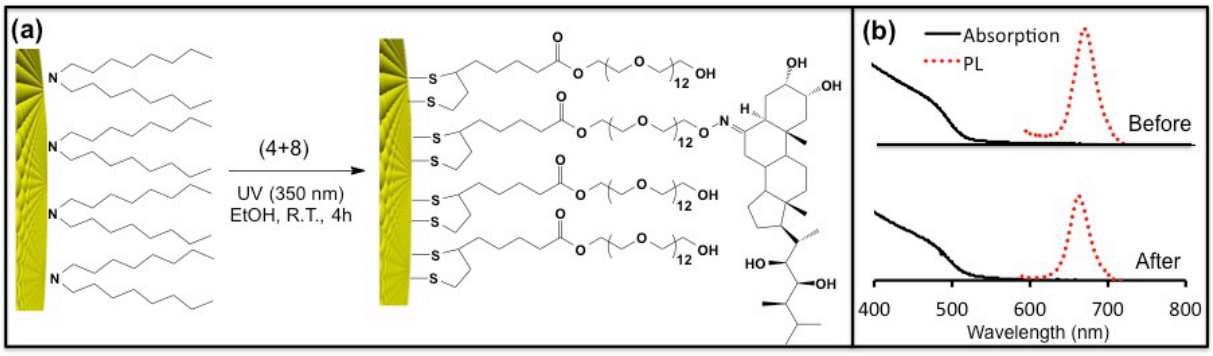

Scheme 3. (a) Thiol ligand exchange to introduce castasterone onto the surface. Mixture of ligands was used to keep the water solubility. (b) Absorption and emission (at 510 nm) of CdSe/CdS quantum dots before and after ligand exchange

Brassinolide **2** was another steroid of interest in our study. We planned to labeled our QDs with Brassinolide for further imaging applications however presence of a lactone ring in the structure of this compounds limited the coupling with alkoxyamine ligand.

To investigate the behavior of 7-membered lactone ring in the condensation reaction with alkoxyamine, we performed a control experiment in which we looked at products of condensation reaction between caprolactone (as a model substrate) and oxyamine terminated TA-PEG600 ligand. ^{1}H NMR and ^{13}C NMR in combination with mass spectroscopy techniques confirmed that there are some condensation products however majorities are the ring-opening product. Scheme 4 shows a condensation of TA-PEG600-oxyamine with 3-methylcyclohexanone *vs.* ring opening with caprolactone.

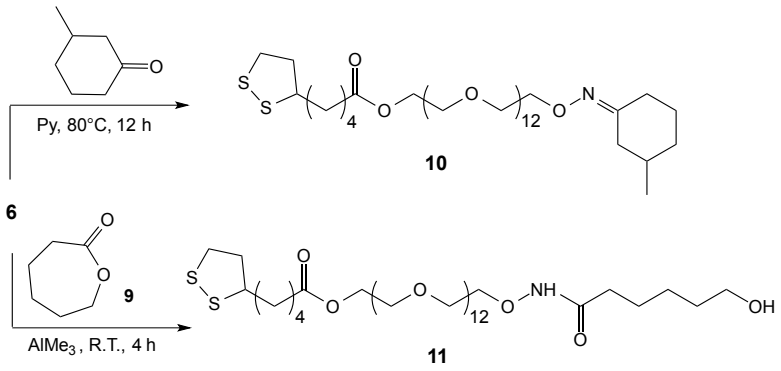

Scheme 4. TA-PEG600-oxyamine condensation with cyclohexanone *vs.* ring opening with caprolactone

The next goal of this study was to look at the surface ligand distribution of modified QDs. Unfortunately we were not able to collect good, high resolution ^{1}H NMR and subsequently ROESY of CdSe/CdS giant QDs capped with PEG600 based ligands due small ligand to surface ratio. Therefore, we designed a model system consisting of small CdS QDs (5nm) to represent CdSe/CdS core/shell giant QDs, short chain cyclohexane terminated TA-DEG (**15**) to represent steroid terminated TA-PEG600 ligands (**7** or **8**), and short chain mesyl terminated TA-DEG capping ligands (**13**) to represent hydroxy terminated TA-PEG600 (**4**) ligands. Scheme 5 shows the synthesis pathway for preparation of mesyl terminated TA-DEG (**13**) and cyclohexane terminated TA-DEG ligands (**15**). The mesyl group in the model system (**13**) was introduced instead of hydroxyl group in the original system (**4**) in order to move the corresponding alpha proton resonances away from the backbone proton peaks and make it easier to track by NMR.

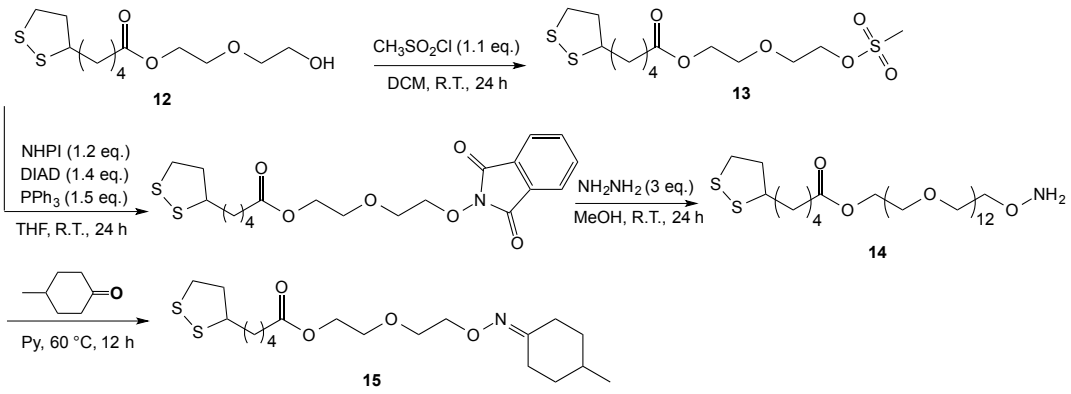

Scheme 5. Synthesis of short chain model ligands for surface distribution study

Scheme 6 shows thiol ligand exchange to introduce 50%-50% mixture of short chain model ligands onto the surface of small 5 nm CdS.

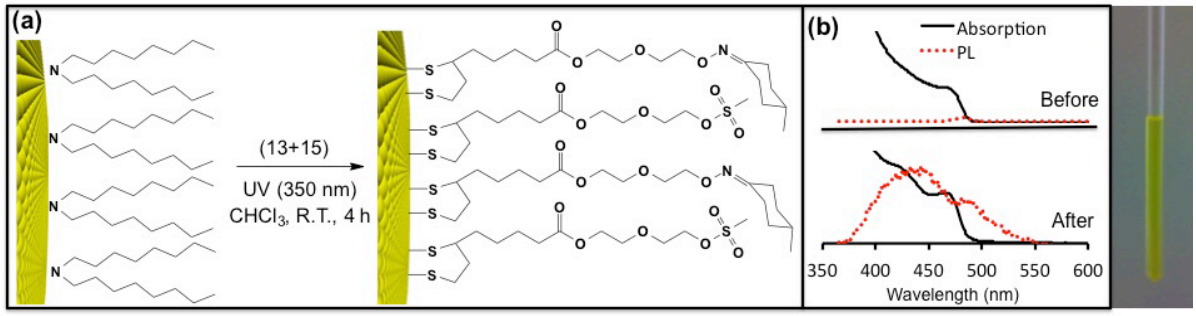

Scheme 6. (a)Thiol ligand exchange, and (b) absorption and emission (at 350 nm) of CdSe/CdS quantum with 50%-50% mixture of ligands on the surface.

As we expected, decreasing the size of the QD helped to increase ligand to surface ratio and resulted in a system that is detectable by NMR. Figure 5 shows T1 relaxation time, ^{1}H NMR, and DOSY of the CdS capped with the 50%-50% mixture of short chain ligands.

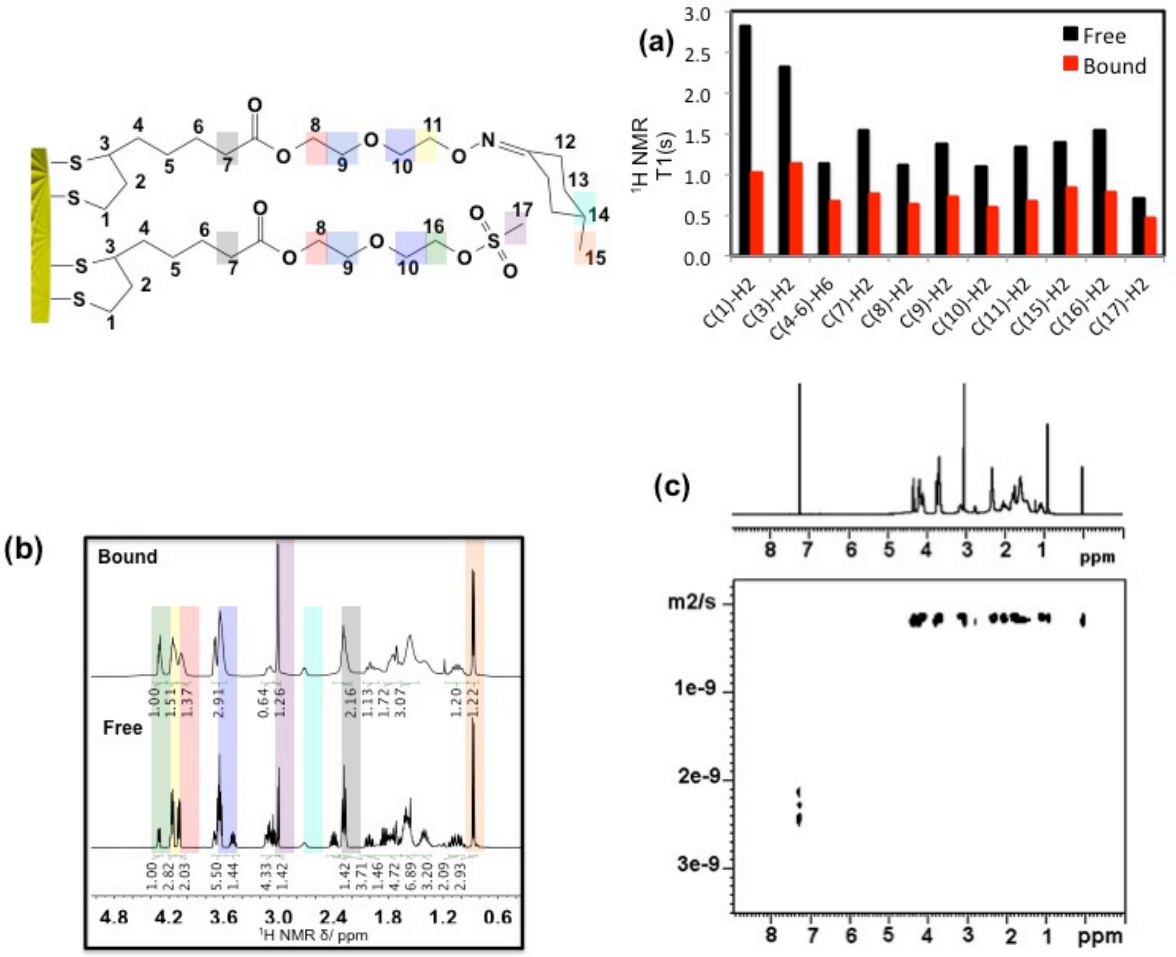

Figure 5. (a) ^{1}H NMR T1 relaxation time, (b) ^{1}H NMR of free vs. bound ligands, (c) representative R.T. DOSY spectrum of 50%-50% mixture of two model ligands on the surface of CdS quantum dot nanocrystals.

Selective gradient-enhanced unidimensional (1D) ROESY experiments of carefully washed samples bearing only surface-bound ligands showed through-space heterocorrelations between dissimilar ligands for the model sample with 50%-50% mixture of mesyl terminated TA-DEG and cyclohexane terminated TA-DEG (Figure 6). For example, 1D ROESY spectrum clearly shows through-space heteroligand coupling between the protons on the methyl end group (C17(H_3)) of mesyl terminated ligand and the protons on the methyl substitute (C15(H_3)) on the cyclohexane terminated ligand.

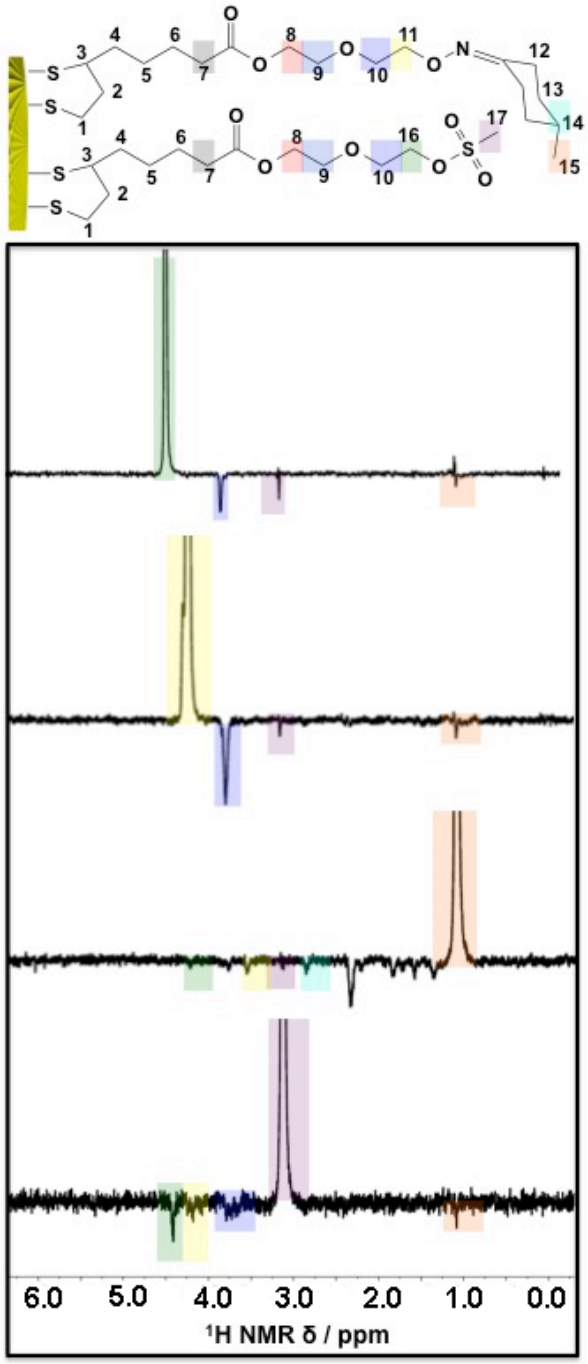

Figure 6. Representative 1D ROESY spectra of 50%-50% mixture of two model ligands on the surface of CdS quantum dot nanocrystals.

Conclusions

We have shown that controlling the surface loading of nanocrystals has direct biologically relevant consequences for the mobility of the particles with both the absorption and desorption rates along with the lateral diffusion across the lipid surface. Furthermore, we have shown through experiment that we can estimate the number of ligands interacting with the surface and how they affect lateral motion. We expect precise control of surface loading to be the next leap forward in designing biologically relevant probes for imaging, drug transfer, and biosensing.

Acknowledgements

J.V. gratefully acknowledges the National Science Foundation for funding of this work through the Division of Chemistry (NSF- 1253058).

References

[1] Mout, R.; Moyano, D. F.; Rana, S.; Rotello, V. M. Surface functionalization of nanoparticles for nanomedicine. *Chemical Society Reviews* **2012**, *41*, 2539–2544.

[2] Suzuki, K.; Hosokawa, K.; Maeda, M. Controlling the Number and Positions of Oligonucleotides on Gold Nanoparticle Surfaces. *Journal of the American Chemical Society* **2009,** 131, 7518–7519.

[3] Borovok, N.; Gillon, E.; Kotlyar, A. Synthesis and Assembly of Conjugates Bearing Specific Numbers of DNA Strands per Gold Nanoparticle. *Bioconjugate Chemistry* **2012,** 23, 916–922.

[4] Zanchet, D.; Micheel, C. M.; Parak, W. J.; Gerion, D.; Alivisatos, A. P. Electrophoretic isolation of discrete Au nanocrystal/DNA conjugates. *Nano Letters* **2001**, *1*, 32–35.

[5] Zhao, W.; Hsing, I. M. Facile and rapid manipulation of DNA surface density on gold nanoparticles using mononucleotide-mediated conjugation. *Chemical Communications* **2010,** 46, 1314–1316.

[6] Zheng, Y.; Li, Y.; Deng, Z. Silver nanoparticle-DNA bionanoconjugates bearing a discrete number of DNA ligands. *Chemical Communications* **2012**, *48*, 6160–6162.

[7] Sperling, R. A.; Pellegrino, T.; Li, J. K.; Chang, W. H.; Parak, W. J. Electrophoretic separation of nanoparticles with a discrete number of functional groups. *Advanced Functional Materials* **2006**, *16*, 943–948.

[8] Pierrat, S.; Zins, I.; Breivogel, A.; Soennichsen, C. Self-assembly of small gold colloids with functionalized gold nanorods. *Nano Letters* **2007**, *7*, 259–263.

[9] Susumu, K.; Mei, B. C.; Mattoussi, H. Multifunctional ligands based on dihydrolipoic acid and polyethylene glycol to promote biocompatibility of quantum dots. *Nature Protocols* **2009**, *4*, 424–436.

[10] Guo, Y. J.; Marchuk, K.; Sampat, S.; Abraham, R.; Fang, N.; Malko, A. V.; Vela, J., Unique Challenges Accompany Thick-Shell CdSe/nCdS (n > 10) Nanocrystal Synthesis. Journal of Physical Chemistry C 2012, 116, 2791–2800.

[11] Sun, W.; Marchuk, K.; Wang, G.; Fang, N. Autocalibrated Scanning-Angle Prism-Type Total Internal Reflection Fluorescence Microscopy for Nanometer-Precision Axial Position Determination. *Analytical Chemistry* **2010**, *82*, 2441–2447.

[12] Pierrat, S.; Hartinger, E.; Faiss, S.; Janshoff, A.; Soennichsen, C. Rotational Dynamics of Laterally Frozen Nanoparticles Specifically Attached to Biomembranes. *Journal of Physical Chemistry C* **2009**, *113*, 11179–11183.

[13] Saffman, P. G.; Delbruck, M. *Proceedings of the National Academy of Sciences of the United States of America* **1975**, 72, (8), 3111–3113.

[14] Mei, B. C.; Susumu, K.; Medintz, I. L.; Mattoussi, H. Polyethylene glycol-based bidentate ligands to enhance quantum dot and gold nanoparticle stability in biological media. *Nature Protocols* **2009**, *4*, 412–423.

[15] Yeagle, P. L. *Biochimica Et Biophysica Acta* **1985,** 822, (3-4), 267–287.

[16] Ramsammy, L. S.; Merz, P. A.; Brockerhoff, H. Association of Cholestanol and Cholestanone with Lisophosphatidylcholine. *Chemistry and Physics of Lipids* **1984**, *34*, 127–138.

CHAPTER 5

MODULAR FUNCTIONAL POLYDENTATE ADMET LIGANDS FOR NANOCRYSTAL SURFACE DOPING: TOWARD FORMATION OF HETEROSTRUCTURES

Abstract

We investigated a different approach to quantum dot surface modification by using a multifunctional polydentate capping ligands. In this study we have used ADMET to randomly oligomerize two dienes: One containing an azide functionality as an active group capable of clicking with an acetylene terminated molecule of interest, and one containing carboxylic acid surface coordinating head groups as a binding diene. Varying the azide-to-acid diene ratio allows control of the relative degree of ligand functionality and nanocrystal surface binding ability. Varying the total dienes-to-Ru catalyst ratio allow control of the extent of ADMET, which will enable us to achieve an accurate control over polydentate ligand size. Our synthesized polymeric ligand is able to wrap around a wide range of nanocrystal compositions. 1D NMR and advanced 2D NMR techniques such as DOSY, as well as IR and size and zeta-potential measurements via Dynamic Light Scattering (DLS) were employed to show type and extent of interaction associated between synthesized polymeric ligand and different types of nanocrystals surface. Extensive DLS studies demonstrated that the resulting acid/azide-containing polydentate ligands can also be readily coated onto the polyethylene glycol capped thick-shelled CdSe/CdS quantum dots and associate with those native ligands to form a double ligand layer on the nanocrystal surface through the hydrogen bonding. However multiple pendant azide functional groups could be subjected to click onto the gold nanoparticles bearing acetylene functionality. TEM images

and EDS line scans also further confirmed formation of such CdSe/CdS-Gold heteroassemblies in the presence of as synthesized polymer containing pre-selected number of azide and acid functional groups.

Introduction

Colloidal semiconductor nanocrystal quantum dots (NQDs) are found to be highly promising materials for applications from solar energy utilization[1] to biological imaging,[2] and catalysis[3] due to their unique size and shape dependent properties. Most of synthetic routs to make high quality nanocrystals require use of oleic acid or oleylamine and/or TOP/TOPO which contain a coordinating head group and a long hydrocarbon chain which brings stability as well as solubility in non-polar hydrophobic solvents.[4] However, ability to engineer the surface of NQDs enables us to improve or modify their shape and optical properties. In this approach we try to explore a new synthetic strategies involving olefin metathesis to modify the physical and chemical properties of NQDs to our advantage by proposing to replace the native nanocrystal (NC) surface ligands with our polymeric ligand that has controlled number of coordinating and doping functionality. We propose a facile and versatile ADMET-based strategy to make a multidentate multifunctional ligand with desired number of carboxylic acid as a coordinating head group and azide as a doping functional group. The replacement of the original organic ligands by our synthesized polymeric ligands enables us to control degree of functionalization introduce per nanocrystals. We investigated a unique class of functional polydentate ligands for quantum dot surface doping built by a modular approach, specifically via Acyclic Diene Metathesis (ADMET). ADMET is a variant of olefin metathesis whereby dienes are linked together under very mild conditions (Scheme 1).[5 6 7 8] Unlike Ring Opening Metathesis Polymerization (ROMP) or Living Free

Radical Polymerization (LFRP), which have been used to encapsulate semiconductor and gold nanocrystals within polymer vesicles,[9,10] ADMET has not yet been applied to nanocrystal functionalization. We will use Acyclic Diene Metathesis or ADMET as a special type of step-growth olefin metathesis to randomly oligomerize two different types of terminal dienes: One functional diene containing an active azide functional group, and one binding diene containing carboxylic acid surface coordinating head groups (Scheme 1a). This process will yield oligomeric polydentate ligands with multiple functional and binding groups. Varying the functional-to-binding diene feed ratio will allow us to control the relative degree of ligand functionality and nanocrystal surface binding ability. Varying the total dienes-to-Ru-catalyst ratio will allow us to control the extent of ADMET; thus we will be able to control overall ligand size and molecular weight.

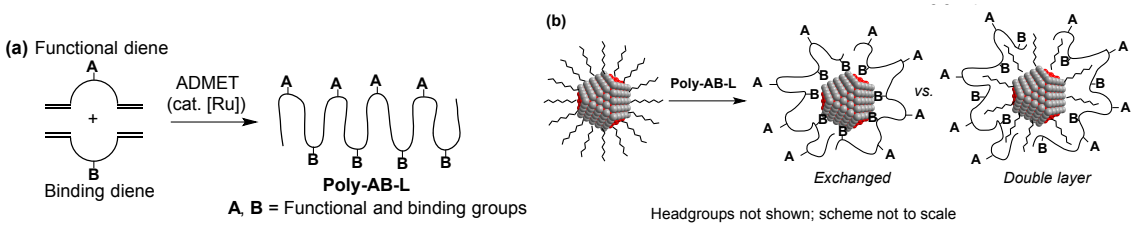

Scheme 1. (a) Ruthenium catalyzed synthesis of functional polydentate ligand via ADMET, (b) ligand exchange illustration *vs.* double layer formation

Experimental

Materials. Ethyl Formate (97%), diethyl malonate (99%), 4-dimethylamino-pyridine (99%), decalin (99%), Grubbs second generation metathesis catalyst, sodium azide (≥99.5%), Celite® 503, 10-undecynoic acid, and bromoacetyl bromide (≥98%) were purchased from Aldrich. Sodium carbonate (K_2CO_3, anhydrous, 99%), sodium chloride (NaCl), and magnesium sulfate ($MgSO_4$, anhydrous) were purchased from Fisher. Diethyl ether, dichloromethane (CH_2Cl_2), and tetrahydrofuran (THF) were purified by passage through

activated alumina and "deoxygenating" columns from Vacuum Atmospheres Co. (Hawthorne, CA). Hexane and ethyl acetate were purchased from Fisher and used as received. Chloroform-d ($CDCl_3$), and dimethylsulfoxide-d6 (DMSO-d_6) were purchased from Cambridge Isotopes Laboratories, Inc. 5-Bromo-1-pentene,[11] undeca-1,10-dien-6-ol,[12] 2-(pent-4-en-1-yl) hept-6-enoic acid,[13] DHLA-TEG, DHLA-TEG capped giant dots [14] bare gold nanoparticles,[15] and CdSe/CdS giant quantum dots,[16] were synthesized following literature procedures. ^{1}H NMR chemical shifts (δ) are reported in ppm relative to residual protiated solvent in $CDCl_3$ (7.26 ppm) or DMSO-d_6 (2.50 ppm). ^{13}C NMR spectra are referenced to residual $CDCl_3$ (77.16 ppm) or DMSO-d_6 (39.52 ppm).

Synthesis. Diene Monomers. *General synthetic procedure.* Un-deca-1,10-dien-6-yl 2-bromoacetate: A solution of undeca-1,10-dien-6-ol (900 mg, 5.36 mmol) in CH_2Cl_2 (10 mL) was added dropwise to a stirred solution of K_2CO_3 (3.70g, 26.78 mmol) mixed with bromoacetyl bromide (1.19 g, 5.89 mmol) in CH_2Cl_2 (50 mL) at 0°C. The solution was allowed to warm up to room temperature (R.T.) and stirred for 12 h under dry N_2. The mixture was filtered through Celite® 503, washed with 1 M HCl (1 × 50 mL), extracted by dichloromethane (3 × 50 mL), and washed with saturated aqueous NaCl (1 × 50 mL). The solution was dried over anhydrous $MgSO_4$, filtered and concentrated under vacuum to yield 1.40 g (4.84 mmol, 90 %) of undeca-1,10-dien-6-yl 2-bromoacetate as pale yellow oils. ^{1}H NMR (400 MHz, $CDCl_3$, 22 ºC) δ 5.72-5.82 (m, 2H, CH_2=CH-); 4.97-5.02 (dd, 4H, CH_2=CH-); 4.95 (m, 1H, -O-CH-); 3.81 (s, 2H, -CH_2-Br); 2.05 (q, 4H, allylic-CH_2); 1.54-1.62 (br, 4H, -CH_2-); 1.35-1.48 (br, 4H, -CH_2-). ^{13}C NMR (100 MHz, $CDCl_3$, 22ºC) δ 167.23 (-O(C=O)-), 138.39 (CH_2=CH-), 115.06 (CH_2=CH-), 76.54 (-O-CH-), 33.58 (allylic-CH_2), 33.48 (-CH_2-), 26.32 (-CH_2-Br), 24.55 (-CH_2-).

ADMET Copolymerization of Diene Monomers. Binding monomer (300 mg of DM-COOH; 1.53 mmol) and functional monomer (88.0 mg of DM-Br; 0.304 mmol) were weighed in an oven-dried vial inside a glove box filled with dry N_2. A small Teflon-coated magnetic bar was added, and the mixture was stirred for 5 min at R.T. In a separate vial, Grubbs second generation catalyst (1.55 mg, 1.83 mmol) (typically, ca. 1500:1 to 100:1 monomer/catalyst) was weighed and completely dissolved in 0.7 mL of anhydrous THF to form an optically clear solution. The catalyst solution was added to the monomer mixture, and the combined liquids were transferred to a re-sealable Schlenk tube equipped with a small Teflon-coated magnetic stir bar. The sealed flask was stirred at R.T. under dry N_2 for 30 min, brought out to the vacuum line and placed in a silicon oil bath pre-equilibrated at 50 °C. Dynamic vacuum was slowly applied while stirring. The mixture was continued to stir for a given length of time (12 h or 48 h) under dynamic vacuum at 50 °C. To stop the reaction and quench the catalyst, the flask was opened to air and the product was diluted with THF.

Azidation. Sodium azide (3eq) was added to the stirred solution of copolymer in THF at R.T. The reaction mixture was allowed to stir at R.T. for 3 days. The crude was filtered and concentrated under vacuum to give the corresponding azide-copolymer with no need for further purification.

Acetylene terminated gold nanoparticle synthesis. A solution of 10-undecynoic acid (10 mg, 54.86 μmol) in chloroform was added to 2 mL crude solution of freshly synthesized bare gold nanoparticle 26 in water. A few drops of 0.1M sodium hydroxide solution was added to make a basic media. The solution mixture was stirred vigorously at room temperature for 10 min. The gold nanoparticles were transferred to the organic layer quickly. Aqueous layer was

decanted and discarded. Organic layer was washed a couple of times with 0.1 M phosphate buffer saline solution and then stored at 4 ºC.

Gold-GQDs heterostructure. Cap exchange of CdSe/CdS giant quantum dots with DHLA-TEG ligands was done following the reported procedure.[9] Newly capped GQDs were washed with mixture of ethanol and chloroform and crashed with hexanes. This cycle was repeated 3 times and precipitate was dried under vacuum for 1 hour. Stock solution of azidocopolymer (100 µL, 300 mg in 2 mL ethanol) was added dropwise to the solution of 50 mg GQDs in 0.5 mL ethanol and the mixture was stirred at R.T. for 10 min. Crude solution of freshly prepared acetylene terminated gold nanoparticles in chloroform was then added dropwise to the mixture (0.1 mL for the sample with small portion of gold and 1 mL for the sample with large portion of gold). Then stock solution of Cp*Ru(COD)Cl catalyst in chloroform (10µL, 0.01 M) was added to the physical mixture of acetylene-terminated gold nanoparticles, giant dots and azidocopolymer. The solution was stirred in dark overnight under N_2 at R.T.

Optical Characterization. Absorption spectra were measured with a photodiode-array Agilent 8453 UV-Vis spectrophotometer. Solvent absorption was recorded and subtracted from all spectra. Steady-state photoluminescence (PL) spectra were measured with a Horiba-Jobin Yvon Nanolog scanning spectrofluorometer equipped with a photomultiplier detector. Nanocrystal quantum dots were diluted in chloroform to give an optical density of 0.05-0.2 at 550 nm. Excitation wavelength was 510 nm, and emission was recorded between 525 and 725 nm. Vibrational infrared spectra were recorded with a Bruker IFS66V FT-IR spectrometer equipped with a DTGS detector with 64 scans at a resolution of 4 cm^{-1}. Samples were prepared as either drop cast thin films on KBr plates or solid KBr pellets. Background

spectra were collected and subtracted under identical conditions. During spectral collection, samples were continuously purged with dry N_2 to minimize water vapor absorbance.

Structural Characterization. Transmission Electron Micros-copy. TEM was conducted on carbon-coated copper grids using an FEI Tecnai G2 F20 field emission scanning transmission electron microscope (STEM) at 200 kV (point-to-point resolution <0.25 nm, line-to-line resolution <0.10 nm). Elemental composition was characterized by energy-dispersive spectroscopy (EDS). Particle Analysis. Dimensions were measured manually or with ImageJ for >50-100 particles. Averages are reported ± standard deviations.

NMR characterization. All NMR spectra were carried out on a Varian 400MR spectrometer operating at a ^{1}H frequency of 399.80 MHz and ^{13}C frequency of 100.51 MHz equipped with one NMR pulse-field-gradient probe. All spectra were recorded using standard pulse sequences from the VNMRJ 3.1 pulse pro-gram library. The ^{1}H NMR spectra were recorded with a spectral width of 12.00 ppm, 16 scans, and a 2 s relaxation delay (d1) between scans. The ^{13}C NMR spectra were recorded with a spectral width of 200 ppm, 64 scans or 2000 scans for copolymers. The standard implementation of the gradient-selected sensitivity-improved inverse (^{1}H-detected) HSQC experiment was used at 400 MHz and had the following parameters: 32-Transient spectral increments were acquired from 9 to 1 ppm in F2 (1H) using 1,200 data points, 160 to 10 ppm in F1 (13C) using 512 increments (F1 acquisition time: 13.6 ms) of 32 NS, with a total acquisition time of 5 h 35 min.

Results and Discussion

Synthesis of monomers. Synthesis of monomer **2** (bromoester) was accomplished via a condensation reaction between the bromoacetyl bromide and undeca-1,10-dien-6-ol (1) [12] (Scheme 2a). The reaction mixture was allowed to stir overnight at room temperature and

was easily monitored for complete conversion by TLC. Bromoacetyl bromide reacts instantly with cold undeca-1, 10-dien-6-ol via a very exothermic reaction in which a steamy acidic gas is given off (hydrogen bromide). Therefore, excess of potassium bicarbonate anhydrous was added to abstract the hydrogen bromide released during the condensation reaction. Once finished, potassium bromide and excess of potassium bicarbonate salts were removed by vacuum filtration through a pad of celite @503. Washing of crude product was performed to remove excess of bromoacetyl bromide. Monomer **2** was recovered as colorless oil with 90% yield and used without further purification. Monomer **3** (acid containing monomer) was synthesized according to the literature.[13]

Copolymerization of diene monomers via ADMET. We have synthesized a series of polydentate ligands from bromide (Br) and carboxylic (COOH) containing dienes. In the presence of a Ru metathesis catalyst, these two diene monomers get co-polymerized in 48 h (Scheme 2b). The second-generation Grubbs catalyst was chosen for its high stability and activity compared to first-generation Grubbs catalysts.[4] The two dienes and product remain liquid upon gentle warming to 50°C, thus the reaction is run neat and does not require any extra added solvent. Dynamic vacuum helps ensure that the reaction proceeds to completion by removing the ethylene byproduct (one equivalent of ethylene is produced for each two monomers linked).

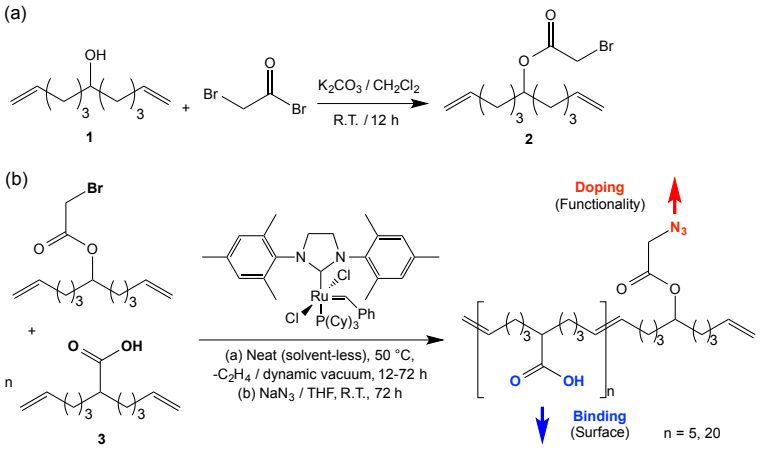

Scheme 2. Synthesis of functional diene monomer precursor (2), (b) functional polydentate copolymer ligand synthesis

Extensive ^{1}H NMR, ^{13}C NMR, unambiguously show that using ADMET, we have been able to precisely tune the degree of polymerization from as high as 380 all the way down to only 8 monomer units per polymer, using Ru catalyst loadings as little as <0.15 mol% (Figure 1). We have also derived an equation to calculate degree of polymerization (DOP) based on the ^{1}H NMR integration. Mathematically

(eq. 1) $$D.O.P. = 2 \times \{(I_{int} / 2) / ([(I_{ter} / 2) + 1] /2)\} +1$$

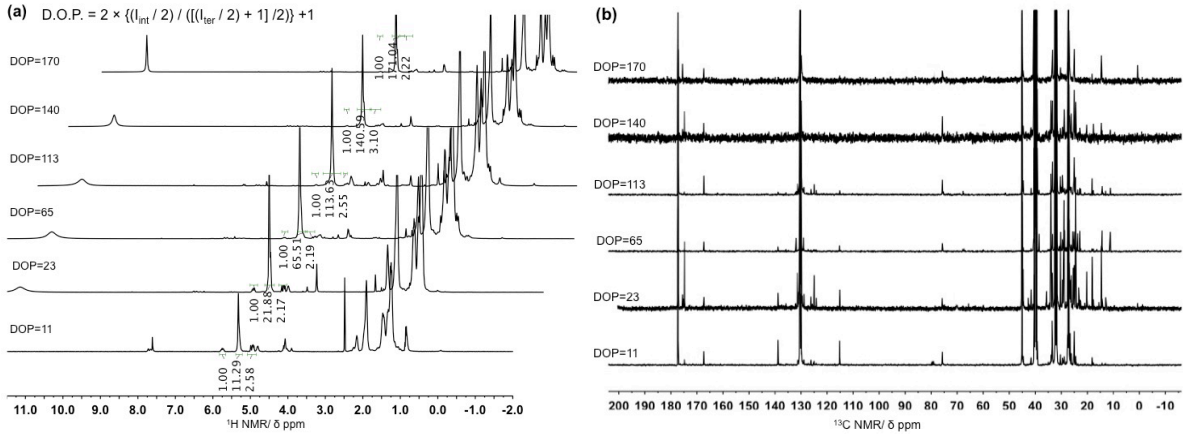

Figure 1. (a) ^{1}H NMR, (b) ^{13}C NMR of different chain length bromoacid copolymer

Table 1 shows a systemic study on the DOP when changing different factors such as monomer ratios, catalyst loading and time.

Table1. Systematic study of catalyst loading and monomer ratio effect on degree of copolymerization

Acid monomer (mmol)	Bromoester monomer (mmol)	ADMET Catalyst (μmol)	Monomer to cat ratio	Monomer to cat ratio	THF (mL)	T (˚C)	Time	DOP From NMR	Poly. Br: Acid ratio by NMR
1.53/300mg	0.311/90 mg	18.4/15.6mg	1:5:0.06	100:1	0.7	50	12h	23	1: 5.1
1.53/300mg	0.311/90 mg	18.4/15.6mg	1:5:0.06	100:1	0.7	50	48h	118	1:5.5
1.53/300mg	0.311/90 mg	18.4/15.6mg	1:5:0.06	100:1	0.7	50	72h	165	1:5.5
1.53/300mg	0.0796/ 22 mg	16.0/13.6 mg	1:20: 0.21	100:1	0.7	50	12h	28	1:21.1
1.53/300mg	0.0796/ 22 mg	16.0/13.6 mg	1:20: 0.21	100:1	0.7	50	48h	38	1:26.4
1.53/300mg	0.0796/ 22 mg	16.0/13.6 mg	1:20: 0.21	100:1	0.7	50	72h	113	1:26.4
0.76/150mg	0.152/ 44 mg	45.9/39 mg	1:5:0.3	20:1	0.35	50	48h	370	1: 4.7
1.53/300mg	0.311/88 mg	5.80/5 mg	1:5: 0.02	300:1	0.7	50	48h	47	1: 4.8
1.53/300mg	0.311/90 mg	3.50/3 mg	1:5: 0.012	500:1	0.2*	50	48h	35	1: 5.8
0.76/150mg	0.152/44 mg	0.88/0.75mg	1:5: 0.006	1000:1	0.35	50	48h	25	1: 5.1
1.53/300mg	0.311/90 mg	1.60/1 mg	1:5: 0.004	1500:1	0.7	50	48h	11	1: 5.8

The relative amount of Br and COOH groups in the final polymer can be controlled by the initial monomer feed ratio (Figure 2a). Even more importantly, the number of monomers per polymer chain or degree of polymerization is dramatically sensitive to, and roughly inversely proportional to the total monomers-to-Ru catalyst ratio used in the synthesis (Figure 2b). Achieving such accurate control over polydentate ligand size would be very difficult or impossible with other polymerization methods such as living free radical polymerization (LFRP).[17,18,19,20,21,22] This is critical for this study because controlling polymer size is a key to apply this type of surface doping to a wide range of nanocrystal sizes and shapes. Short oligomers are more likely to be small enough to wrap around one nanocrystal at a time (there is no indication that having more than one oligomer chain per nanocrystal could be a problem). This argument is strongly supported by some recent studies on surface modification using non-ADMET polydentate ligands; these studies showed that short

polyacrylic acid oligomers with as few as 10-20 monomer units are able to wrap around typical 3-5 nm colloidal quantum dots with very robust binding.[23] [24] [25] We speculate that larger nanocrystals will require longer polydentate ligands, and that very large polymers could bind to more than one nanocrystal at a time leading to undesirable particle aggregation.

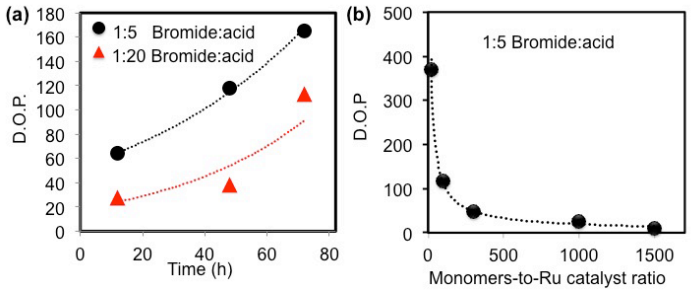

Figure 2. (a) DOP *vs.* reaction time for 1:5 and 1:20 ratio between bromo: acid monomers, (b) DOP *vs.* catalyst loading for 1:5 bromo: acid ratio

We introduced azide functionality by a simple post synthetic modification of the COOH-Br copolymer with NaN_3 in THF since azide known to be incompatible with Ru metathesis catalyst.[26] Reaction of the COOH-Br copolymer with excess of NaN_3 in tetrahydrofuran (THF) cleanly gives COOH-N_3 copolymers. Presence of azide in our copolymer has been confirmed by appearance of a strong signal at 2100 cm^{-1} in Infrared spectrum corresponding to azide asymmetric stretching frequency (Figure 3a).

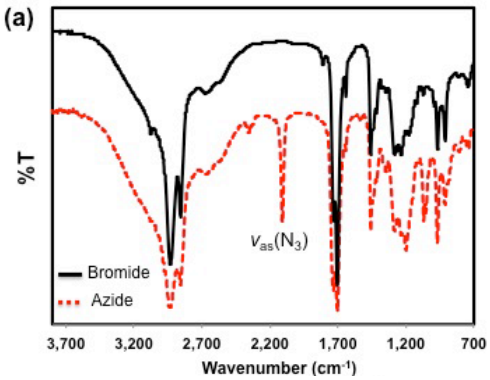

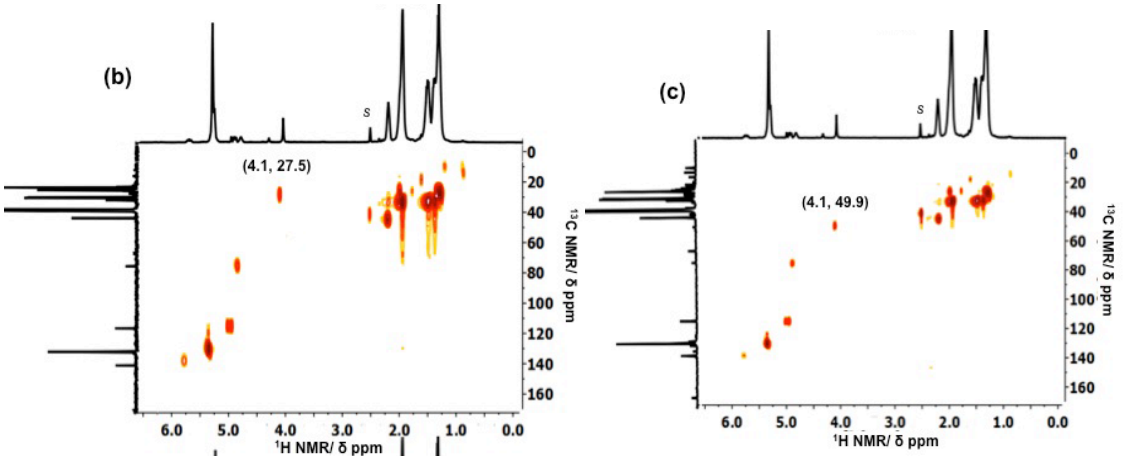

Figure 3. Bromide to azide transformation (a) Infrared spectrum of bromo-acid copolymer (solid black) and azido-acid copolymer (dotted red), (b) HSQC of bromo-acid copolymer, and (c) HSQC of azido-acid copolymer

In addition to IR, ^{1}H NMR and ^{13}CNMR studies, further advanced two-dimentional Heteronuclear Single Quantum Coherence spectroscopy (HSQC) demonstrated that the chemical shift of the methylene peak in alfa position has changed from (4.11, 27.96) in bromine ppm to (4.11, 49.91) ppm in azide (Figure 3b, 3c). The resulting azide-containing polydentate ligands can be readily clicked with functional acetylenes.

Does functional polydentate ligands bind to the quantum dot surface? Some recent studies on surface modification using non-ADMET polydentate ligands showed that short oligomers with as few as 10-20 monomer units are able to wrap around typical 3-5 nm colloidal quantum dots with very robust binding.[24 25 27] Our synthesized multi functional oligomers are more likely small enough to bind one nanocrystal at a time, and we do not expect that the presence of more than one oligomer chain per nanocrystal will cause a problem even in the case of large nanocrystals. However we speculated from DLS studies that longer chain polymers are able to wrap around more than one nanocrystal at a time and therefore cause undesirable particle aggregation. To test the feasibility of this approach we perform a surface

passivation of our synthesized polymeric ligand onto a couple of metal oxide nanocrystals with different sizes such as CuO_2 (60nm) and ZnO (5nm) (Scheme 3).

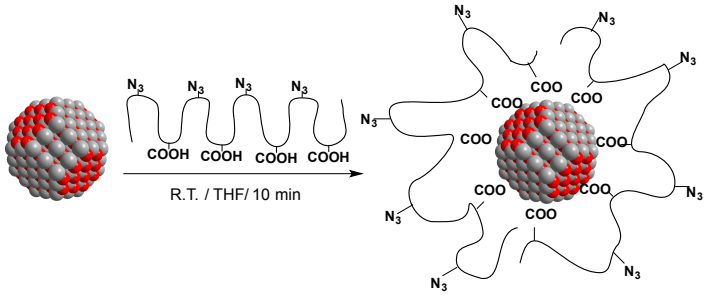

Scheme 3. Multifunctional polymer as a passivating ligand for bare metal oxides

We simply sonicated a mixture of our synthesized polymer and metal oxide powder for less than 5 min in THF, where the particles were initially insoluble. We speculate that both CuO_2 and ZnO particles became partially soluble in organic solvents after conjugation with our multifunctional ligands. IR analysis also revealed that asymmetric carboxylate stretching frequency originated from acid, $\nu_{as}(COO^-)$ shifts from 1710 cm^{-1} in the free ligands to 1610 cm^{-1} for Cu_2O and 1590 cm-1 for ZnO in the surface-bound ligands; while the asymmetric carboxylate stretching frequency originated from ester carbonyl, $\nu_{as}(CO)$, and azide, $\nu_{as}(N_3)$ remained unchanged at ca. 1730 cm^{-1} and 2100 cm^{-1}, respectively (Figure 4).

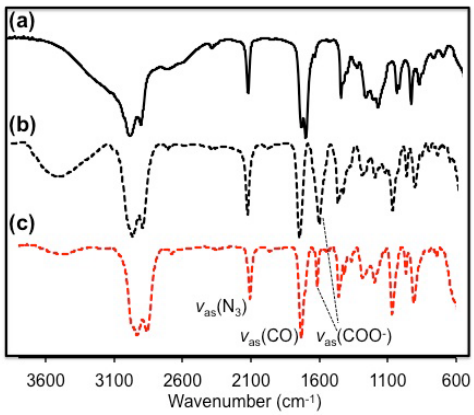

Figure 4. Infrared spectroscopy of (a) free azido-acid copolymer, (b) polymer capped Cu_2O, and (c) polymer capped ZnO

Proof of concept: Heterostructure assemblies- Tetraethylene glycol (TEG)-terminated CdSe/CdS QDs was synthesized by DHLA-TEG ligand exchange method under 350 nm UV lamp in ethanol.[28] Figure 5 illustrates the TEM images, size distribution diagram, and absorption/emission spectrum of CdSe/CdS QDs after DHLA-PEG ligand exchange.

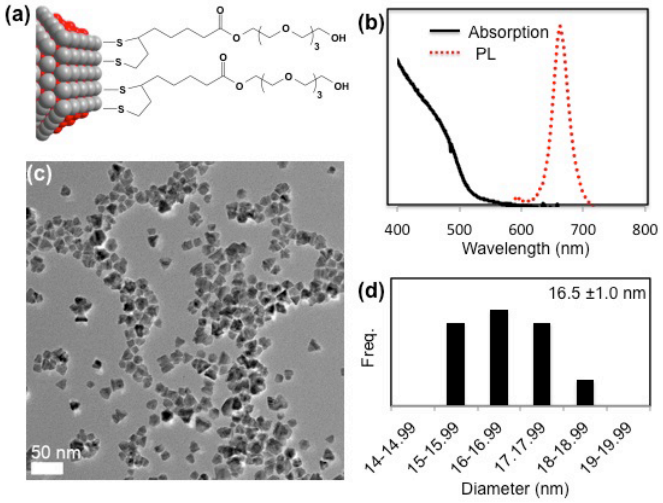

Figure 5. (a) Surface chemical structure, (b) absorption (solid black) and emission (dotted red) spectra, (c) TEM image, and (d) size histogram of TEG-terminated CdSe/CdS QDs

Scheme 4 demonstrated that the resulting acid/azide-containing polydentate ligands can also be readily coated onto the polyethylene glycol capped thick-shelled CdSe/14CdS quantum dots and associate with those surface ligands to form a double ligand layer on the nanocrystal surface through the hydrogen bonding.

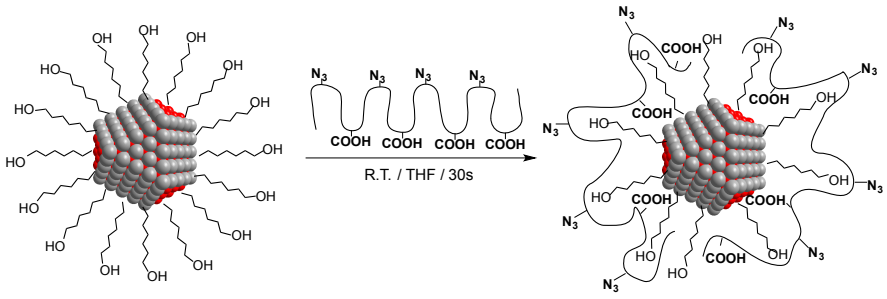

Scheme 4. Multifunctional polymer ligand wrapped around the DHLA-TEG-capped CdSe/CdS via hydrogen bonding

DLS investigation has been done by monitoring the hydrodynamic diameter of PEG-terminated giant dots against addition of multifunctional azido-acid copolymer. Addition of every 0.1 mL of polymer solution to PEG-capped GQDs solution in ethanol would increase the hydrodynamic diameter of giant QDs by 1 nm that is roughly correspond to the diameter of copolymer (Figure 6).

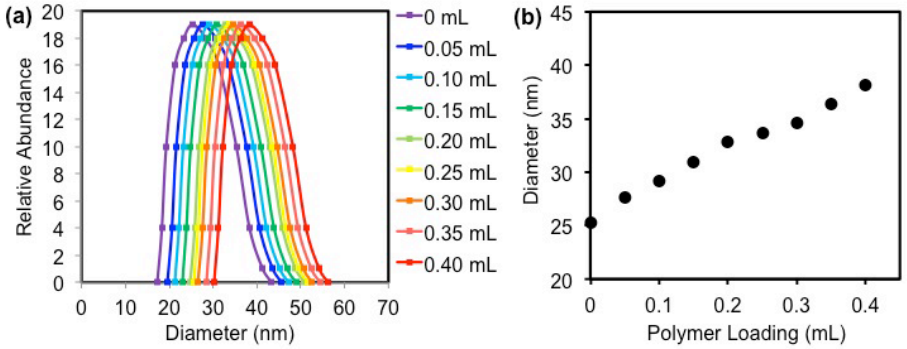

Figure 6. (a) DLS study on increasing hydrodynamic radius of double layer by dropwise addition of copolymer, (b) linear trend of CdSe/CdS QDs *vs.* polymer loading

No aggregation was observed in this case which could be an evidence of having more than one nanocrystal being wrapped by polymer. Therefore it is safe to conclude that our synthesized polymer will wrap around a single nanocrystal via hydrogen bonding to make a GQD-polymer double layer (Scheme 4). The corresponding assembly with multiple carboxylic acid functional groups involves in hydrogen bonding with TEG on the surface of CdSe/CdS QDs, however, multiple pendant azide functional groups can be clicked onto the gold nanoparticles bearing acetylene functionality.

Scheme 5 shows surface passivation of 6 nm bare gold nanoparticles by 9-decynoic acid in basic media (pH>7).

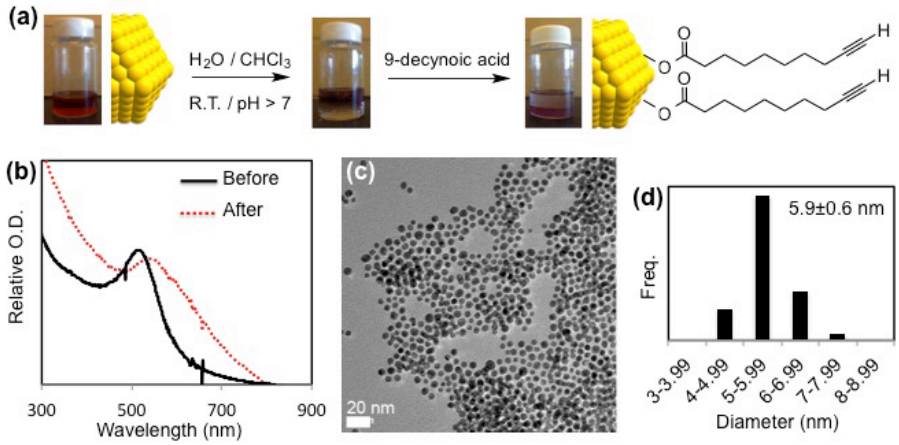

Scheme 5. (a) Synthesis, (b) absorption spectra before and after surface modifications, (c) TEM image, (d) and size distribution of acetylene-terminated Au-NP

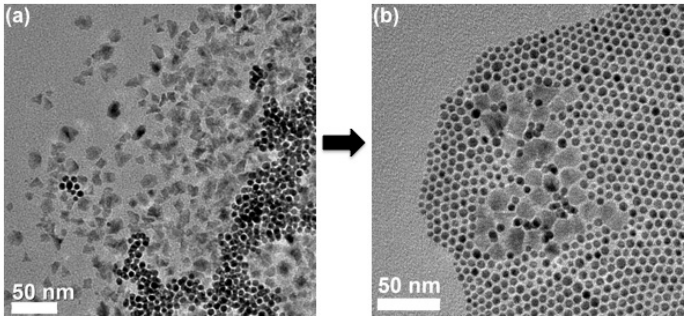

Figure 7. (a) Physical mixture of acetylene terminated Au-NP and polymer wrapped CdSe/CdS double layer in the absence of Ru catalyst, (b) heterostructure assembly *via* click after Ru catalyst addition

The resulting acetylene terminated Au-NPs were clicked onto the azide pendants of our double layer system (CdSe/CdS wrapped with copolymer) in the presence of ruthenium catalyst. (Figure 7 & 8).

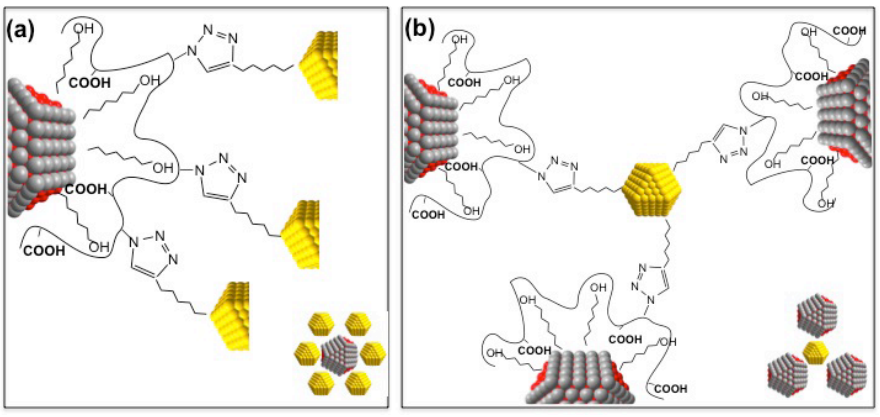

Figure 8. Au-CdSe/CdS heretostructure linkage via click reaction with (a) high, and (b) low Au concentration

TEM images and EDS line scans confirmed formation of such assemblies (Figures 9). We are more likely to get a radioactive shape heterostructure (Figures 9a) when we use lower concentration of Au NPs and flower shape heterostructure (Figures 9d) when we use more concentration of Au NPs. Formation of Au-QD heteroassembly was also confirmed by disappearance of asymmetric azide stretching infrared frequency (2100 cm^{-1}) after GQD-polymer double layer was clicked with the acetylene terminated gold (Figure 10).

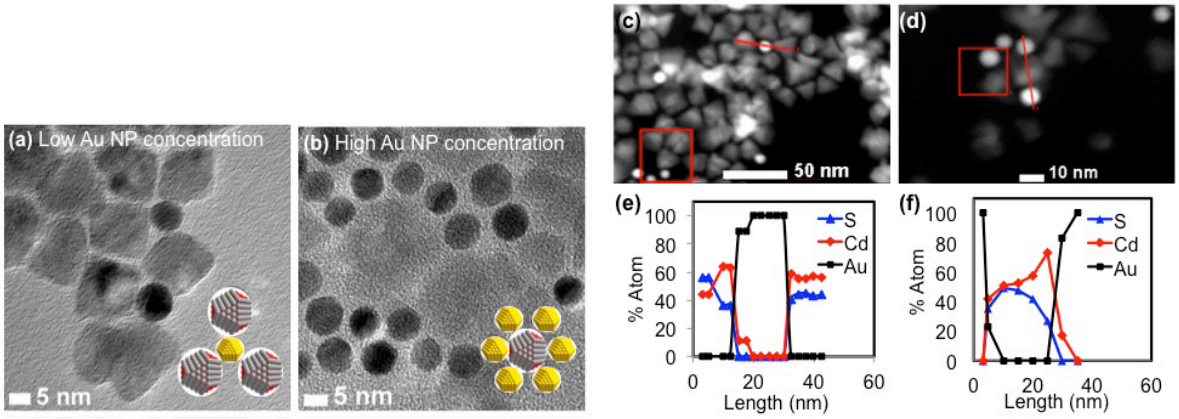

Figure 9. (a,b) TEM images, and (c-f) EDS line scans of heterstructure with low (a,c,e) and high (b,d,f) Au-NP concentration

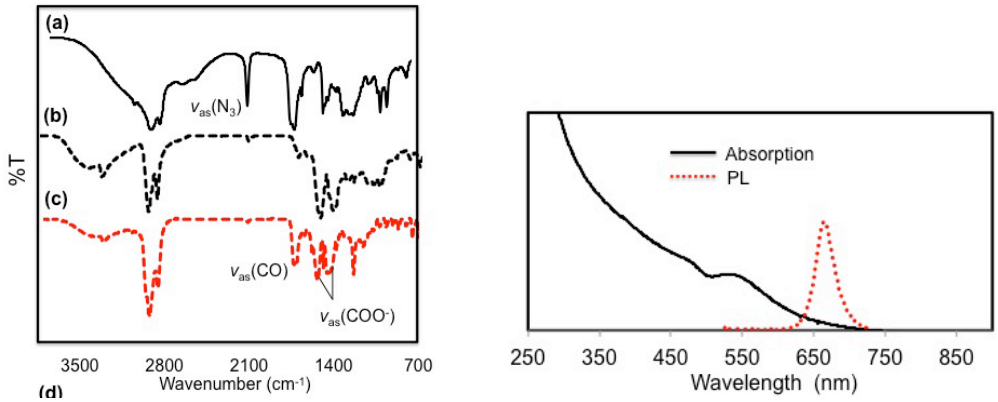

Figure 10. Infrared spectroscopy (a) free azido acid copolymer, (b) Acetylene terminated Au-NP, and (c) Au-CdSe/CdS hereto-structure; (d) absorption and emission spectrum of Au-CdSe/CdS heretostructure

Conclusions

Using ADMET and applying very mild condition we were able to synthesis multifunctional polymer ligands with multiple azide and carboxylic acid groups. Our synthesized multifunctional ligand was able to wrap around a single nanocrystal by associating in hydrogen bonding with QD's surface ligands to form double layers. The corresponding double layer system with azide pendant functional group was then click onto the gold nanoparticles bearing acetylene functionality in the presence of Ruthenium catalyst to form heterostructures of QD-Au.

Acknowledgements

J.V. gratefully acknowledges the National Science Foundation for funding of this work through the Division of Chemistry (NSF- 1253058).

References

[1] Kamat, P.V., Meeting the clean energy demand: Nanostructure architectures for solar energy conversion. *J. Phys. Chem. C* **2007**, *111*, 2834–2860.

[2] Alivisatos, A.P.; Gu, W.; Larabell, C., Quantum dots as cellular probes. *Annu. Rev. Biomed. Eng.* **2005**, *7*, 55–76.

[3] Lim, B.; Jiang, M.; Camargo, P. H. C.; Cho, E. C.; Tao, J.; Lu, X.; Zhu, Y.; Xia, Y., Pd-Pt bimetallic nanodendrites with high activity for oxygen reduction. *Science* **2009**, *324*, 1302–1305.

[4] Park, J.; Joo, J.; Kwon, S. G.; Jang, Y.; Hyeon, T., Synthesis of monodisperse spherical nanocrystals. *Angew. Chem., Int. Ed*. **2007**, *46*, 4630–4660.

[5] Baughman, T. W.; Wagener, K. B., Recent advances in ADMET polymerization. In Metathesis Polymerization, Buchmeiser, M. R., Ed. Springer-Verlag Berlin: Berlin, 2005; Vol. 176, pp 1–42.

[6] Mutlu, H.; de Espinosa, L. M.; Meier, M. A. R., Acyclic diene metathesis: a versatile tool for the construction of defined polymer architectures. Chemical Society Reviews 2011, 40, 1404–1445.

[7] Schwendeman, J. E.; Church, A. C.; Wagener, K. B., Synthesis and catalyst issues associated with ADMET polymerization. Advanced Synthesis & Catalysis 2002, 344, 597–613.

[8] Opper, K. L.; Wagener, K. B., ADMET: Metathesis Polycondensation. Journal of Polymer Science Part a-Polymer Chemistry 2011, 49, 821–831.

[9] Skaff, H.; Lin, Y.; Tangirala, R.; Breitenkamp, K.; Boker, A.; Russell, T. P.; Emrick, T., Crosslinked capsules of quantum dots by interfacial assembly and ligand crosslinking. *Adv Mater* **2005,** *17*, 2082–2086.

[10] Basu, A.; Liu, X., Olefin metathesis on nanostructures. *J. Organomet. Chem.* **2006,** *691*, 5148–5154.

[11] Hok, S.; Schore, N. E., Synthesis of 2-arylcycloalka-2,4-dienones using sulfone-based methodology. Journal of Organic Chemistry 2006, 71, 1736-1738.

[12] Hopkins, T. E.; Wagener, K. B., Amino acid and dipeptide functionalized polyolefins. Macromolecules 2003, 36, 2206–2214.

[13] Leonard, J. K.; Turek, D.; Sloan, K. B.; Wagener, K. B., Polyethylene Prodrugs Using Precisely Placed Pharmaceutical Agents. Macromolecular Chemistry and Physics 2010, 211, 154–165.

[14] Mei, B. C.; Susumu, K.; Medintz, I. L.; Mattoussi, H., Polyethylene glycol-based bidentate ligands to enhance quantum dot and gold nanoparticle stability in biological media. Nature Protocols 2009, 4, 412–423.

[15] Chen, W.; Deng, H. H.; Hong, L.; Wu, Z. Q.; Wang, S.; Liu, A. L.; Lin, X. H.; Xia, X. H., Bare gold nanoparticles as facile and sensitive colorimetric probe for melamine detection. Analyst 2012, 137, 5382–5386.

[16] Guo, Y. J.; Marchuk, K.; Sampat, S.; Abraham, R.; Fang, N.; Malko, A. V.; Vela, J., Unique Challenges Accompany Thick-Shell CdSe/nCdS (n > 10) Nanocrystal Synthesis. Journal of Physical Chemistry C 2012, 116, 2791–2800.

[17] Golas, P. L.; Matyjaszewski, K., Marrying click chemistry with polymerization: expanding the scope of polymeric materials. *Chem. Soc. Rev.* **2010,** *39*, 1338–1354.

[18] Matyjaszewski, K.; Tsarevsky, N. V., Nanostructured functional materials prepared by atom transfer radical polymerization. *Nat. Chem.* **2009,** *1*, 276–288.

[19] Min, K.; Matyjaszewski, K., Atom transfer radical polymerization in aqueous dispersed media. *Cent. Eur. J. Chem.* **2009,** *7*, 657–674.

[20] Oh, J. K.; Bencherif, S. A.; Matyjaszewski, K., Atom transfer radical polymerization in inverse miniemulsion: A versatile route toward preparation and functionalization of microgels/nanogels for targeted drug delivery applications. *Polymer* **2009,** *50*, 4407–4423.

[21] Matyjaszewski, K., New catalysts for controlled/living atom transfer radical polymerization (ATRP). *Science and Technology in Catalysis* **2002,** *145*, 3–11.

[22] Coessens, V.; Pintauer, T.; Matyjaszewski, K., Functional polymers by atom transfer radical polymerization. *Prog. Polym. Sci.* **2001,** *26*, 337–377.

[23] Smith, A. M.; Nie, S., Minimizing the hydrodynamic size of quantum dots with multifunctional multidentate polymer ligands. Journal of the American Chemical Society 2008, 130, 11278–+.

[24] Uyeda, H. T.; Medintz, I. L.; Jaiswal, J. K.; Simon, S. M.; Mattoussi, H., Synthesis of compact multidentate ligands to prepare stable hydrophilic quantum dot fluorophores. Journal of the American Chemical Society 2005, 127, 3870–3878.

[25] Duan, H. W.; Kuang, M.; Wangi, Y. A., Quantum Dots with Multivalent and Compact Polymer Coatings for Efficient Fluorescence Resonance Energy Transfer and Self-Assembled Biotagging. Chemistry of Materials 2010, 22, 4372–4378.

[26] Kanemitsu, T.; Seeberger, P. H., Use of olefin cross-metathesis to release azide-containing sugars from solid support. *Org. Lett*. **2003**, *5*, 4541–4544.

[27] Liu, L.; Guo, X. H.; Li, Y.; Zhong, X. H., Bifunctional Multidentate Ligand Modified Highly Stable Water-Soluble Quantum Dots. Inorganic Chemistry 2010, 49, 3768–3775.

[28] Susumu, K.; Mei, B. C.; Mattoussi, H., Multifunctional ligands based on dihydrolipoic acid and polyethylene glycol to promote biocompatibility of quantum dots. Nature Protocols 2009, 4, 424–436.

CHAPTER 6

GENERAL CONCLUSION

In summary, we have investigated a new surface ligand modification strategy, so called “doping”, to introduce native active surface ligands and remove need of routine ligand exchange in semiconductor nanocrystal quantum dots. This method also designed to control the degree of loading or “valency” per nanocrystal quantum dots. We show that quantum dots capped with chemically active native ligands can be synthesized directly from a mixture of ligands with similar chain lengths. We are able to successfully maintain the ratio between active and inactive-terminated ligands on the nanocrystals surface by simply changing the corresponding ratio in the initial mixture.

Moreover, combination of one-dimension and two--dimension solution NMR techniques confirm that mixtures of ligands with similar chain lengths homogeneously distribute themselves on the nanocrystal surface. However, mixtures of ligands with different chain length tend to form rafts. NMR studies also show that island or raft configurations of ligands over homogenous distribution increase the local concentration of specific ligands on the surface and eventually enhance the surface chemical reactivity in quantum dots.

To show that controlling the surface loading of nanocrystals has direct biologically relevant consequences, we incorporated different percentage of steroid onto the surface of fluorophore giant quantum dots *via* DHLA-PEG ligand exchange. Particles with different loading of cholestanone show dissimilar absorption and desorption rates along with the lateral diffusion across the lipid surface. Particle landing on the lipid membrane is directly proportional to steroid loading due to cholestanone integration with the lipid bilayer. Therefore, samples with higher steroid loading infuse themselves more with the lipid

membrane compare to those with no or little steroid. Furthermore, we show through experiment that we can estimate the number of ligands interacting with the surface and how they affect lateral motion. In addition, 1D gradient ROESY technique for a simulated model system shows homogeneous distribution of surface ligands.

We investigated a different approach to quantum dot surface modification using ADMET to synthesis multifunctional polymer ligands with multiple azide and carboxylic acid groups. Varying the Ru catalyst to monomer ratio allows us to control the extent of ADMET during the polymerization process. The synthesized multifunctional ligand can wrap around a single nanocrystal by participating in hydrogen bonding with QD's surface ligands to form double layers. The corresponding double layer system with azide pendant functional group was then click onto the gold nanoparticles with acetylene functionality in the presence of Ruthenium catalyst to form heterostructures of QD-Au.

This study can provide a new avenue to understand the organic/inorganic boundary of other and more complex nanoparticle/ligand systems.